

Development and Testing of a High-Country Electric Vehicle

Alexander Ryde

B.E. (Hons)

A thesis submitted in fulfilment of the requirements for the degree of Master of Engineering
in Electrical and Computer Engineering at the University of Canterbury, Christchurch,
New Zealand.

February 2022

Abstract

HiCEV (High-Country Electric Vehicle), is an electric vehicle conversion project which aims to produce a prototype to test the viability of replacing traditional internal combustion engine (ICE) powered farm vehicles with those having an electric drivetrain. Previous work has been performed on a 70-series Land Cruiser, replacing the existing ICE system with an electric motor and power-train. The project was taken over, by the author, as vehicle hardware was largely pre-installed in the vehicle; however, due to the presence of several faults, most significantly, in the electric vehicle control module (EVCM), significant redesign, rewiring, and reprogramming was required to enable vehicle functionality.

Modifications were made to the vehicle to facilitate operating without the EVCM, using the built-in motor control within the inverter. This had the secondary effect of reducing the complexity of the systems, by reducing the number of I/O pins available for switching and monitoring several of the vehicle sub-systems. To work around the EVCM, the inverter took input from several peripherals within the vehicle as well as receiving information from the Battery Management System (BMS), through CAN bus communication.

Testing on HiCEV was carried out to establish the operation of the vehicle, and how it relates to both theory as well as the project objectives. It became evident early on in testing that due to the cell tap wiring in the BMS, the vehicle was being shut down as a result of high measured internal resistances within cells. To enable further testing on the vehicle, the capacity for the BMS to shut down the vehicle was bypassed. Testing yielded that motor and inverter characteristics largely resembled the expected theoretical outcomes, with the motor accomplishing peak torque outputs of 320 Nm at lower vehicle speeds with the torque output beginning to lower at 3600 rpm. The motor and inverter configuration ended up accomplishing a peak power of 130 kW, noticeably greater than the original 95 kW produced by the previous power systems; considerably, due to the torque availability at lower speeds, producing a noticeably greater acceleration than most ICE vehicles. Further testing on specific cells within the pack did yield that there were early signs of degradation, which may inhibit long term reliability; in most cells, signs of degradation were expected and minimal given the age of the cells in the vehicle, which is close to 10 years.

Acknowledgements

First and foremost, I would like to thank my supervisor Dr Paul Gaynor, whose continued guidance and advice kept the project on track. I would also like to thank Glenthorne Station, for sponsoring HiCEV and making this all possible. Additionally, thank you to all UC technical staff, without your input and support this project would not have been possible. Special thanks to Edsel Villa and Ken Smart for your continued support and assistance in testing and fixing HiCEV.

I would also like to extend my gratitude to my family for their unwavering support throughout the project, and for taking me in during the pandemic.

Table of Contents

Abstract.....	ii
Acknowledgements.....	iii
List of Figures	vii
List of Tables	ix
Acronyms	x
Chapter 1: Introduction	1
1.1 EV Background	1
1.2 HiCEV.....	2
1.3 Project Motivation	2
1.4 Project Requirements	3
1.5 Previous Work.....	4
1.6 Overview	5
Chapter 2: Theory of Operation.....	6
2.1 Inverter.....	6
2.2 Resolver.....	7
2.3 Motor Control	8
2.4 Battery Management System	16
2.5 CAN Signal Protocol	20
2.6 UART Signal Protocol	21
Chapter 3: HiCEV Systems and Modifications.....	23
3.1 Inverter.....	25
3.2 Battery Management System	29
3.3 Motor	33
3.4 Charger.....	35
3.5 LV Systems and Ignition	38
3.6 HV Box.....	41
3.7 Power Distribution Box	43
3.8 Braking System.....	44
3.9 Cooling Systems	46
3.10 General Reliability	48
Chapter 4: Experimental Results.....	49
4.1 Testing Overview.....	49
4.2 Batteries.....	51
4.3 Inverter.....	66

4.4 Motor Characteristics	73
4.5 DC/DC Converter.....	76
4.6 LV Systems	77
4.7 Drive Testing	80
Chapter 5: Discussion and Conclusions.....	81
5.1 Project Objectives	81
5.2 Future Work.....	82
5.3 Conclusions	83
References	84
Appendix	90

List of Figures

Figure 1 Simplified 3-Phase Inverter Topology [20].	6
Figure 2 Sinusoidal PWM vs Inverter Output for single phase operation [21].	7
Figure 3 Resolver functionality schematic and expected output waveforms [22].	7
Figure 4 Cross-Sectional Diagram of PMAC Motor [26].	8
Figure 5 Electrical Equivalence circuit for PMAC motor [28].	9
Figure 6 Torque-Speed characteristic curve for PMAC type motors [30].	10
Figure 7 Power-Speed characteristic curve for PMAC motors [32].	11
Figure 8 Phase Angle representation of Space Vector States produced by a two-level inverter [33].	12
Figure 9 Graphical representation of quadrature and direct components of force applied to PMAC rotors [35].	13
Figure 10 Clarke transform phases α and β , referenced to the 3-phases used in motor control [37].	14
Figure 11 Field-Oriented Control feedback loop [35].	15
Figure 12 Discharge Voltage profile for LiFePO ₄ cells, used commonly in EVs [46].	17
Figure 13 Charge Curve for CCCV Charge mode used in Li-Ion cells [50].	18
Figure 14 Cell tap schematic for typical Passive Balance Algorithm BMS [52].	19
Figure 15 Wiring Schematic for CANBUS [57].	20
Figure 16 Standard CAN Frame [61].	21
Figure 17 Electrical Block Diagram for HiCEV	24
Figure 18 Inverter Schematic.	25
Figure 19 Acceleration Pedal Configuration [23].	28
Figure 20 BMS Main I/O Schematic	30
Figure 21 BMS Cell Tap Internal Schematic.	31
Figure 22 Torque-Speed Curve Remy HVH-115 [65].	33
Figure 23 Power-Speed Curve Remy HVH-115 [65].	34
Figure 24 Charger Schematic.	35
Figure 25 Voltage Profile used to estimate State of Charge.	36
Figure 26 BMS CCL Enforcement Profile.	37
Figure 27 Schematic of aftermarket 12 V components.	38
Figure 28 Ignition System Schematic	39
Figure 29 HV Box Schematic.	41
Figure 30 HV box Physical Layout.	42
Figure 31 Power Distribution Box Schematic.	43
Figure 32 Brake Pump Controller Schematic.	44
Figure 33 Schematic of heat transfer in a liquid cooling loop [67].	46
Figure 34 Pack state of charge estimation during charge.	52
Figure 35 Pack Voltage at end of charge cycle.	52
Figure 36 Charge Currents through a full charge cycle.	53
Figure 37 Various cell voltages during BMS passive cell balancing.	54
Figure 38 Pack Voltage during drive testing.	54
Figure 39 Pack Current during drive testing.	55
Figure 40 Pack state of Charge during discharge.	55
Figure 41 Voltage Profile updated for Winston 100Ah Cells	56
Figure 42 Pack estimated State of Charge using Orion factory calibrated Winston 100 Ah cell profile settings under 6 A continuous current charging.	57
Figure 43 Pack voltage during charge with updated cell profile.	57

Figure 44 Individual cell voltages throughout charge period.	58
Figure 45 Cell Resistances calculated by Orion BMS during discharge test.	59
Figure 46 Cell 71 Voltage Measurements over 20 s measurement period.	62
Figure 47 Inverter Current dropping to 0 on shutdown, compared to voltage hysteresis.....	67
Figure 48 Inverter Temperature and Current Profile.....	69
Figure 49 Long-Term operation Inverter temperature profile.	70
Figure 50 Quadrature Current vs Accelerator Input	71
Figure 51 Requested Quadrature Current vs Measured Quadrature Current	71
Figure 52 Efficiency vs Motor Speed.....	72
Figure 53 Torque and Speed Characteristics 1 st Gear Acceleration.....	73
Figure 54 Power and Speed Characteristics in 3 rd Gear Acceleration Test.....	74
Figure 55 Power and Speed Characteristics during 1 st Gear Acceleration test	75
Figure 56 Power and Torque Characteristics during 1 st Gear Acceleration test.....	75
Figure 57 CAN High Signal.....	77
Figure 58 CAN bus using external termination resistor on BMS.	78
Figure 59 Modified Ignition System Schematic	79

List of Tables

Table 1 HiCEV Specifications	4
Table 2 Vehicle Components	24
Table 3 Inverter EEPROM programmed variables.	27
Table 4 12 V peripherals and corresponding current ratings.	38
Table 5 Expected Thermal losses in Electrical Components.	46
Table 6 Testing Overveiw.....	50
Table 7 Battery Cell Calculated Internal Resistances compared to Orion measurements.	60
Table 8 Battery Internal Resistances, and Discharge Voltages, compared with Orion measurements.	61
Table 9 Internal Resistances from Discharge Test using Orion BMS 2.	61
Table 10 Benchtop Cell discharge test.....	63
Table 11 Charger Thermal Test Results.	64
Table 12 Charger Thermal Test with Airflow Applied.	65
Table 13 Motor parameters updated in inverter software.	68
Table 14 Motor Break Speed per Gear	73

Acronyms

AC Alternating Current
BEMF Back-Electromotive Force
BMS Battery Management System
CAN Controller Area Network
CC Constant Current
CV Constant Voltage
CCCV Constant Current Constant Voltage
CRC Cyclic Redundancy Check
DC Direct Current
EEPROM Electrically Erasable Programmable Read-Only Memory
EMF Electromotive Force
EOF End of Frame
EV Electric Vehicle
EVCM Electric Vehicle Control Module
FOC Field-Oriented Control
FYP Final Year Project
GUI Graphical User Interface
HiCEV High Country Electric Vehicle
HV High Voltage
ICE Internal Combustion Engine
IP Ingress Protection
LV Low voltage
LVVTA Low-Volume Vehicle Technical Association
MCU Microcontroller Unit
MOSFET Metal-Oxide Semiconductor Field-Effect Transistor
NMOS N-Channel Metal-Oxide Semiconductor (Field-Effect Transistor)
PM Permanent Magnet
PMAC Permanent Magnet Alternating Current (Motor)
PWM Pulse-Width Modulation
RMS Root Mean Square
RS232 Recommended Standard 232
RTR Remote Transmission Request
SCI Serial Communications Interface
SOC State of Charge
SOF Start of Frame
SVM Space Vector Modulation
SVPWM Space Vector Pulse-Width Modulation
UART Universal Asynchronous Receiver-Transmitter
UC University of Canterbury
VFD Variable Frequency Drive
WoF Warrant of Fitness

Chapter 1: Introduction

1.1 EV Background

Electric vehicles are becoming increasingly popular due to mounting environmental and economic concerns worldwide. Deepening worries over global climate change, due in part to carbon emissions from ICE vehicles, contribute to pressures to re-evaluate transport in modern society [1].

Economically, electric vehicles pose a significant advantage over internal combustion engine (ICE) counterparts, culminating from the reduced cost of electric energy as opposed to ICE vehicle alternatives [2]. Recently in NZ, this has been compounded by governmental incentives to switch to more fuel efficient and sustainable transportation options; through exemptions in road user charges, introduction of rebates and increasing taxation on diesel alternatives [3]. Despite these incentives, there are still substantial concerns from general consumers and industry which inhibit the adoption of electric vehicles. This is largely based on practicality matters; however, due to the manufacturing process of EVs and electricity generation, there is still scepticism over the environmental advantages posed by electric vehicles.

Electric Vehicles provide many advantages over ICE alternatives which provide road users with a competitive alternative. EVs are likely to be at the forefront of the global drive towards carbon neutrality, with transport contributing an estimated 29% of all CO₂ emissions in the US for the year of 2019; notably, the largest contributor of all sectors [4]. Though climate change is providing the primary motivation for this, the benefits to consumers are also alluring, as running an EV has been estimated to be similar to paying as little as 30c per litre despite the significant up-front cost of buying a new EV [5]. There is also the benefit that EVs can simply be charged from the grid, which allows them to be charged virtually everywhere, despite the concerns some may have with charge times. This could provide great benefit to many, especially in remote areas, as they adapt to overnight charging as opposed to rapid refuelling.

Recent technological advances in battery manufacturing and widespread charging stations have significantly improved the viability of electric vehicles for regular consumers by addressing many of the practicality concerns with early EVs. Resistance to EVs from consumers is generally based on range, convenience, and safety concerns. Early EVs were significantly limited in terms of the battery technology that was available at the time. The result was early vehicles had limited range, with early Nissan Leaf models producing nominal ranges of 117 km [6]. Modern EVs have improved upon this substantially, with the equivalent 2021 Leaf more than tripling this rated range at 385 km and Tesla offering vehicles capable of driving up to 665 km on a single charge [7, 8]. This in part, resolves much of the concern regarding the convenience of EVs as charge times become less relevant with increased range. Despite this, charge times do remain an issue for many sectors, as for many in occupations which require travel, the convenience of refilling a tank in minutes cannot be easily surpassed. The concerns with charge times are being exacerbated by improved power density in electric vehicles, with Tesla charge times varying from 5-12 hours, with the highest times experienced for the newer models with increased range [7]. With this trend, the longer charge times do mean that the EVs still pose a significant inconvenience to many who may want to use their vehicle for long distances. Infrastructural workarounds, through fast chargers, which shave charging times down to 30 minutes or less, are improving the viability for long distance EVs; however, their availability in NZ has yet to reach a point where they are justifiable for consumers for long distance trips, when compared to using ICE powered vehicles [8].

Safety concerns have also been raised recently as a drawback for electric vehicles. The primary source of this apprehension stems from the Lithium-Ion batteries which are used in EVs and the abundance of anecdotal evidence regarding EV fires and risks they pose to occupants of a vehicle in a crash. Though there is some evidence to support this, the reality is, combustion in Lithium-Ion batteries is invariably due to a fault, overheating or physical damage from crashes [9]. Some sources argue that EVs are able to reach higher general safety levels than ICE vehicles due to reduced physical size of components contributing to larger crumple zones, fewer volatile liquids in the vehicle and lighter physical weight of the vehicle reducing the severity of crashes [10].

Electric Vehicles have many advantages going for them, however, there is still a well-founded doubt towards the technology. One common argument is that grid power is not 100% clean and the manufacture of the core components is particularly questionable. In NZ, the grid is partially reliant on coal, oil and natural gas for generation, making up as much as 15-20% of annual electricity generated in the past decade [11]. Though the government is aiming to improve this situation, with an objective to become 90% renewable by 2025, and 100% renewable by 2035; disruptive technology, like EVs, could potentially significantly increase the load and therefore renewable infrastructure required [12]. The concern which arises from this, is that EVs are simply exchanging carbon emissions from the vehicle itself, to the generation of electricity. This issue is far more substantial on a worldwide level; where combustible energy, primarily fossil fuels, make up an estimated 67% of electricity generated [13]. Fortunately, climate initiatives have brought this number down steadily, and alternatives like nuclear power, are able to generate electric power without carbon emissions though brings up other concerns with the radioactive waste. Despite the 'zero-emission' reputation touted by EVs, opponents bring up the energy cost in production of EVs, and notably the transport of raw materials using cargo ships, the ethics of mining battery materials and the lack of recycling infrastructure. These concerns are valid, however, in large part, ICE vehicles also suffer from similar drawbacks [14, 15].

1.2 HiCEV

The High Country Electric Vehicle (HiCEV) is an electric vehicle conversion project commissioned to the University of Canterbury by Glenthorne station. The project aims to produce an EV prototype to test the viability of running electric vehicles in a farm environment as a replacement for traditional ICE vehicles. HiCEV has been an ongoing project for the University, with multiple engineering programme final year projects (FYPs) and a previous Master's Student, Pierce Hennessy, having completed significant work towards the conversion of the vehicle [14]. A considerable amount of this work was with the mechanical transformation from the original drivetrain of a 70 Series Toyota Land Cruiser and getting the prototype functioning. Due to more recent developments, notably malfunctioning hardware in the electric vehicle control module (EVCN), extensive work has been required to restore this prototype vehicle's functionality. Additionally, because of the unique requirements of a farm vehicle, substantial new additions and revisions have been required to reliably operate the vehicle.

1.3 Project Motivation

The project sponsor, Glenthorne Station, originally commissioned the vehicle to UC with the intention of prototyping an electric vehicle that could test the feasibility of converting an entire fleet of vehicles to EVs for farm operation. The perceived benefits of EVs for a farm environment include not only green initiatives, but also some practicality improvements on regular farm vehicles. At the time the project was initiated in 2012, the EV market was limited to low-range smaller road vehicles, like the Nissan Leaf or the early Tesla Model S. This left a hole in the market for practical utility vehicles that could greatly benefit from the reduced ongoing costs that are offered by EVs. The

additional benefits to the farm, by making use of the electricity network, is that they become more self-sufficient and also have the potential to make some considerable time savings for the farm in normal operation.

More recently, incentives for operating EVs on farms are increasing, with the climbing ongoing costs of operating ICE vehicles, government levy introductions to diesel powered vehicles, and the growing awareness of global climate change.

Electric vehicles are becoming increasingly popularised due to the reduced costs of production, and the ongoing improvements in practicality for general usage; however, the stand-out cause for the shift toward EVs is primarily being driven by climate initiatives, of which New Zealand is on the forefront. Though it is still too soon to practically convert the majority of vehicle users to EVs, largely in part due to up-front cost and range concerns, prototyping the viability of EVs enables them to be used more widely, and incentivises their adoption when the technology has caught up to the demand. In NZ, the majority of electricity consumption comes from renewable energy which is a major motivation for NZ road users to move towards the EV market. This enables owners of EVs to feel confident that for the most part, they are reducing their carbon footprint.

1.4 Project Requirements

The general functionality of HiCEV is the most important requirement for the vehicle, inclusive of safety, operability, peripheral operation and reliability. Additionally, HiCEV has a unique set of requirements due to the nature of it operating as a farm vehicle; as well as the requirements from governing bodies, namely the Low-Volume Vehicle Technical Association (LVVTA), within NZ for it to be operable on NZ roads [15]. The LVVTA has guidelines and requirements for the electrical safety of the vehicle, which must be met to operate HiCEV on New Zealand roads. The location where it is intended for use, Glenthorne Station, is surrounded by rivers, creeks, lakes and hills; which dictate requirements for waterproofing, power output, reliability and safety [16].

Functionality requirements for HiCEV largely resemble that of a normal road car. The objective being, that HiCEV remains an operational prototype of what could, feasibly, replace the existing fleet of farm utility vehicles. As an EV, compromises need to be made with regards to the general operability of the vehicle; however, for the most part the basic functionality can remain intact from the original build of the vehicle. One key objective for the vehicle was that it remained similar to the original vehicle in terms of power output and drivability. For this reason, the vehicle components were chosen, by Pierce Hennessy (the Masters student who developed the original HiCEV systems), to compliment this by creating a similar power to weight ratio. Additionally, HiCEV has some other unique inclusions because of this requirement, notably the original gearbox is intact to preserve the authenticity of driving a manual farm vehicle along with providing the necessary wheel-level torque range for farm utility application.

Glenthorne station is a high-country farm spanning 25000 hectares with geographic features like creeks and hills contributing to rough terrain. The nature of the location, being that it is high in elevation also means that the vehicle will likely be exposed to extreme climate, with temperatures as low as -20° C or as high as 35° C. This environment poses a threat to EVs with regards to waterproofing, cooling, and reliability. For this reason, HiCEV has an additional requirement to maintain an IP67 level of waterproofing. IP67 is a standard for waterproofing which specifies that the enclosure is dust tight and protected from temporary submersion in water [17]. This was used as a minimum standard for the overall water-proofing for many of the HV components in the vehicle such that practical farm use will not damage the vehicle, or pose any safety risk.

The LVVTA is an organisation which inspects modified vehicles and determines their safety for use on New Zealand roads. Most relevantly, the LVVTA sets and enforces the standards for electric and hybrid conversions on vehicles, which ideally, HiCEV will meet so that it can be used on and off road safely. The LVVTA makes considerations towards the electrical and mechanical adjustments to the vehicle for the general safety of the occupants, post-modification [15]. Table 1 below shows the requirements and specifications for HiCEV to meet safe operation requirements.

Table 1 HiCEV Specifications

Requirement:	Specifications:
Weather-Proofing	<ul style="list-style-type: none"> - IP67 specified sealing on all HV components. - General waterproofing of LV components, and positioning of exposed terminals physically higher in the vehicle. - Use anti-freeze coolant with water-cooled units.
LVVTA Requirements	<ul style="list-style-type: none"> - Mounting of cables every 350 mm or less. - Provide Battery disconnects. - Mount a 'kill switch', or emergency shutdown switch, in the cab accessible to the driver. - Be able to meet all WoF requirements for NZ Roads - Colour code all HV wiring (>50 V) orange - Provide HV warning labels to all boxes containing terminals of greater than 50 V. - Ensure the battery compartment is capable of withstanding 30x its weight in impact force. (i.e., 1kg, must withstand 300N)
Functional Requirements	<ul style="list-style-type: none"> - Keep existing wiring loom to operate peripherals. - Tune motor control for gearbox operability. - Build in ability to charge from any AC power point. - Include regenerative braking to allow the vehicle to run longer and provide additional ability to emulate conventional vehicle driving behaviours.

1.5 Previous Work

HiCEV has been an ongoing project for the University of Canterbury since 2012 and has had a significant amount of student input throughout that period. The bulk of the hardware transformation had been completed by these previous students having installed the motor, inverter, charger, BMS and batteries. The primary fault with the vehicle in early 2020 was the EVCM which controlled and monitored all the peripherals, was malfunctioning. Alongside this, the vehicle had many other concerning features, notably the assembly of the cabling, mounting of hardware and cooling which all needed to be worked on towards the goal of meeting all the specifications for the vehicle.

Significant work had been done to get the vehicle into a working state, including the integration of all core components of the vehicle, with the failing EVCM inhibiting the functionality from many of the fundamental systems of the vehicle. The result of this is that for the vehicle to function, the vehicle wiring would have to be fundamentally redesigned to operate around the inverters built-in control module as opposed to the EVCM. Most of the existing wiring was recyclable, having been specified and installed by previous FYP groups, and the modules in the vehicle were still in a functional condition. Many of the peripherals however, were controlled by the EVCM and had to be re-designed so they could operate with either, inverter control, or automated such that they would not pose significant concern for the driver.

1.6 Overview

The objective for this thesis is to highlight the fundamental electrical operation of HiCEV, explain the existing and modified components of the vehicle and verify reliable and expected operation. Chapter 2 introduces the fundamental principles of EV operation which are used in HiCEV through both hardware and software implementations. The electrical hardware in the vehicle, including modification and existing hardware, is covered in chapter 3. The results from vehicle testing is detailed in chapter 4, with particular emphasis on reliability and reference to theory. A discussion on how progress meets with the project requirements and future work that will likely need to be carried out for HiCEV is covered in chapter 5.

Chapter 2: Theory of Operation

HiCEV peripherals rely on a wide array of functionality and features for operation. This is inclusive of the motor control, battery management and charging, inverter, auxiliaries, and communication protocols; which all have a significant role in the functionality of HiCEV. The operability of the vehicle is largely reliant on the integration of these components and the functionality they each provide.

2.1 Inverter

Inverters are used in a wide array of applications in modern devices and are an essential component of EV power trains. The operation of an inverter is to switch DC currents across a load to produce a pseudo-AC waveform on the output. Power inverters are commonly found in motor drives, solar installations and motor homes.

Inverters are typically made up of half-bridges consisting of NMOS transistors for switching the output state for each connected node. Single phase inverters consist of an H-bridge which can be switched alternately to apply either a positive or negative voltage across a load; whilst 3-phase inverters, such as the inverters used in motor control, make use of 3 half-bridges. Filtering can then be used to smooth the current on the output to produce a sinusoid-like current output. The simplified topology of a three-phase inverter, like the one used in motor drives, can be seen in Figure 1 below.

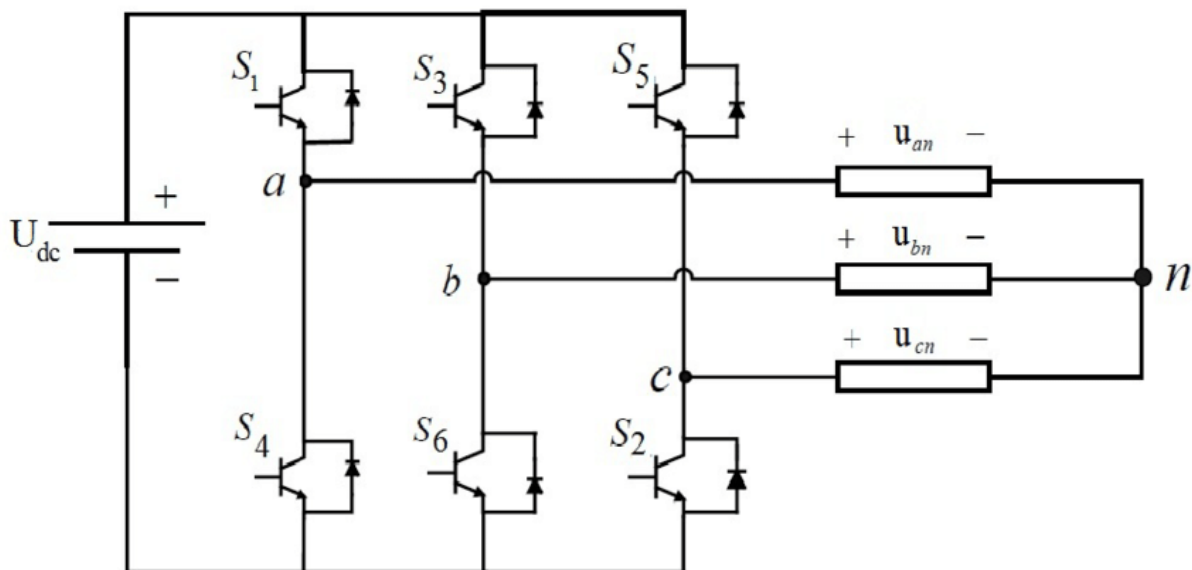


Figure 1 Simplified 3-Phase Inverter Topology [18].

This topology for the 3-phase inverter enables the controller to switch a voltage across the 3-phase load, u , through the switching of the power transistors. Each phase can be individually controlled to vary the phase angle of the voltage as viewed from the load. In three phase permanent magnet (PM) type synchronous motors, like the one in HiCEV, the stator is typically connected via a star-connection. In a motor, current flows through the conducting switches in the inverter, such that effectively balanced 3-phase current flows through the three phase motor stator windings. This allows control methods to be applied to rotate the magnetic field around the stator of the motor, thus driving the permanent magnet rotor.

This switching operation can be modulated using various control strategies, often sinusoidal PWM, to produce a relatively smooth 3-phase AC output waveform. In practice, this can be applied to 3-phase motor windings to magnetise the stator in PMAC motors; which, can be used to drive the rotor. Figure 2 shows the typical control waveforms for single phase sinusoidal inverter operation, and the output waveforms generated [19].

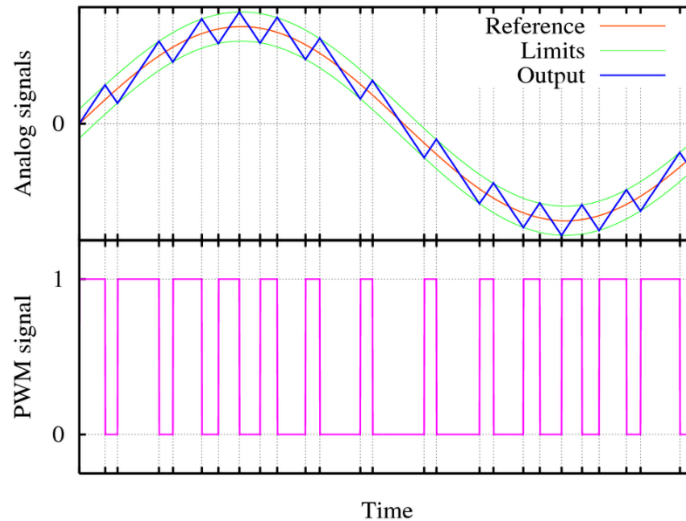


Figure 2 Sinusoidal PWM vs Inverter Output for single phase operation [19].

The inverter topology also enables PM synchronous motor loads to perform regenerative braking. For this to occur, the switching order of the transistors are adjusted, such that the inverter operates as a controlled rectifier. In this mode of operation, the rotating magnetic field from the motor's allows controlled current flows back into the voltage source (batteries).

2.2 Resolver

Resolvers are an analogue positional sensor used in motor control for determining the position of the rotor. Resolvers function by energising a rotary coil, which is attached to the rotor, with a high frequency excitation provided by a voltage source. This rotating coil has a magnetic field, produced by the current flowing through it, which is used to induce a voltage on two secondary coils which are mechanically placed with 90° separations. The induced voltage in the secondary coils will resemble the frequency of the excitation voltage; however, the magnitude of the excitation in each direction can be used by a controller to determine the position of the rotor and tune the controller accordingly. Figure 3 shows an electrical schematic for a resolver, and the expected output waveforms from the coils during rotational operation [20].

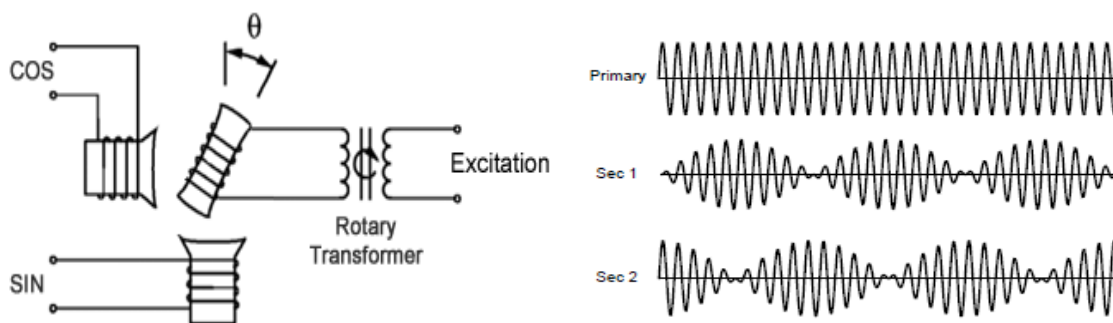


Figure 3 Resolver functionality schematic and expected output waveforms [20].

2.3 Motor Control

Motor control is a fundamental aspect of HiCEV, enabling the motion and regenerative braking of the vehicle making use of Field-Oriented Control (FOC). The motor used in HiCEV is a Remy HVH-250-115 3-phase permanent magnet synchronous AC motor, which is driven by a Cascadia Motion Systems PM150DX inverter [21]. The inverter has built-in motor control, utilising FOC, which can be adjusted in software to program the desired functionality from the motor.

2.3.1 Synchronous AC Motors

Permanent Magnet Synchronous AC motors (PMAC) are structured with a permanent magnetic rotor often in the centre of the motor, which typically contains multiple pole-pairs to facilitate smooth operation. Conventionally, the stator takes the form of 3-phase windings usually around the rotor; these windings surround laminated steel to reduce eddy currents in the stator, guide the magnetic field, and limit the effects of hysteresis [22]. Figure 4 below shows the cross-sectional construction of a very basic PMAC 3-phase synchronous motor [23], similar to the HVH250 used in HiCEV.

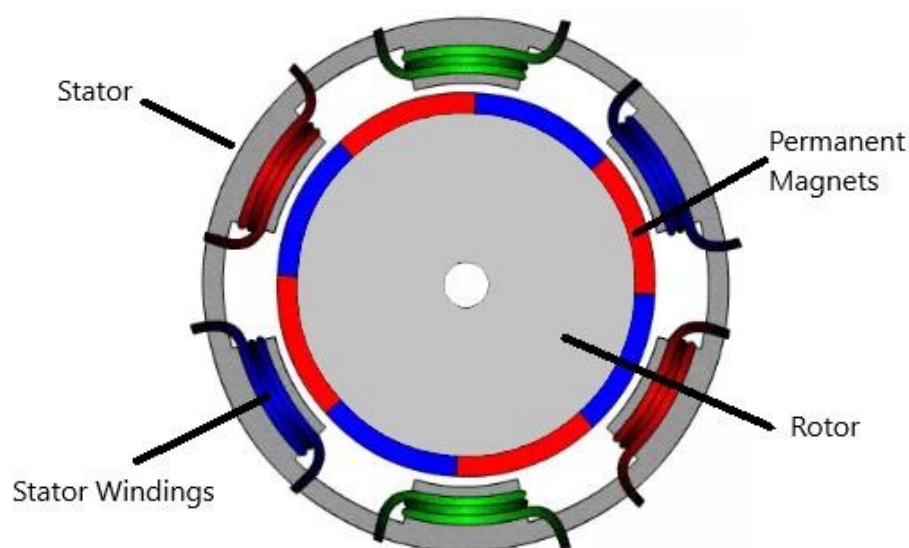


Figure 4 Cross-Sectional Diagram of PMAC Motor [23]

In a synchronous machine, the rotation of the rotor magnetic field is aligned (synchronous) with the stator rotating magnetic field throughout the motor. For this reason, the motor speed is determined by the rate at which currents are switched through the coil, which is known as variable frequency drive (VFD). However, the majority of PMAC motors contain multiple pole-pairs, which alternates the optimal line frequency to achieve various speeds. The speed of the motor can be determined by applying **Error! Reference source not found.** below;

$$N = 120 (f/P) \text{ rpm} \quad (1)$$

Where, N is the motor speed, in revolutions per minute (rpm), f is the AC line frequency, and P is the number of poles [24].

To maintain rotation, the magnetic field applied to the stator must be constantly adjusted such that the torque angle is maximised for the position of the rotor. To produce the maximum torque, the rotor position, will lag the stator magnetic field by the maximum torque angle of the motor 90° . In a 3-phase system, the torque angle is maintained by three input waveforms 120° out of phase referenced to each other.

The fundamental structure of permanent magnet AC synchronous motors include 3-phase stator windings in a star-configuration. Present on each winding is a leakage resistance, leakage inductance and a back-EMF voltage (BEMF) [25]. The BEMF generated by the operation of permanent magnet motors can be explained by the applications of Faradays law of electro-magnetic induction [26]. Faraday’s law states that in a time-varying magnetic field will induce an EMF, which is described by **Error! Reference source not found..**

$$e = -N \frac{\Delta\phi}{\Delta t} \quad (2)$$

Where e is the induced back EMF, N is the number of windings in the coil, and $\frac{\Delta\phi}{\Delta t}$ is the change in magnetic flux with reference to time.

These characteristics can be used to produce an electrical equivalence circuit for the PMAC motor, consisting armature resistance and inductance, and a frequency dependent voltage source, representing the magnitude of the back-EMF. This equivalence circuit can be seen in Figure 5.

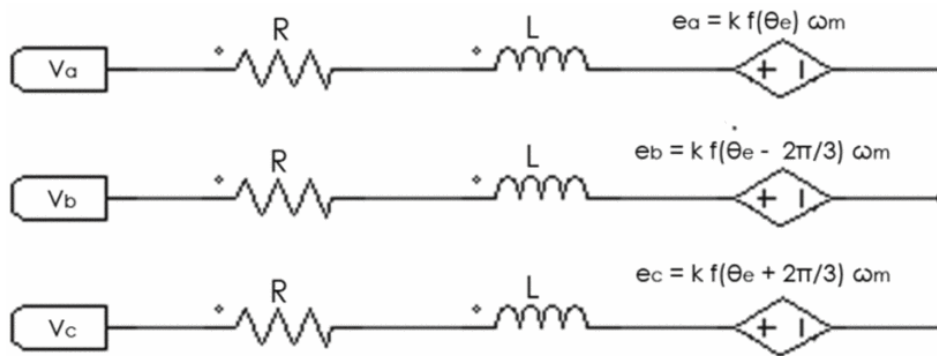


Figure 5 Electrical Equivalence circuit for PMAC motor [25].

2.3.2 PMAC Motor Characteristics

Motor operating characteristics provide a significant role in the expected performance of a system like an EV. Permanent magnet motors are often used in EVs due to their relatively easy controllability and high efficiency. Operating characteristics, with regards to torque, speed and power, can be used to control and manage the performance of these system.

In permanent magnet motors, mechanical torque is produced by the effect of the magnetic field circulating within the stator interacting with the rotor permanent magnet poles. For this reason, magnetic field strength is a primary contributing factor to the torque observed by a motor. In a PMAC motor, the magnetic field should be optimised, through control, such that the magnetic field leads the rotor magnetic field to meet the load torque requirements while minimising the current amplitude.

Given that, mechanically, force is proportional to torque, the expected torque produced by a motor is proportional to the current supplied to the motor. PMAC motors produce torque characteristic curves similar to the one in Figure 6 [27].

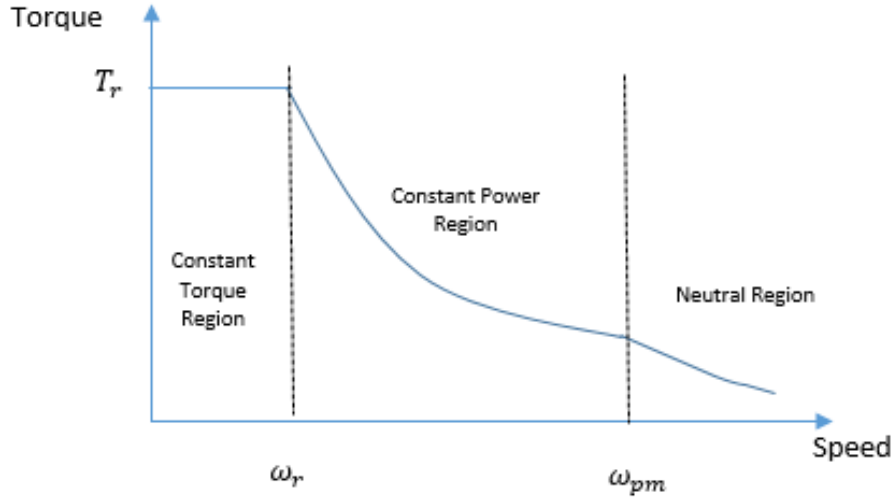


Figure 6 Torque-Speed characteristic curve for PMAC type motors [27].

In PMAC type motors, the peak operating torque is limited by the product of the rotor and stator magnetic flux. Consisting of permanent magnets, the rotor maintains a constant flux magnitude; consequently, the stator flux, proportional to armature current, has the most significant impact on the peak torques obtainable. Though the torque can be said to be proportional to the current, other limiting factors, such as magnetic core saturation, flux leakage, back EMF, and motor conductor material, can have substantial impact on the peak and rated torque characteristics. At low speed, the peak rated currents can generally be safely applied to the motor, enabling a constant torque operation region at the rated torque for the motor.

At higher rotor speeds, the back EMF induced in the stator coils by the rotor flux, limits the peak current of the motor. The back-EMF opposes the applied voltage reducing the effective voltage across the energised stator coils; thus, limiting the peak current that can be applied to the motor based on the armature impedance. The rated speed in PM type motors, is the speed at which the maximum constant torque for the motor begins to degrade based on the effects of the back EMF. Armature impedance is a sum of inductive and resistive impedances within each phase of the motor, resulting in the following basic motor voltage equation.

$$V_A = Ri_A + L \frac{di}{dt} + e_A \quad (3)$$

Mathematically, it can be observed that with constant resistive and inductive components, increasing back EMF must result in a decreasing current, and $\frac{di}{dt}$ product; the consequence of which, is a reduced peak torque at higher speeds.

The power-speed characteristic curve can be derived from these operating conditions, given the following expressions for mechanical and electrical power.

$$P = \omega \cdot T_r \quad (4)$$

$$P = V \cdot I \quad (5)$$

During operation, the peak electrical power is proportional to the current-voltage product, equivalent to the mechanical torque-speed product. At low speed, the average voltage applied to the motor, through PWM commutation, scales proportionally to the speed of the motor; this occurs until the motor reaches its peak power operating point [28]. At the motor peak power operating point, the back-EMF limits the peak operating current, clamping the continuous power output of the motor at higher operating speeds. This trend can be seen in Figure 7 showing the typical rated power-speed characteristic for a PMAC motor [29].

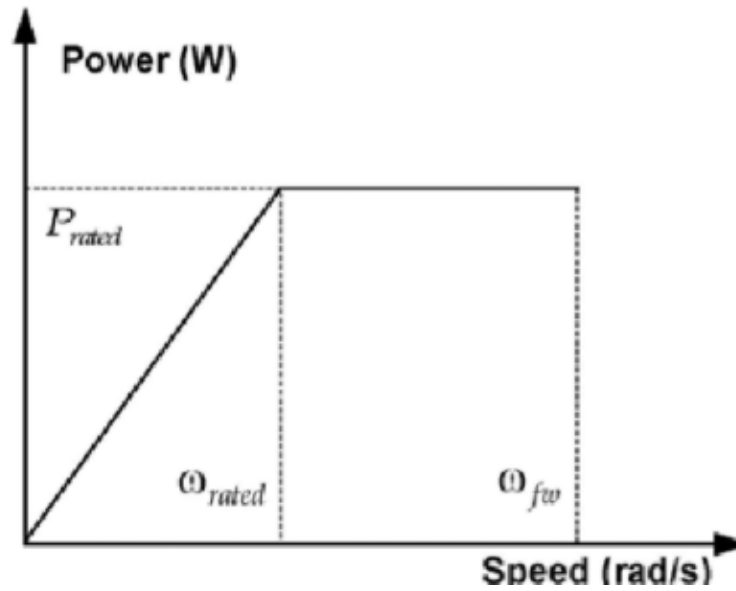


Figure 7 Power-Speed characteristic curve for PMAC motors [29].

2.3.3 Space Vector Modulation

The specific control method applied in HiCEV is space vector modulation, also known as field-oriented control. Due to the nature of 3-phase two-level inverters, there is a finite number of phase angle states the controller can be switched to dependant on which of the phases is energised. These finite states are known as space vectors and are shown in Figure 8 below.

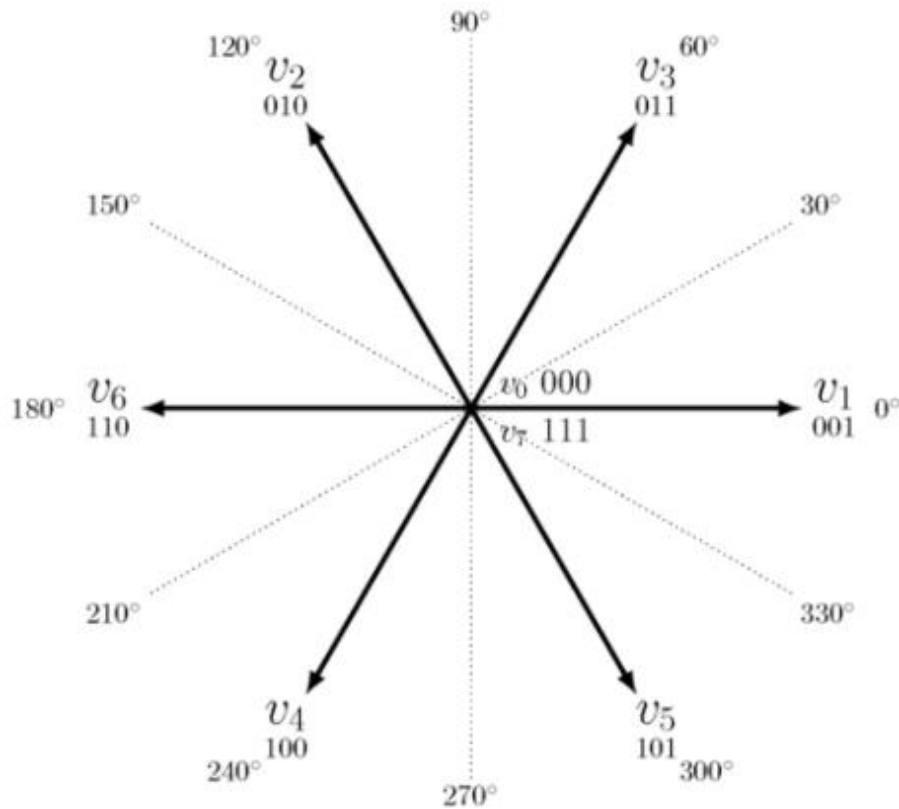


Figure 8 Phase Angle representation of Space Vector States produced by a two-level inverter [30].

Each space vector state can be equated to a switch state for the inverter, for instance, 001 position represents the state where phase A is connected to the voltage source and phases B and C are connected to ground. The notation represents the state of each inverter half-bridge for each space vector, with each number representing a binary, on or off state for phases CBA in that order. The state for 000 represents the state where no phases are energised, and state 111 represents the state for all phases being energised. Because of the 60-degree commutation of BLDC and PMAC type motors, an unavoidable by-product of these motors is torque ripple. This is induced as the result of a 'stator magnetic field jump' which occurs from inverter switching; various control methods aim to address this ripple by rapidly switching between states to smooth the experienced magnetic field rotation around the motor [31].

Space Vector Modulation aims to smooth the operation of PM motor types by producing any voltage vector through rapid commutation between the eight achievable states. With rapid switching, any phase angle for the voltage vector can be accomplished by switching between the states, for instance, a phase angle of 30° can be accomplished by switching between state 001 and 011, with a 50% duty on each state. The voltage magnitude can also be reduced by making use of the 000 and 111 states to provide a 'dead-time' for the inverter, lowering the overall on time for applied voltage. Ideal operation for space-vector control would use the 3 inverter phases to produce a smoothly rotating voltage vector, thus magnetic field, which leads the rotor of the PMAC type motor.

2.3.4 Field-Oriented Control

Field-oriented control is a method which aims to maximise the force applied to the rotor of a PM machine by maintaining a magnetic field perpendicular to the rotor. The magnetic field in the stator of a PM motor can be represented as effects from two orthogonal vectors, direct and quadrature; where the direct vector is the magnetic field component which is in-phase with the rotor, and the quadrature leads the rotor by 90° . Field-Oriented control aims to control both the direct and quadrature components of the magnetic field in the stator, maximising the torque applied to the rotor by minimising the direct component of the magnetic field [32]. In practise, motors typically have multiple pole pairs within the rotor, configured to reduce overall torque ripple and improve efficiency by reducing air-gap between rotor and stator magnetic fields. Consequently, in most PM motor configurations, it is impossible to achieve a perfect quadrature force vector in relation to the rotor position. Despite this, algorithms can still control quadrature and direct currents to accomplish relative maximum performance for the motor. Figure 9 below demonstrates graphically the quadrature and direct vectors of the forces applied to the stator in a basic PMAC motor.

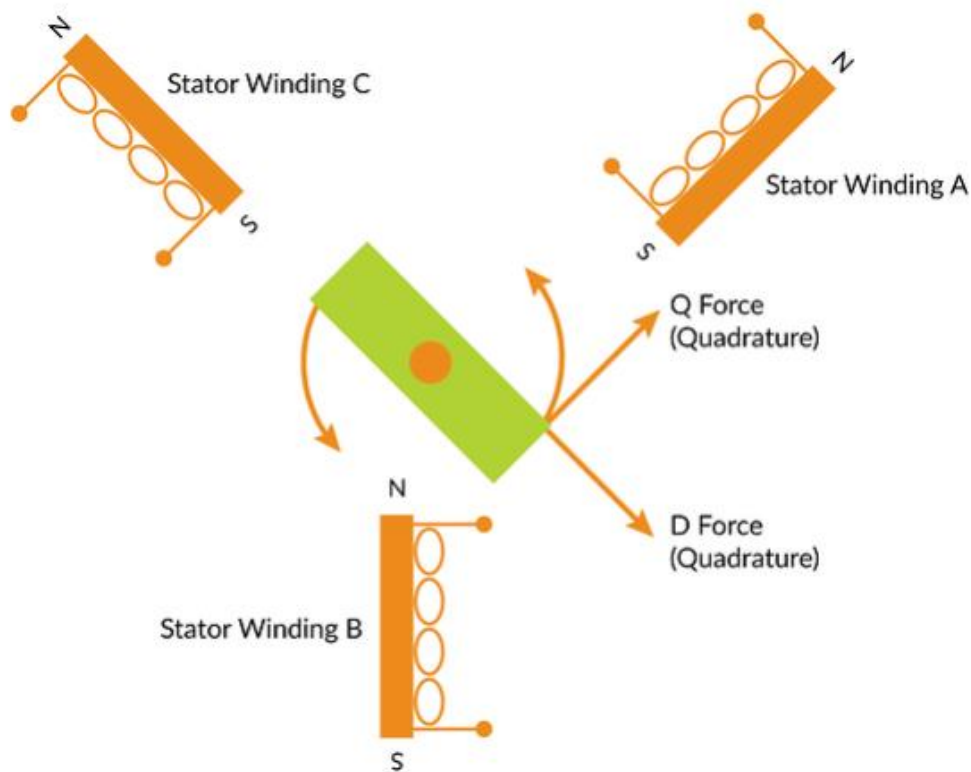


Figure 9 Graphical representation of quadrature and direct components of force applied to PMAC rotors [32].

Controlling the quadrature and direct components of the force applied to the stator requires the 3-phase commands to be converted into a 2-phase reference representing the control variables I_Q and I_D . This is performed in two stages, firstly converting the 3-phase reference to a 2-phase reference, known as a Clarke Transformation; secondly converting the 2-phase reference to a rotating 2-phase reference representative of the rotor position, known as a Park Transformation [33]. The Clarke transform is performed by multiplying the vectors for the a, b and c phase components by a reference matrix. The reference matrix is representative of the factor which each phase has on the new 2-phase reference axes, with phase A being in phase with α , phase B being 120° out of phase with α , and phase C being -120° out of phase with α . A graphical representation of the new phases, α and β , can be seen in Figure 10 below.

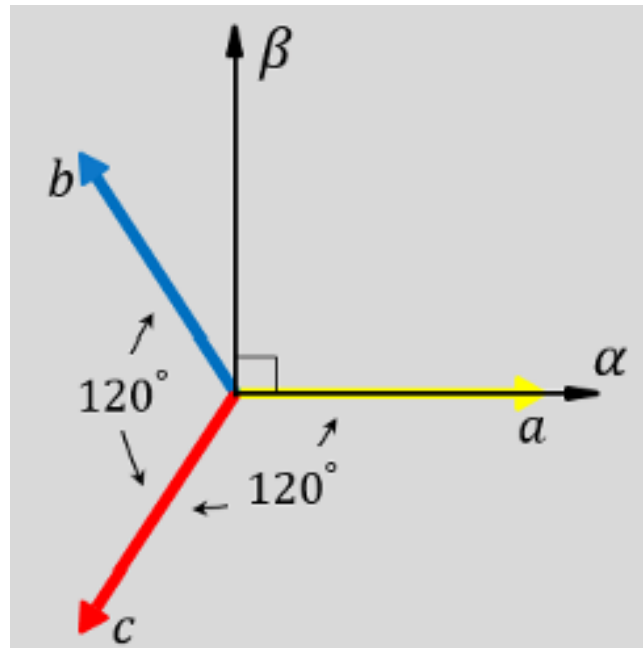


Figure 10 Clarke transform phases α and β , referenced to the 3-phases used in motor control [34].

The equation used in the Clarke transform sums the effect each phase has on the new 2-phase representation using α and β . This equation can be seen below [35].

$$\begin{bmatrix} I_\alpha \\ I_\beta \\ 0 \end{bmatrix} = \frac{2}{3} \begin{bmatrix} \cos(\theta) & \cos(\theta - 120) & \cos(\theta + 120) \\ \sin(\theta) & \sin(\theta - 120) & \sin(\theta + 120) \\ 1/2 & 1/2 & 1/2 \end{bmatrix} \begin{bmatrix} I_A \\ I_B \\ I_C \end{bmatrix} \quad (6)$$

A Park transformation is performed on the resultant 2-phase representation of the current vectors in the system. Given that the motors actual position is known, the magnitude of the vectors, I_α and I_β , can be extrapolated out to give the magnitude of the control variable vectors, I_D and I_Q . This process known as a Park transform, works by summing the effect I_α and I_β have on the current at actual position of the motor, and goes by the following equations [33].

$$I_D = I_\alpha \cdot \cos(\theta) + I_\beta \cdot \sin(\theta) \quad (7)$$

$$I_Q = I_\beta \cdot \cos(\theta) - I_\alpha \cdot \sin(\theta) \quad (8)$$

Field-Oriented Control performs control on these variables, I_D and I_Q , taking in multiple control inputs, with I_D demand being set to 0, and I_Q command determined by the desired torque in the system. Both variables I_D and I_Q have independent PID control, which is used to generate I_D and I_Q command currents which is inversely transformed to produce I_α and I_β commands. These current commands are used with a space vector PWM generator which provides the commands for the inverter. Figure 11 below shows the overall control pathway for a system using Field-Oriented control.

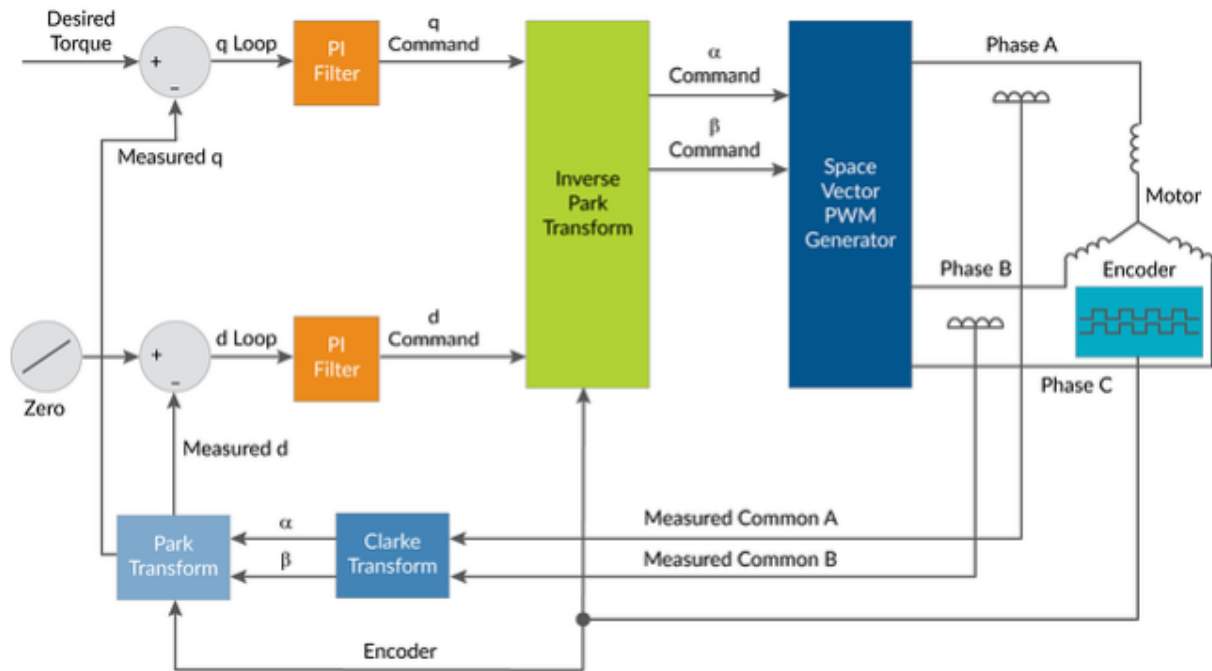


Figure 11 Field-Oriented Control feedback loop [32].

2.4 Battery Management System

2.4.1 Battery Technology

Lithium-Ion batteries are widely used in modern electronics and EVs due to their relatively high energy density, which can be over 6 times greater than lead-acid alternatives [36]. The high energy density enables weight to be kept down and physically smaller battery requirements for EVs, providing benefits to efficiency and practicality. Lithium-Ion battery chemistry varies by application, in EVs LiFePO₄ batteries are often used due to high relative discharge rates, longevity, and temperature resilience. However, these desirable features come at the expense of reduced energy density, with LiFePO₄ batteries typically exhibiting 90-120 Wh/kg, and other Li-Ion chemistries producing up to 200 Wh/kg [37].

2.4.2 Battery Chemistry

The simplest battery cells chemically consist of an anode, negative terminal, and a cathode, positive terminal, separated by an electrolyte. The power supplied by the batteries is reliant on the movement of ions across the electrolyte, in Lithium-ion cells the charged ions moving through the battery are Li⁺ ions [38]. During discharge, Li⁺ ions are produced by a reduction reaction which occurs at the cathode, and an oxidation at the anode, within the battery the Li⁺ ions move across the electrolyte from anode to cathode; the movement of Li⁺ ions accounts for much of a cells internal resistance. The redox of Li⁺ ions are reversible in the cells by applying a current source across the batteries which enables the batteries to be recharged. The chemical equation for the redox in LiFePO₄ batteries, which are used widely in EVs can be seen below [38].



2.4.3 Battery Characteristics

In all electrochemical redox reactions, the nodes produce a potential difference due to the gain or loss of electrons at the node. Commonly, this potential is compared to a reference point, known as the standard hydrogen electrode, which has a potential of 0 V [39]. This standard electrode potential, E⁰, is the primary determining factor for a cells nominal voltage, with many Li-Ion chemistries producing between 3.3 and 4.2 V due to the standard electrode potential of the redox reactions taking place. However, the standard electrode potential is only a measure of the electrode conditions in a standard environment, and as such, the cell voltage is highly susceptible to temperature, pressure and ion-concentration.

Lithium-ion voltage characteristics are also affected by limitations within the battery and the effects of internal resistance. Factors which contribute to the internal resistance of battery cells can be constant or variable. Constant factors include characteristics of the battery design, such as anode and cathode material, physical separation distance, material exposed surface area, or the electrolyte [40]. Alternatively, factors like temperature, state of charge and cell degradation, have a variable effect on the internal resistance of battery cells. Internal resistance can be a contributing factor to voltage drops in lithium-ion cells, which are particularly sensitive to high currents. High load current induced voltage drops can often be caused by the slowed diffusion of Li⁺ ions across the battery due to chemical factors contributing to internal resistance [41].

The state of charge in Lithium-Ion batteries is an estimated characteristic based on temperature and voltage characteristics, which have a known correlation with the cell status. For general use, the voltage profile of the cell can be used to estimate the cells SOC; however, temperature (Entropy) can have a significant effect on the voltage profile [42]. Lithium cells produce a variable voltage profile, based on the concentration of Lithium ions, the voltage profile for LiFePO₄ cells can be seen below.

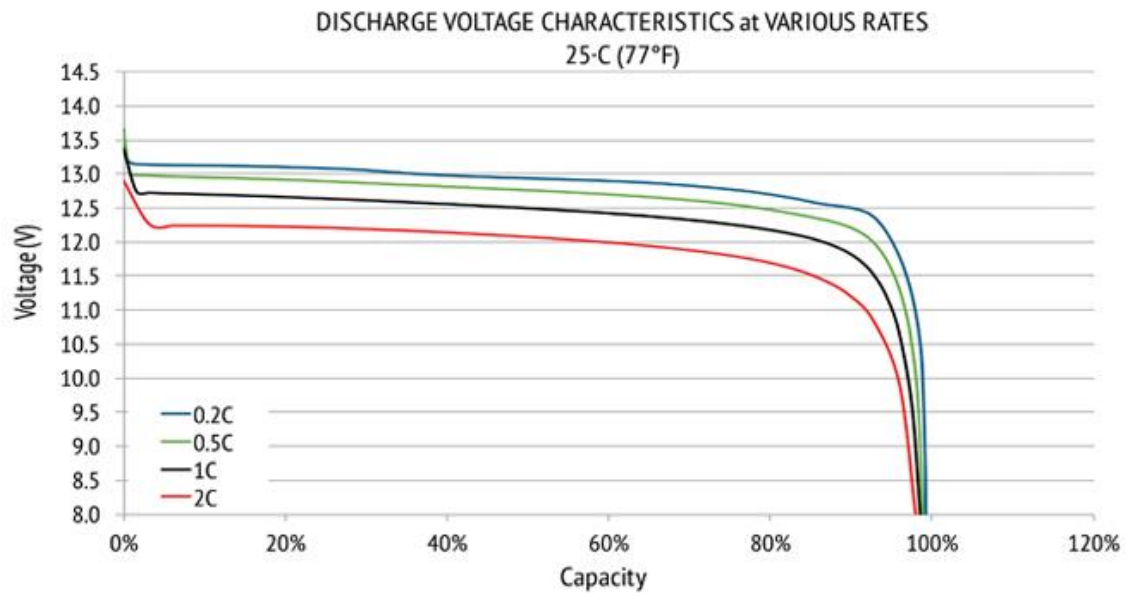


Figure 12 Discharge Voltage profile for LiFePO₄ cells, used commonly in EVs [43].

Notably, the voltage profile varies considerably due to thermal effects on the conductivity of Li⁺ through the electrolyte and redox reaction rates. In the intermediary zone, with middling Li⁺ concentrations, the voltage profile of the battery remains relatively stable, known as the equilibrium voltage [42]. Due to the variation in the battery characteristics, state of charge, is generally an estimation based on known voltage profiles for battery cells.

2.4.4 Battery Charging

Lithium ion cells, like other batteries, are prone to degradation over time, through both the charging and discharging of the cells. Both high SOC, and high charging currents have been linked to accelerating the degradation of Lithium ion cells [44]. There are two primary charging methods applied for battery cells, constant-current, and constant-voltage. Constant current charging applies a controlled, generally low, current to the cells and modulates the voltage to increase with the cell voltage. CC charging with higher currents can be used to charge Li-ion cells quickly, however, comes at a trade off with battery lifespan; whilst low charge currents exhibit a low charge rate which is typically inconvenient for EV applications. Constant voltage charging applies a constant voltage across the battery terminals and the charge current is determined by battery characteristics, such as battery voltage, and load resistance. In practice, this results in a high charge current for low cell voltages which can contribute to rapid degradation in battery cells; however, constant voltage charging enables the user to control the charge voltage, thus reducing the risk of over-charging the cells to excessive SOC [45].

An alternative charging option is often used to reduce the degradation of battery cells from both the influences of over-charging and high charge currents, Constant Current – Constant Voltage (CCCV). CCCV charging involves charging cells to a pre-set SOC using CC mode charging to reduce over-current during charging for the cells, and topping the cell up to the desired SOC utilising CV mode charging to ensure the cells are up to acceptable voltage [46]. Charge currents and voltages for various SOC levels can be seen in Figure 13 below.

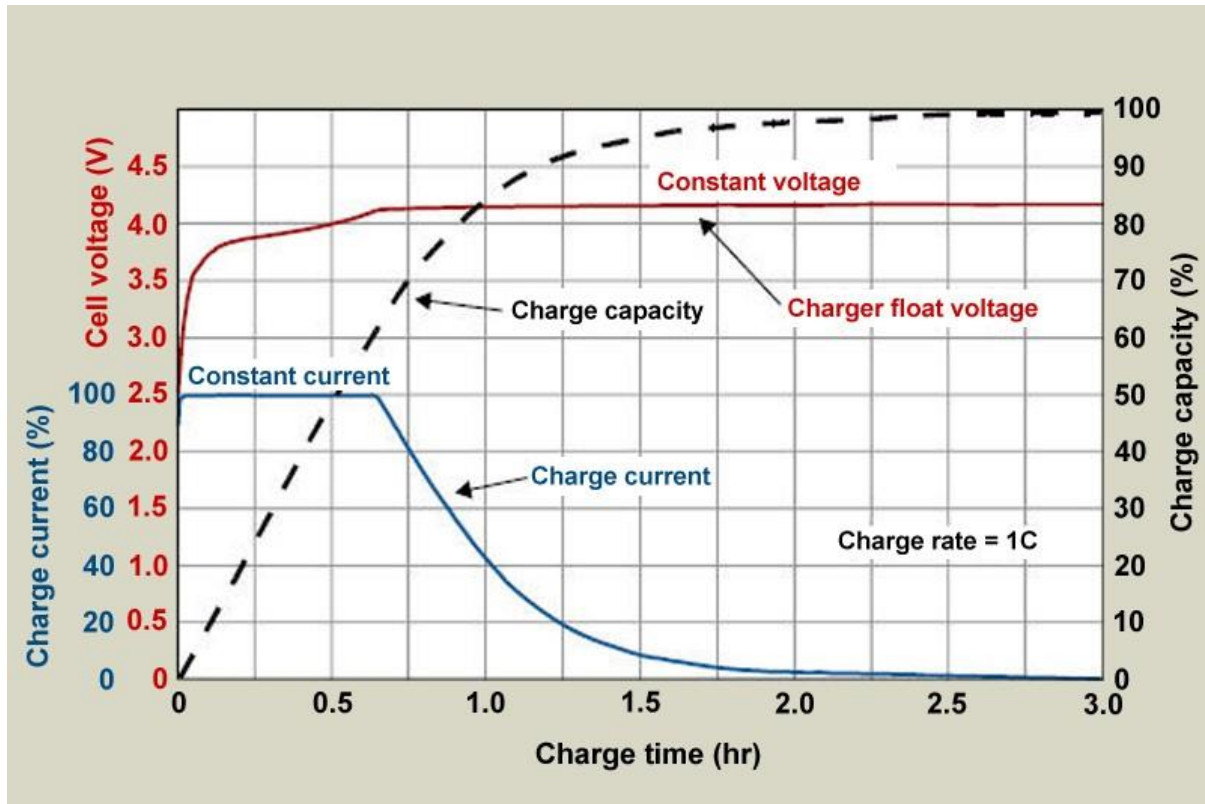


Figure 13 Charge Curve for CCCV Charge mode used in Li-Ion cells [47].

2.4.5 BMS Operation

Lithium-Ion cell voltages are typically relatively low, 3.2-4.2 V, for which reason, battery cells are often connected in series to produce a higher voltage useful for driving high-power devices at lower currents. Cells connected in a battery pack each exhibit independent cell characteristics and are prone to charge, discharging and degrading at varying rates. Battery Management Systems typically contain support for monitoring of cell characteristics, controlling connections to the cells and cell balancing. The BMS is also able to approximate the state of charge for a battery pack, based on the voltage of the cells within the pack, given a known voltage profile for the cells.

Battery Management Systems are used to monitor individual cells in a network, with thermal sensors, voltage sensors and current sensors. In series connected battery packs, current sensing is typically performed using a series connected shunt, or current transducer type sensor, to estimate the pack current. Voltage sensing is typically applied to individual cells within the network, using cell taps. When referenced to ground, the voltage of series connected cells would increase through the network, for this reason, the ADC inputs in the BMS calculate the potential difference between each cell, and the cell before it in the network to accurately determine the voltage at each cell. Utilising these known characteristics, the internal resistance of each cell can be estimated, provided there is charge movement in the battery pack [48].

BMS architecture usually contains safety features, to disengage battery cells in the event of a fault. In a fault or crash, the short-circuit current from Lithium-Ion cells can exceed 1000 A, and heat cells further damaging them. To prevent this from causing irreparable damage to the battery pack, a charge and discharge relay is typically controlled by the BMS to isolate the batteries in a fault event. Additional protection is provided by the BMS through limiting charge currents, based on estimated SOC for battery cells, to prevent heating during regenerative braking in EV applications [49].

Cell balancing in BMS devices use SOC estimations for each cell to ensure the cells in the pack are charged uniformly. There are two fundamental methods for cell balancing in Li-ion battery packs, passive and active. Passive cell balancing usually occurs through the cell taps, enabling the BMS to apply a resistive load to discharge independent cells within the pack. Typically, passive balancing occurs after charging to prevent risk of over-discharging cells through the cell balancing process and is disabled once cell voltages drop to when approximately at 80% SOC [50]. Active cell balancing usually requires additional complexity, and material cost, over passively balancing cells; however, offers the benefit of balancing cells during charge and discharge operations. The objective of active cell balancing is to charge the lower voltage cells from the overcharged cells in the system. In Li-Ion systems, this is done by connecting cells in parallel, via a bi-directional power electronic converter [51]. Power electronic converters used with active cell balancers typically have transformers which galvanically isolates the connection for each cell in the system; though alternative methods store energy from one cell in a capacitor or inductor and discharge into under-charged cells in the system [52]. It is important to not directly connect cells in battery packs, cells are often connected in series with differing terminal voltages, which makes active balancing quite challenging. Due to the complexity, cost and physical size required by active cell balancing, most battery management systems employ passive balancing techniques through the battery cell taps. A schematic for the cell-tap configuration in a typical Battery Management System can be seen in Figure 14.

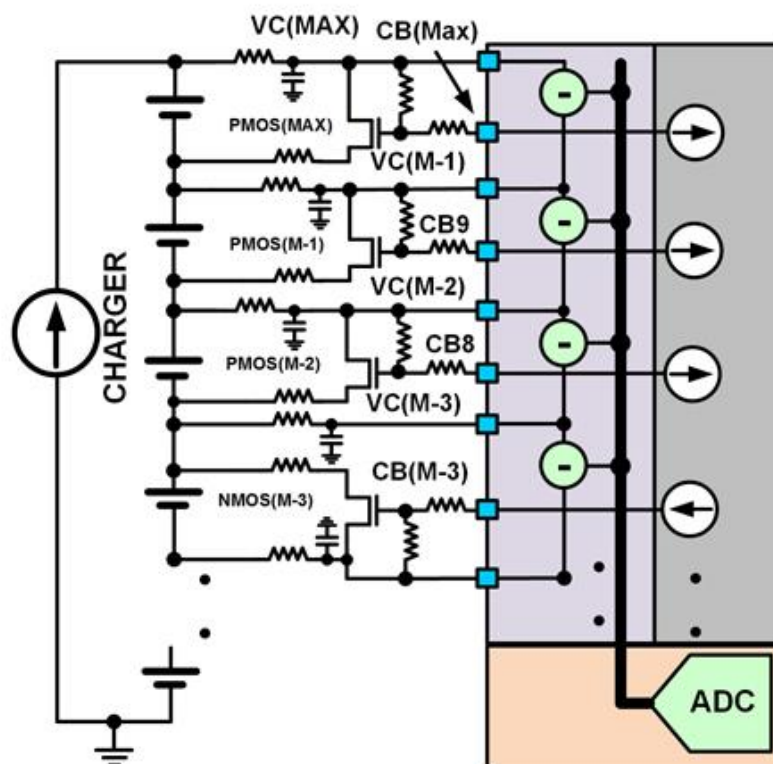


Figure 14 Cell tap schematic for typical Passive Balance Algorithm BMS [49].

BMS cell taps are wired to sense the cell voltage for each cell independently and passively balance the pack using shunt resistors on each cell. The schematic above demonstrates how passive balancing systems are wired, with BMS controlled FETs able to close a connection across a discharge resistor to bring the SOC of overcharged cells down independently. Additional protection is often added to these systems, using individual cell fusing, and Zener diodes to detect overvoltage and protect against short circuits in cell tap wiring [53].

2.5 CAN Signal Protocol

CAN bus, or Controller Area Network Bus, is a signal protocol developed for use in electronically noisy environments, like vehicles, to facilitate reliable and accurate data transmission between components. CAN typically consists of two wires connected as a differential bus pair, a grounded mesh, 'shield', is often used to surround CAN bus connections to mitigate the effects of electrical noise. The CAN signal protocol is designed to house multiple devices, or 'nodes', which are each independently 'addressed' along the bus enabling the devices to all communicate directly using CAN. The physical connection of the bus requires each device to be connected in parallel to the CAN high and CAN low differential pair, with a separation resistor of $120\ \Omega$ at each end of the bus as shown in Figure 15.

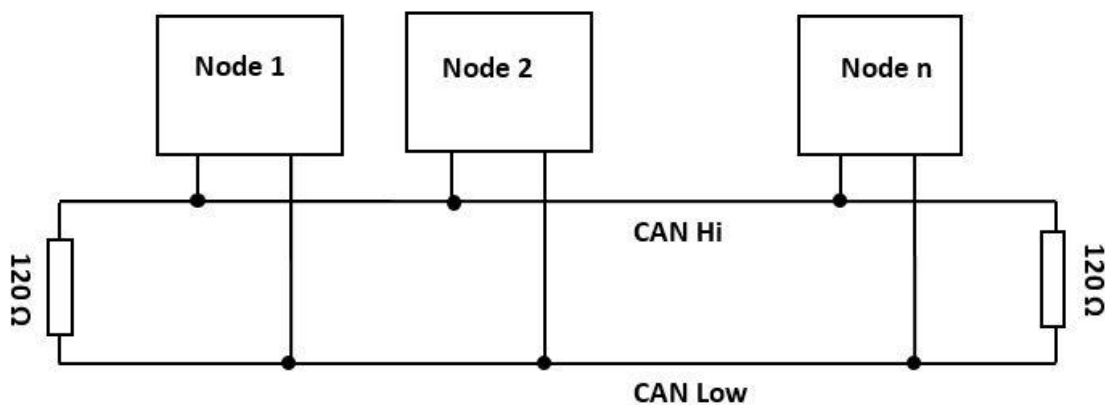


Figure 15 Wiring Schematic for CANBUS [54].

The CAN bus physical wiring is set-up for all nodes to individually access the bus to send and receive data. Data is sent as logic bits, 0 or 1, using the differential pair; during operation, when the bus voltage on both signal wires is approximately 2.5 V, it can be interpreted as a '1', whilst to send a '0' the high signal is pulled up whilst the low signal is pulled down [55]. This system provides many advantages over single signal operation, such as reducing errors in noisy environments and reliability, and extended range. The drawback however, stems from the signal speeds typically attainable in CAN bus systems when compared to other low-distance, full-duplex signal protocols.

In CAN bus systems each node has independent control over the bus, which introduces the requirement for arbitration to prevent signal clashing. During typical operation, each device is programmed to broadcast relevant data, command, and updates to other devices at timed intervals, or during specific events. The result of this, is that bus is prone to multiple devices attempting to send data simultaneously. As opposed to using master-slave operation, or specific control; each device in the network has a unique numeric identifier (usually hexadecimal representation), which also determines the priority it has over bus control, where the lowest identifier has the highest priority [56].

CAN protocols have a specific data transmission ‘frame’ which is consistent across devices that is used to identify the receiving devices and check for errors while transmitting. The signal frame consists of eight sections, to begin the data transmission, send data, check data, and signal the end of the frame. In CAN networks there is no synchronisation or clock for each frame, but rather, receiving devices continuously sample the bus to decode the message, given the clock rate for messaging in the bus is a known constant. For this reason, bit sampling can cause errors when reading information off the bus, exacerbated by noisy signal environments, giving cause for error checking in the CAN message frame [57]. Figure 16 below shows the data frame for a CAN transmission.

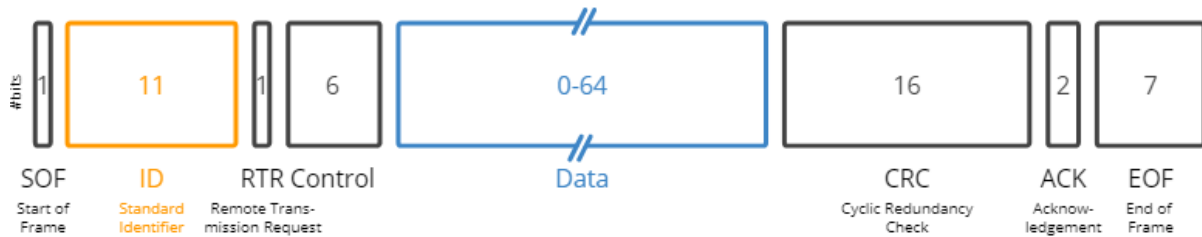


Figure 16 Standard CAN Frame [58].

The start of frame bit is a single bit for the node transmitting to pull the bus to a logic ‘0’ to signal to other nodes that the device intends to send data. During the ID phase, the device transmits its own identifier, which is when collision detection occurs; the ID is transmit in bits with the MSB sent first, as the ‘0’ bit is dominant, the first node to transmit ‘1’ and detect the bus is occupied will stop transmitting, this translates to priority being assigned to the node with the lowest numeric identifier. The RTR, or remote transmission request, is a single bit sent to determine whether the node intends to send or receive data. The control bits send information regarding the length of the data transmission, signalling between 1 and 8 bytes. The remaining tasks are to ensure that the data has been retrieved correctly by the receiving node. The cyclic redundancy check uses a mathematical outcome for a polynomial using the data as input variables which is calculated by the transmitting node, and the receiving node can verify the data integrity by ensuring that the outcome of this polynomial is identical to the transmit value in the CRC [59]. If this is the case, the receiving node can acknowledge that the data has been received correctly, and the end of frame is signalled by a wait period of 7 ‘1’ bits, if a ‘0’ occurs during the EOF, the message will be repeated [60].

2.6 UART Signal Protocol

UART is an asynchronous serial communication protocol which is often used to communicate between devices, that in its simplest form uses three connections between devices. Unlike CAN, UART is limited to communication between two devices that are directly connected using Tx, Rx and GND connections. Tx and Rx, transmit and receive pins, for each device is connected to the opposing connection on each device enabling full duplex communication.

UART messages resemble the format of CAN, however, only consists of four sections. UART begins with a start bit, followed by a single byte of data, a checking ‘parity’ bit and 2 stop bits. As the data length is consistent with UART, and the transmit and receive pins are distinct, the control required is notably less sophisticated than larger networks. UART devices create a data frame in a buffer prior to sending data, which consists of a start bit, the message, a parity bit, and a stop bit. In UART, the start bit is ‘0’ which grounds the bus signalling the receiver that message is about to be transmit. Following this, the data is sent with a parity bit followed by one or two ‘1’ stop bits, which restore the bus to a higher voltage level when not in use.

In UART, a parity bit is used to identify if any errors occurred in the transmission; the parity bit has two possible states, '0' which indicates even parity, or '1' which indicates odd parity. The parity bit is determined by summing the number of '1' bits sent in a transmission, with even parity the number is even and with odd parity the number is odd. If the parity sent by the transmitter doesn't match the parity calculated by the receiver, the receiver knows that the received data is changed.

Chapter 3: HiCEV Systems and Modifications

Modifications were made to HiCEV's electrical and mechanical systems based on the requirements for the project, and the existing vehicle components. Prior to modifications, the vehicle was set up for EVCM control of a variety of sub-systems. This involved including the EVCM to drive various signals between the inverter, BMS, HV and LV distribution boxes. The EVCM control added to the complexity of hardware in HiCEV, as it enabled multi-stage ignition for the motor controller, and independent switching for vehicle peripherals.

The EVCM enabled independent control of sub-systems, including 12 V peripherals, increasing the complexity of the vehicle wiring. Though more efficient, controlling each sub-system meant independently relay controlling the cooling systems for various peripherals, which was performed by the '12 V distribution box'. The EVCM also monitored vehicle systems, via CAN, and reported to cab mounted displays to communicate with the driver, control the inverter, and monitor the vehicle to ensure safe operation.

The EVCM unfortunately experienced faults throughout the project's lifespan, notably the pre-charge for the inverter, for which the EVCM was no longer usable. Though fundamentally, this problem could be readily dealt with via output pin reconfiguration, due to programming software licensing costs, it was simply unachievable to reconfigure the EVCM. Several attempts were made at identifying to the EVCM that the vehicle was operating as intended, however, failures meant that the EVCM start-up process would not complete, rendering the vehicle non-operational.

The pre-modified vehicle also had several disconnected modules, notably the inverter, as well as several different components, most considerably the air-cooled DC/DC converter. The re-installation of several components as well as the integration and testing of new components make up a considerable portion of the changes to the HiCEV design. Though modules within the vehicle typically perform the same functions they did prior to modifications, the components within each module have largely been updated, re-wired, and re-mounted to better suit the specific requirements of HiCEV. The removal of the EVCM most notably meant that controlling various vehicle features moved from EVCM control, to BMS, Inverter, Charger and Ignition control via relays powering various stages and peripherals to the vehicle. In practise, this sums to a large reconfiguration to the vehicle systems for the most part requiring the vehicle to be rewired.

HiCEV operates on a modular design, using off-the-shelf components and integrations to perform required functionality. The primary components of the vehicle include the Inverter, BMS, Motor, and Charger, which are integrated through the 'Power Distribution Box', 'High Voltage Box', LV systems, and the communications connections. Previously, these were integrated using an EV control module, however, due to faults the EVCM was discarded from the vehicle, and the integrations it had with the vehicle had to be re-evaluated. The EVCM was used for motor control, vehicle start-up checks, monitoring systems, and independently controlling vehicle sub-systems. This was solved by utilising the built-in control and vehicle peripheral monitoring within the Inverter hardware, however, some functionality had to be removed. A revised block-diagram for the systems in the HiCEV can be seen in Figure 17.

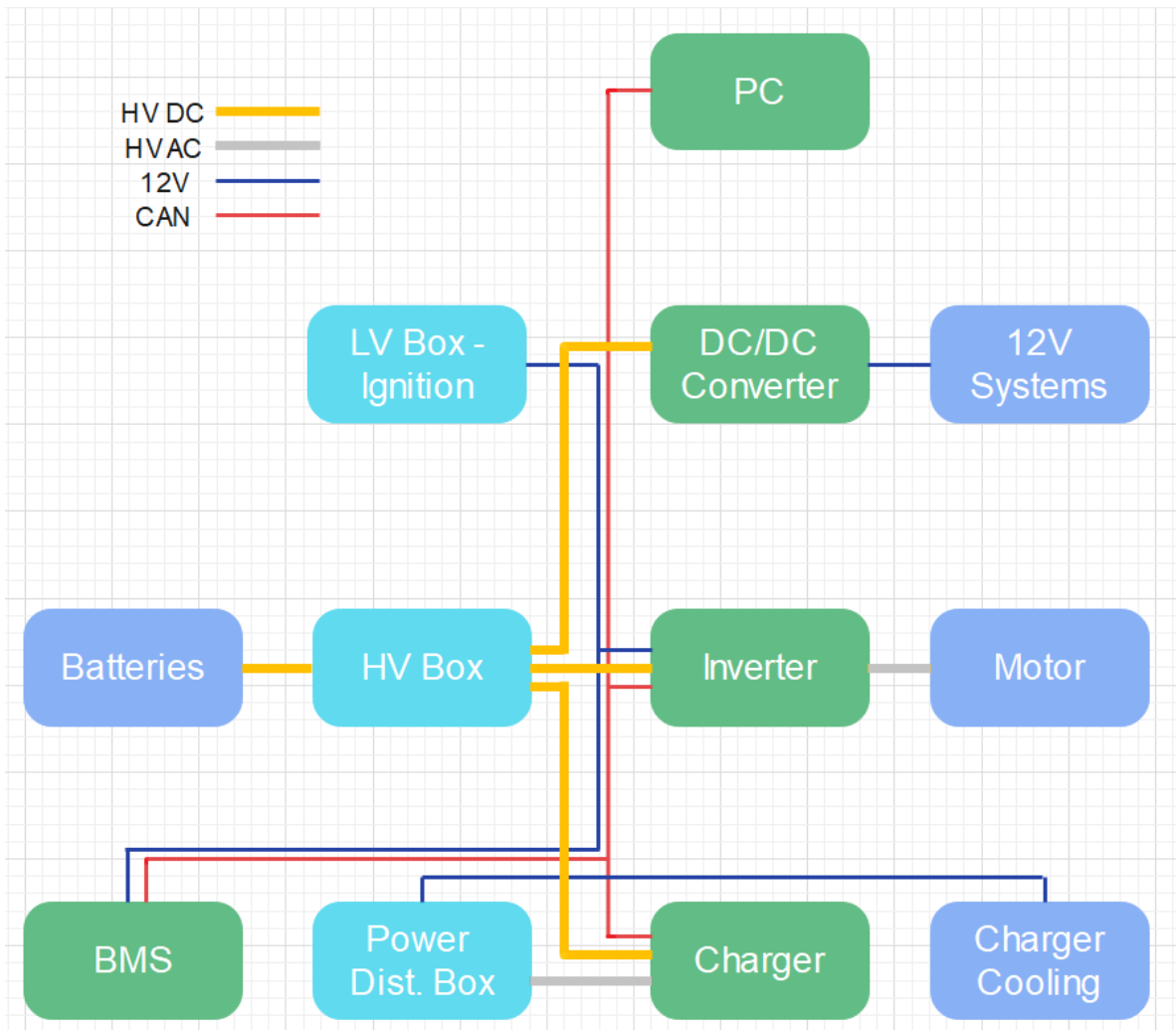


Figure 17 Electrical Block Diagram for HiCEV

HiCEV also has various monitoring, signal, safety, and control connections which link the components to provide complete functionality to the vehicle.

The integration of components on the HiCEV is largely done through the CAN Bus, Ignition systems and communication via Digital I/O ports. A parts list for the off-the-shelf components in the HiCEV can be seen in Table 2 below, which describes fundamental role of each of these parts.

Table 2 Vehicle Components

Component	Function
Cascadia Motion Systems PM150DX Inverter	Power Electronic Driver for motor control; software controller for vehicle, and integration with vehicle peripherals.
Orion BMS	Monitors Battery Pack, and communicates directly with the charger and inverter to maintain safe SOC, temp and cell health.
Remy HVH250-115	PMAC Motor.
Current Ways 3 kW liquid-cooled Charger	Charges main battery pack at 6 A, and drives cooling systems when vehicle powered down.
Sevcon DC/DC Converter	Provides Power for 12 V systems from the main DC Bus, charges backup 12 V battery.

3.1 Inverter

The inverter in the HiCEV is a Cascadia Motion Systems PM150DX, which provides the functionality of vehicle controller, motor controller and motor driver. The PM150DX is a 150 kW inverter, designed to integrate with the core components of the vehicle to provide functional control to the motor, using traditional and existing vehicle components.

The PM150DX consists of two signal connection headers which interface with vehicle control peripherals to perform motor control. The motor also interfaces with the inverter through HV connections to the inverter, resolver, and temperature sensing. The inverter requires some support circuitry, which is largely housed by the HV box, and Ignition systems, however, notably also interfaces directly with acceleration potentiometer and the brake switch, from the brake lights. A schematic of inverter connections is shown in Figure 18 below.

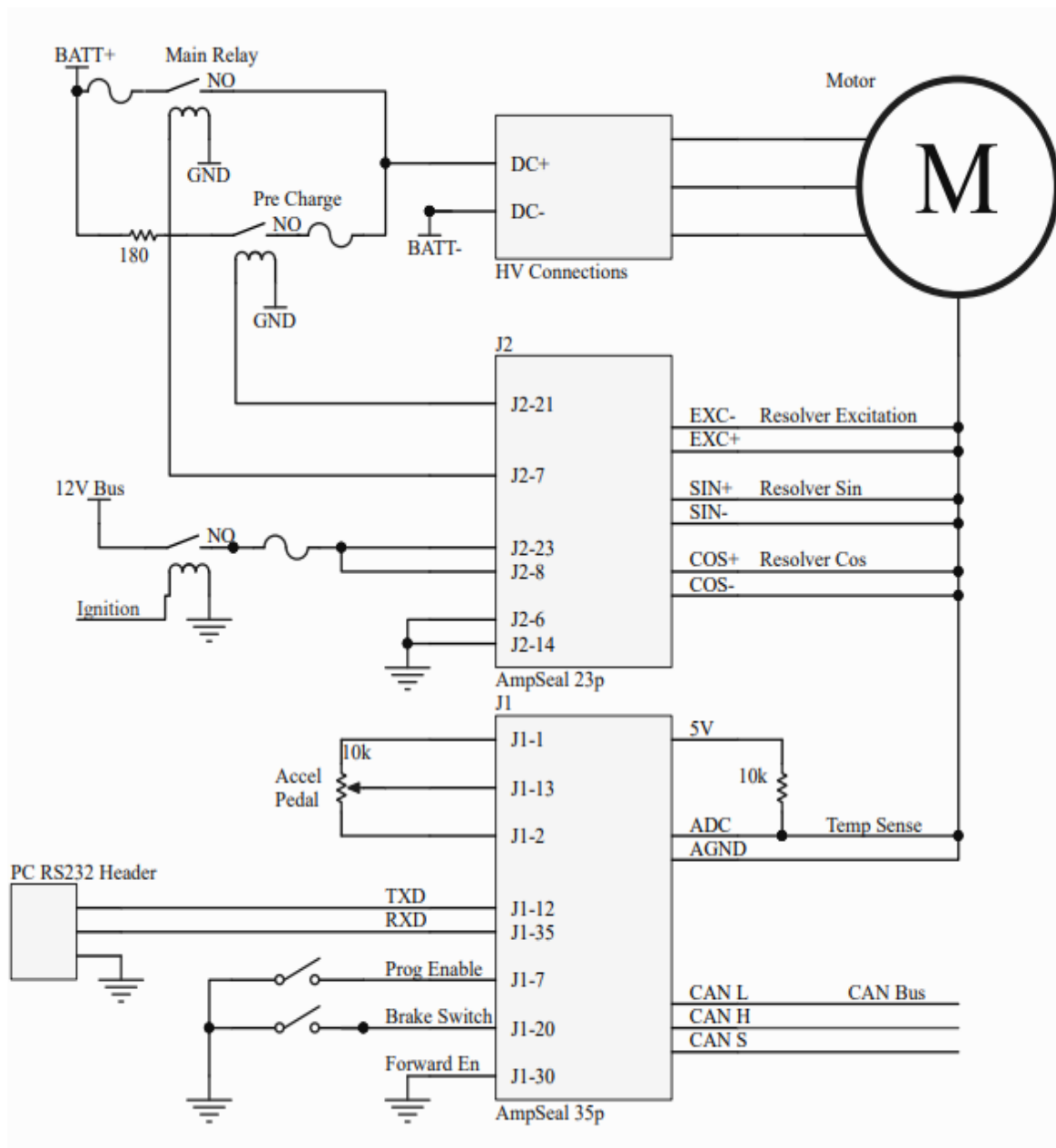


Figure 18 Inverter Schematic.

The schematic displayed in figure 18 resembles the recommended operation for the inverter, which was modified due to the specific requirements of HiCEV. The connections to the inverter can be categorised into HV, communications and programming, and vehicle interfacing. The inverter also features built-in control software, fault detection, and internal monitoring; inclusive of bus voltage, DC current, and temperatures.

The HV wiring for the inverter is connected through the HV box, which houses the main bus, and pre-charge relay. As a high-power device, the inverter is susceptible to voltage ripple on the main bus; this voltage interference can stem from high-frequency switching currents, sudden loading of batteries from internal or external sources, or changing torque loading of the motor. For this reason, the inverter has a large DC bus decoupling capacitor which smooths the HV bus voltage ripple by storing and discharging energy through transient currents. Charging the bus capacitor directly from the battery pack, a non-current limited source, can create large peak inrush currents due to minimal series resistance. The theoretical maximum inrush current, can be modelled by equation 11.

$$I = C \frac{\Delta V}{\Delta t} \quad (11)$$

The internal bus capacitor on the PM150DX is an 880 μF , 800 V DC, rated capacitor, in the HiCEV operated at approximately 360 V during nominal battery conditions. To reduce the inrush current, a pre-charge bypass is installed on the main bus, which routes the main battery supply through a resistor and an independent 10 A fuse. This pre-charge resistor increases the effective time constant, RC , for the bus capacitor, thus reducing the $\frac{\Delta V}{\Delta t}$ product and limiting the peak inrush current during start-up. In the HiCEV, a 600 Ω resistor is used, which gives a theoretical time constant of 0.528 s, and a charge time of approximately 2.6 seconds.

The pre-charge and main bus relays are controlled by inverter software, notably, using high-side relay drivers. High-side relay drivers are used in this case, for the safety benefits offered in fault conditions; with a high side driver, the connected state for the relay is that the high side must be energised for the relay to switch state. In an EV, this is beneficial, as faults, or crashes, resulting in cable damage could potentially ground a connection to the chassis, with a low-side driver, a connection may remain grounded after a crash, thus leaving the main bus connected after such an incident.

The inverter formerly used CAN messaging to communicate and receive motor control commands from the EVCM. However, the option to operate using its own motor control replaces this with a requirement to communicate with the BMS for cell information during operation. The inverter has a built in CAN protocol designed to receive specific battery cell information from the BMS, namely, the maximum charge and discharge current limits. These parameters are used in motor control, notably, lower discharge current limits will cause the control to scale the peak torque available from the accelerator accordingly; and, reduced charge current limits will scale the regenerative braking to prevent overheating battery cells. The BMS determines the discharge current limit (DCL) and charge current limit (CCL) based on programmed values, however, risk factors, such as exceedingly high or low bus voltage, high cell resistance, or temperature, will cause these current limits to be reduced due to built-in BMS control.

RS232 is also used by the inverter to communicate with a PC which is used for programming the inverter, and real time retrieval of operating information. The PM150DX utilises EEPROM memory which contains software and controller information that can be re-programmed using the Cascadia Motion Systems GUI. The EEPROM view in the GUI, displays variables and their programmed states, some being discrete Boolean variables, whilst others represent particular operating conditions such as accelerator voltage, or, quadrature current. Because of this set up, the inverter’s additional functionality is largely determined by specific pre-programmed states from the manufacturer, which limits its flexibility when compared to the EVC. A table of relevant programmed states, for the operation of HiCEV can be seen in Table 3. Many EEPROM values have been updated to account for specific hardware in HiCEV.

Table 3 Inverter EEPROM programmed variables.

Variable	Value	Functionality
Key_Switch_Mode_EEPROM	0	Provides a simple On/Off operation when power is applied to the ignition inputs.
IQ_Limit_EEPROM ID_Limit_EEPROM	4250 (425 A)	Limits the peak I_D and I_Q commands to 410 A, based on motor, and battery, specifications.
Motor_Torque_Limit_EEPROM	3300 (330 Nm)	Sets the maximum torque that can be commanded by the controller while operating.
Regen_Torque_Limit_EEPROM	400 (40 Nm)	Sets the maximum regenerative braking torque that can be applied while ‘coasting’.
Torque_Rate_Limit_EEPROM	50 (5 Nm/s)	Limits the rate at which Torque Commands can be adjusted for regenerative braking.
Brake_Mode_EEPROM	0	Switch Mode, as opposed to using a potentiometer.
Regen_Ramp_Rate_EEPROM	2000 (2 s)	This limits the rate at which regen braking torque is applied to smooth braking.
Pedal_Lo_EEPROM Pedal_Hi_EEPROM	80 400 (0.8 – 4 V)	Sets the Min and Max voltage for the accel pedal.
Accel_Min_EEPROM Accel_Max_EEPROM	115 368 (1.15 – 3.68 V)	Sets the Min and Max voltage, at which the control starts to register torque command, to provide a buffer for noise.
Coast_Lo_EEPROM Coast_Hi_EEPROM	130 140 (1.3-1.4 V)	Sets a range, where 0 Torque is commanded from the controller, below the min point regenerative braking is enabled.
Kp_Torque_EEPROM Ki_Torque_EEPROM Kd_Torque_EEPROM	100 4 0	PID Controller gains to modify vehicle control.

The software also accounts for how the various features of the inverter interface with the peripheral and hardware components of the vehicle. HiCEV peripherals are calibrated with the inverter to enable proper operation and drivability. Notably, the control logic, associated with relays, switches, and inputs, like the braking, forward enable, and accelerator pedal. Forward and reverse enable systems in HiCEV are unique due to the manual transmission. As the gearbox has a reverse gear, the reverse enable is not used and instead uses the internal pull-up resistor to ensure it is not enabled, whilst similarly, the forward enable switch is shorted to ground such that the motor is always in forward operation.

The acceleration input has also been configured to move the vehicle into coast mode when the driver stops accelerating. This essentially, automatically applies regenerative braking, based on the voltage input from the accelerator potentiometer. The implementation for this feature has been programmed to resemble ‘engine braking’ in ICE vehicles, providing minor braking capability which is notably larger in lower gears than it is in higher gears. The set up for coasting on the accelerator pedal can be seen in Figure 19 below [21]; from which, you can see that the inverter is programmed to regenerate up to 40 Nm during low pedal voltages, and has a small ‘dead zone’ where the pedal voltage requests 0 Torque. In practice, this voltage range has been chosen to be a small value in HiCEV, such that the vehicle regeneratively brakes only when the pedal is completely released.

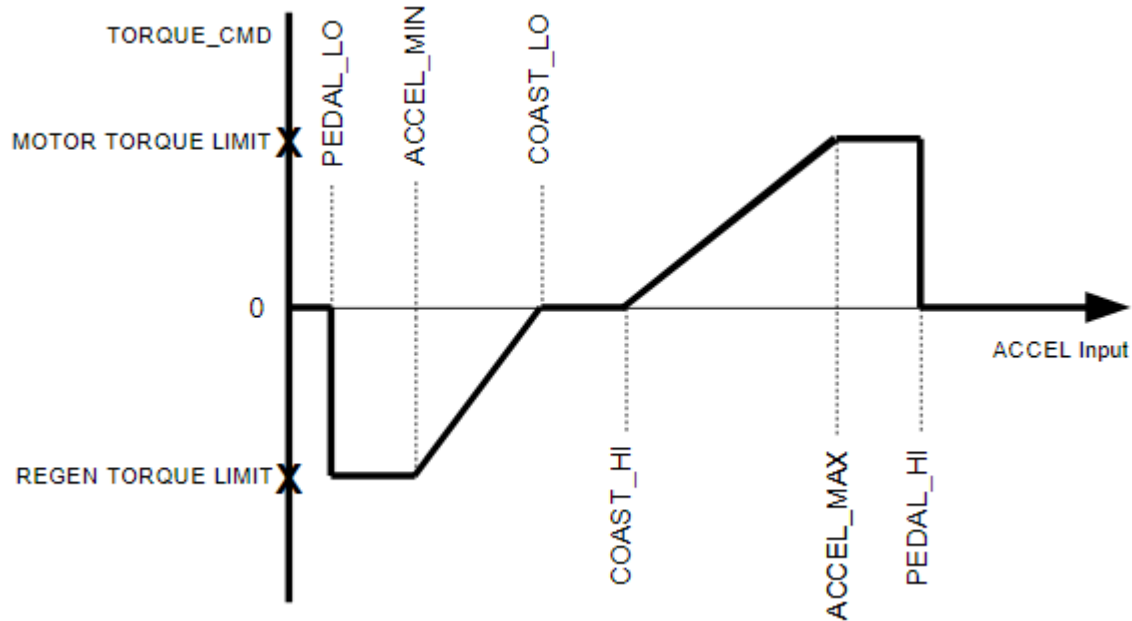


Figure 19 Acceleration Pedal Configuration [21].

The inverter also has data acquisition modes enabled for retrieving real time information on the operation characteristics using the RS232 port. This is performed using SCI data acquisition, through serial capture software on a PC. This data is broadcast as 20 columns of 32-bit data (4 bytes), where ASCII symbols representing hexadecimal values are broadcast to the PC. Though the data acquisition is in real-time, the drawbacks of this method stem from susceptibility to noise on the RS232 connection, inability to interpret data in real time, and data processing required to view the results. For this purpose, a program in python has been produced by the author to quickly import the table of data into data-frame, and graphically represent real values, this program has been captured in Appendix 1. Due to the formatting of the data, and noise errors, substantial data cleansing is required. A table representing the data points retrieved through SCI can be seen in Appendix 2. Notably, in the inverter software the SCI transmission is given low-priority which results in inconsistent time intervals between data-points, using reported timing values, the power on time for the inverter can be extrapolated.

3.2 Battery Management System

The battery management system in the HiCEV is an Orion BMS, with 108 Cell taps to independently monitor each of the 108 Winston LYP100AHA cells. The BMS interfaces directly with both the HV and Power distribution boxes to control charge and discharge on the main HV bus. Cell monitoring is performed through a series connected current sensor, independent voltage, and resistance characterisation through cell taps.

The battery pack in the HiCEV consists of 108 Winston 100 Ah LiFePO₄ cells, in a series connected arrangement. Each cell has a nominal voltage of 3.2 V, with a range from 2.5 – 4.2 V, which gives the battery pack a nominal voltage of approximately 350 V, and a peak voltage of upwards of 450 V. These cells also offer many benefits, through their low self-discharge rate or less than 1% SOC monthly; which makes it easy to maintain charge stability across the battery pack through long periods in storage, and reduces the risk of reaching high depth of discharge (DOD), which is harmful for the longevity of cells. Additional benefits of LiFePO₄ battery chemistry used in the Winston battery cells is the rated 5000 charge cycles, provided DOD doesn't exceed 80%, which assuming daily usage would enable over 10 years of charge cycles before battery cells need replacing due to excessive degradation [37].

The BMS interfaces with both the charger and all vehicle loads through the use of the discharge enable and charger safety signal. These signals drive relays which physically isolate the connections to the HV bus; in HiCEV, this is used to provide a charger interlock function. When the charger is plugged in, the BMS has an input to the ready charge, which remains active, when the charger has completed the charger cycle. Similarly, when powered on, the BMS receives power from the ready power pin, and is thus able to monitor both conditions. When the charger is plugged in, attempting to start-up the vehicle will fail as the discharge enable will prevent any load from being connected to the cells. Because the BMS receives power on the first stage of ignition, when all accessories turn on, it is worth noting that the BMS may trigger this interlock without any physical sign of the vehicle being active. This concern is especially prominent as the switch requires a button press to fully disengage the accessories, a step which is easy to forget.

The BMS interfaces directly with the inverter, PC, and charger using the CAN protocol during operation. CAN interface is used for programming, charge control, and real-time updates for the inverter. In addition to this, the BMS interfaces with cell sensors, ignition, power distribution box, and the high-voltage box. The BMS also controls much of the start-up procedure, A schematic for BMS control circuitry can be seen in Figure 20.

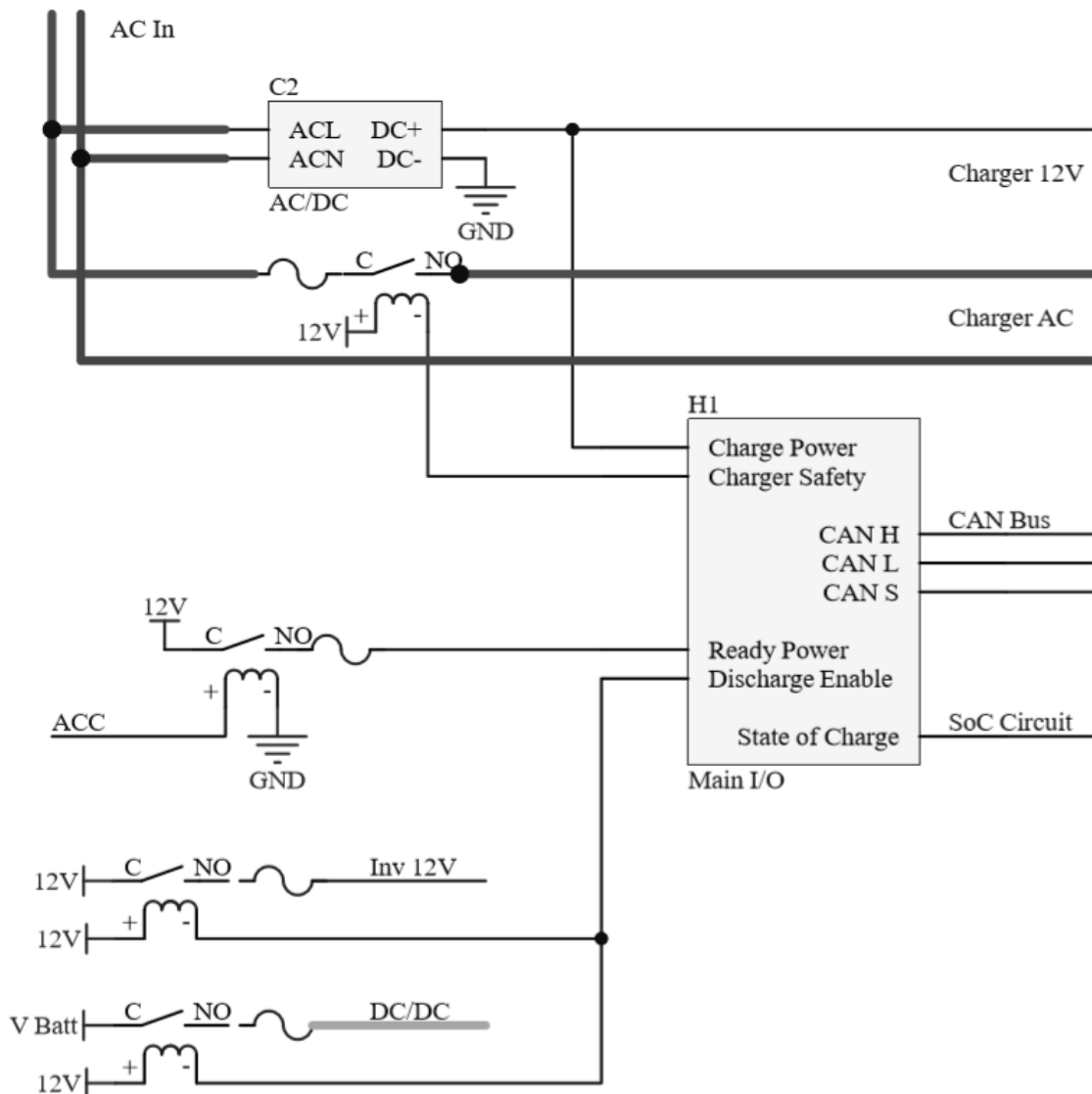


Figure 20 BMS Main I/O Schematic

The BMS plays a major role in the “ignition” systems for the vehicle in the absence of the EVCM. With the replacement of many of the core functions of the vehicle going to the inverter, the additional functionality of the EVCM was lost. A considerable component of this was peripheral control, and the start-up procedures. With the EVCM, the BMS operated off an ‘Always-on Power’, such that the BMS was monitoring cells while the rest of the vehicle was switched off and able to immediately communicate with the EVCM upon powering up. With this removed, the BMS is the first device which is powered on for both charging and discharging as it functions as a controller for HiCEV’s most volatile component. Operationally, the power supply for the BMS comes from two separate sources, depending on the function; for charging, an AC/DC converter is used to power the ‘Charge Power’ on the BMS, whilst during discharge, the ‘Discharge Power’ is battery connected through the ignition system. Internally, the BMS has a charge interlock, which prevents both charge and discharge from being simultaneously active, which it controls through relays able to cut power from the charger in the Power Distribution box, or cut all loads, by turning of the inverter power supply, and the DC/DC Power supply. The switching order for start-up requires that the BMS discharge enable is active before the Inverter can perform pre-charge and thus start the vehicle. This causes a noticeable, but slight, delay when starting the vehicle, however, ensures driver and hardware safety.

With the EVCM removed, the BMS utilises internal safety checks to determine the peak discharge and charge currents for the cells, and uses this to drive relays to disengage cell connections. The drawback for this method of cell monitoring is that the BMS is generally inactive whilst the vehicle is neither charging, or discharging, which limits its ability to maintain the balance of cells and monitor potential faults. The 'always-on power' is still available, though unnecessary, to the BMS through the 12 V battery at the rear of HiCEV; however, leaving this in long term storage would deplete the 12 V lead-acid battery which would prevent the vehicle from operating when required. The state of charge for the battery pack is an estimated figure, taken from battery measurements, primarily temperature and voltage; as temperature can cause SOC estimations in LiFePO₄ cells to drift by up to 50% [61]. The I/O pin for this figure, is a 0-5 V analogue representation of the SOC from 0 to 100%, which can be used with external circuitry to create a 'fuel gauge' for the vehicle.

The Orion BMS has 108 cell taps independently providing passive monitoring and cell balancing to the battery pack. Each cell connection consists of a fused input, which uses a zener diode for reverse polarity and over-voltage protection. The cell voltage is also monitored by an ADC which is referenced to the cell voltage of the previous cell in the series connected pack. The BMS also uses digital output to drive a switch, which when conducting, bypasses the battery cell, discharging the cell through a 'shunt' resistor to balance the cell SOC with the rest of the pack. A schematic for this can be seen in Figure 21 below.

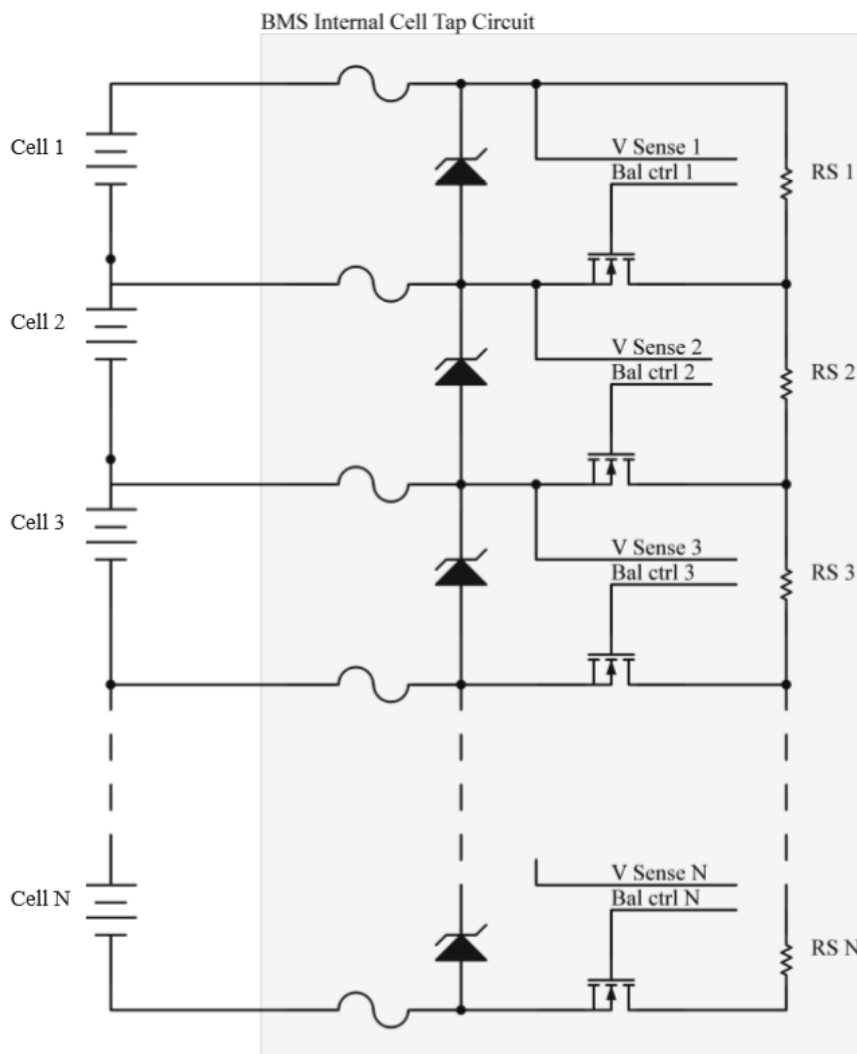


Figure 21 BMS Cell Tap Internal Schematic.

The Orion BMS system uses passive balancing, as opposed to active balancing due in part to the simplicity of the systems required, and the cost reduction which goes along with this. The shunt resistors are sized to dissipate up to 200 mW per cell, when the battery pack is in a high SOC. This works off a fundamental component of Li-Ion cells, that they typically exhibit similar, very small (μA), self-discharge rates and remain relatively balanced when left in storage. Consequently, once balanced, a pack can sustain relatively low SOC differences when left in storage or throughout the discharge cycle. The Fuses in this system are designed to operate as a failsafe, to protect the internal BMS in the event of a fault, or incorrect wiring; however, as the fusing is internal and non-resettable, the system requires servicing if a cell is connected incorrectly.

The BMS is also configured to use CAN to communicate with both the inverter and the charger during operation. Communication with the inverter is limited to current limits which are in the interest of cell health, based on the depth of discharge and temperature of the cells. Similarly, the BMS monitors the SOC for the battery pack, and reports a maximum charge current limit, and pack voltage to the charger. This maximum CCL is used to integrate CCCV charging as the BMS de-rates the current and increases the charge voltage at higher SOC.

3.3 Motor

The HiCEV uses a Remy HVH250-115, which is a PMAC type motor, driven by the Cascadia PM150DX, specifically designed to be integrated into EVs. The motor consists of 3-phase HV windings surrounding a rotor with permanent magnet, and contains its own thermistor and resolver to communicate control information with the inverter. These connections integrate directly with the Inverter via high-current, HV leads, and through a smaller signal connection which drives the resolver and temperature sensors.

The signal header on the motor facilitates both the resolver and temperature sensing of the motor. As these sensors are mounted near the motor, with high switching currents, they are highly susceptible to noise. Considerations have been made, however, difficult to implement, to reduce the magnitude of these issues. Examples of such considerations include, the use of shielded HV cable, placement of HV cable away from signal connectors, and use of twisted pairs on resolver connections. Shielding the HV cable reduces the electromagnetic noise emitted from the high current cabling. Despite this, at high currents the motors signal cables, which are in close proximity, are highly susceptible to this noise. For this reason, signal connections to the resolver and thermistor utilise twisted pairs, and are routed separately to the HV leads to reduce the effects of crosstalk.

The HVH250 is a PMAC type motor and can be operated at a variety of voltage levels to produce unique torque and power characteristics. The torque and power characteristics for the Remy HVH250 can be seen in Figure 22 and Figure 23 below.

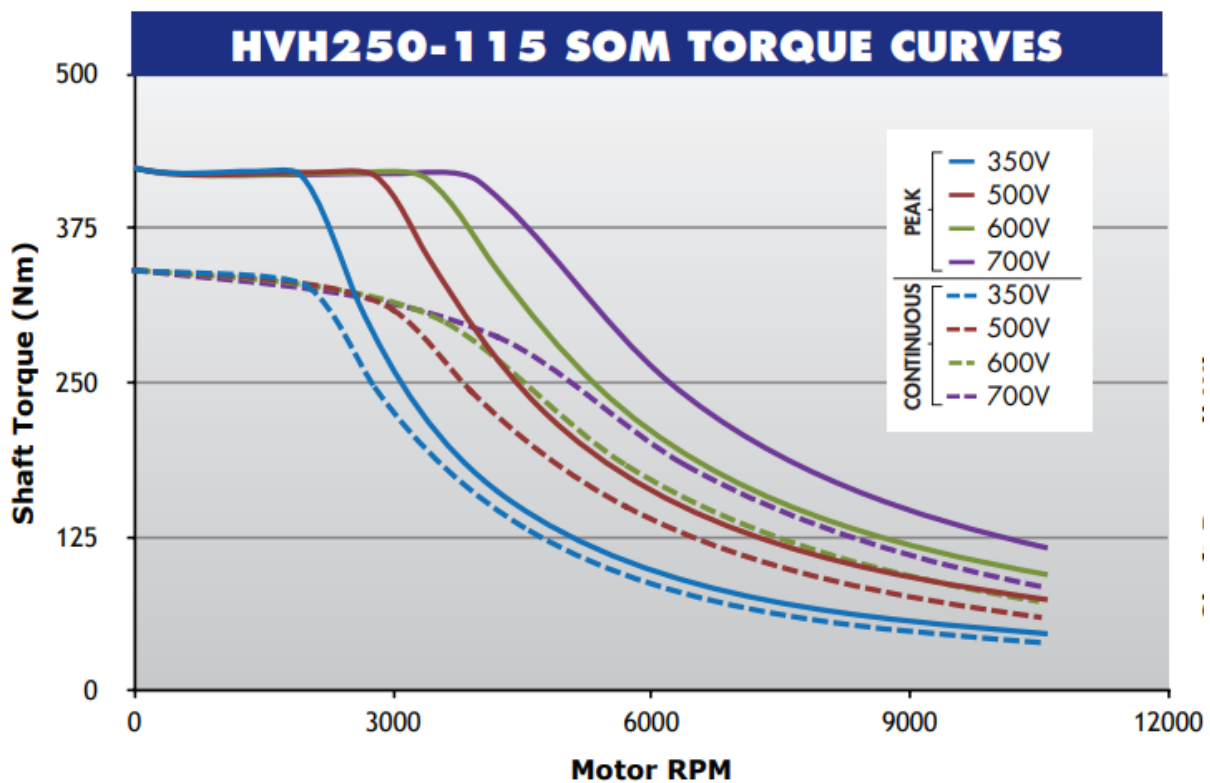


Figure 22 Torque-Speed Curve Remy HVH-115 [62].

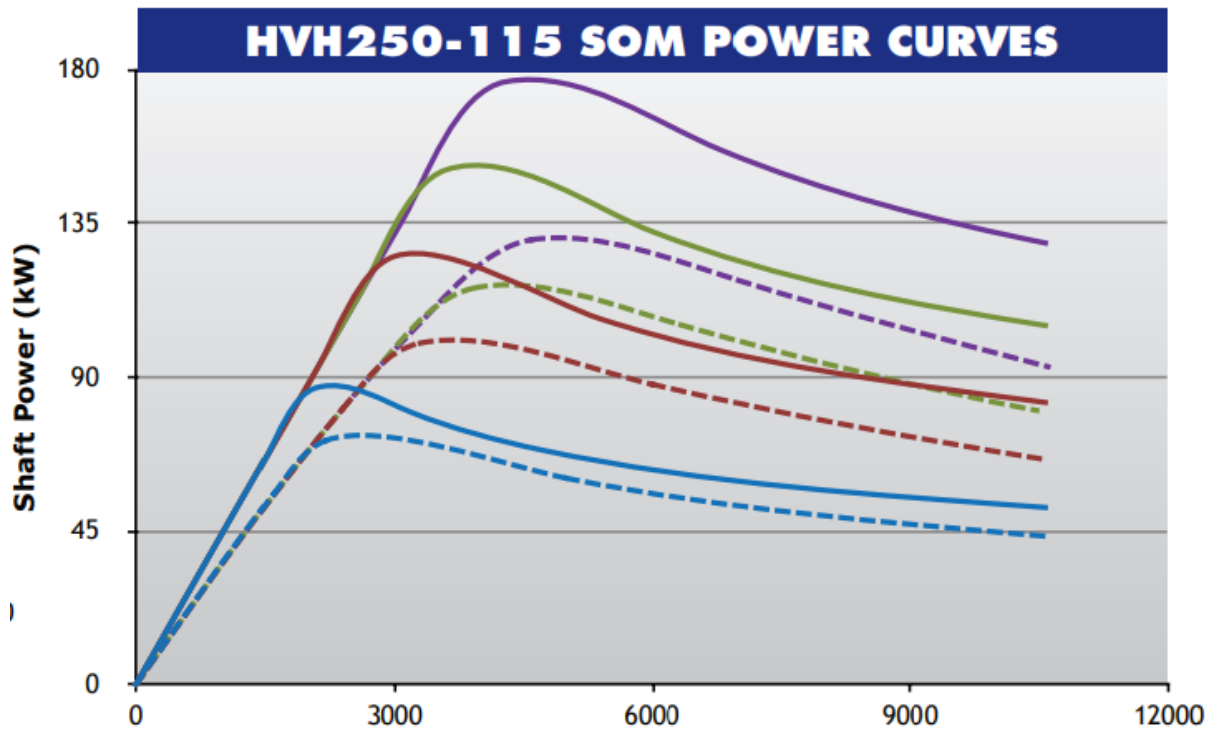


Figure 23 Power-Speed Curve Remy HVH-115 [62].

The HVH250 operational characteristics vary based on the voltage applied to the motor; wherein, HiCEV operates at approximately 360 V, depending on the level of charge within the pack. The effect of this operating voltage is twofold. The lower operating voltage means that the constant torque region is reduced due the magnitude of the back-EMF exceeding the supply voltage at a lower operating speed. Consequently, the peak voltage current product, or electrical power, is reduced based on this supply voltage constraint. For this reason, HiCEV's operating power is unlikely to exceed 115 kW based on the peak pack voltage of 380V. However, due to the battery voltage characteristics, it is also likely that the HV bus will operate at a lower level under heavy loading, reducing the overall power output even further. HiCEV exploits these operating characteristics by pairing the motor with a weaker rated, 150 kW inverter.

3.4 Charger

As an EV conversion, HiCEV uses an off-the-shelf charger, which enables it to be charged via any standard AC socket. Though this provides the benefits of versatility, it comes at a cost of charge times, as the off-the-shelf unit has limitations in the charging rate, due to its small physical size. The charger in HiCEV, is a CurrentWays 3 kW liquid-cooled unit, which is a CAN controlled device that works directly with the Orion BMS for charge control. The charger also utilises its own separate 12 V supply, which is used to drive HiCEV's cooling components. A basic schematic illustrating how the charger integrates with HiCEV can be seen in Figure 24 below.

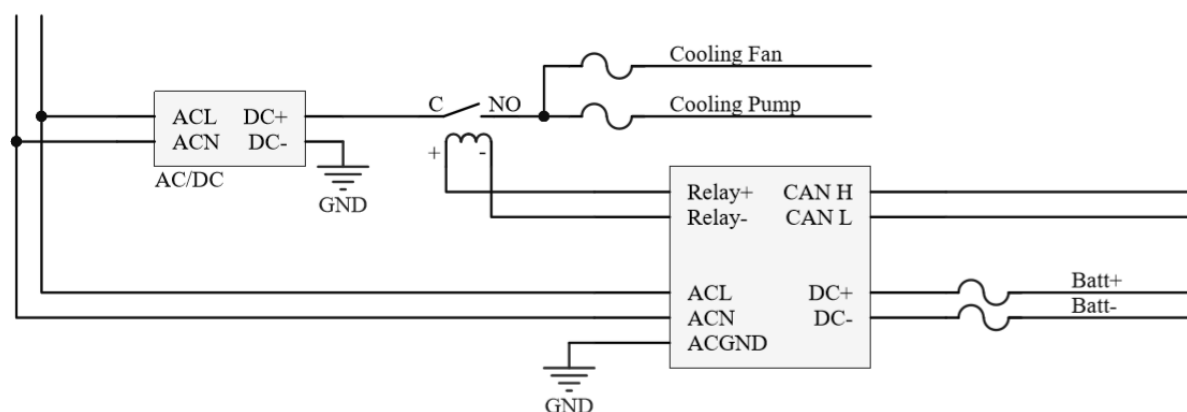


Figure 24 Charger Schematic.

When HiCEV is charging, the main ignition and accessories are switched off, which is why a separate 12 V supply is added via an AC/DC converter. The charger, has been configured to operate its own cooling systems independently, however, the relay control lines are only capable of sourcing up to 200 mA. The cooling pump and fan, are therefore required to be power on from the AC/DC converter to operate correctly while the vehicle is charging. The control of the pump and fan is left to the charger, which automatically switches the relay on when internal temperatures exceed 40 °C.

The charger is controlled by the BMS, which communicates charge current limits as the pack SOC increases. During a typical charge cycle, the battery charge current limits will only be reduced at very high SOC as the peak current supplied by the charger is already particularly low compared with the charge current the cells are compatible with. The typical charge current of approximately 8 A is a limiting factor on the charge time for HiCEV; assuming a typical DoD of 80%, and the pack operates with its nominal 100 Ah, the typical time to charge the vehicle is up to 10 hours. Though this would enable the user to perform overnight charging and use the vehicle during the day, it may pose potential inconveniences for further uses. The consequence of this means of charge control is that until high SOC, the charger typically operates with a constant-power, method of control, which is functionally similar to constant-current; however, current is reduced slightly as cell voltages increase.

The BMS estimates charge and discharge current limits, based on temperature and state of charge profiles. Figure 25 shows the profile which is programmed into the BMS to estimate the state of charge, based on the voltage of the cells.

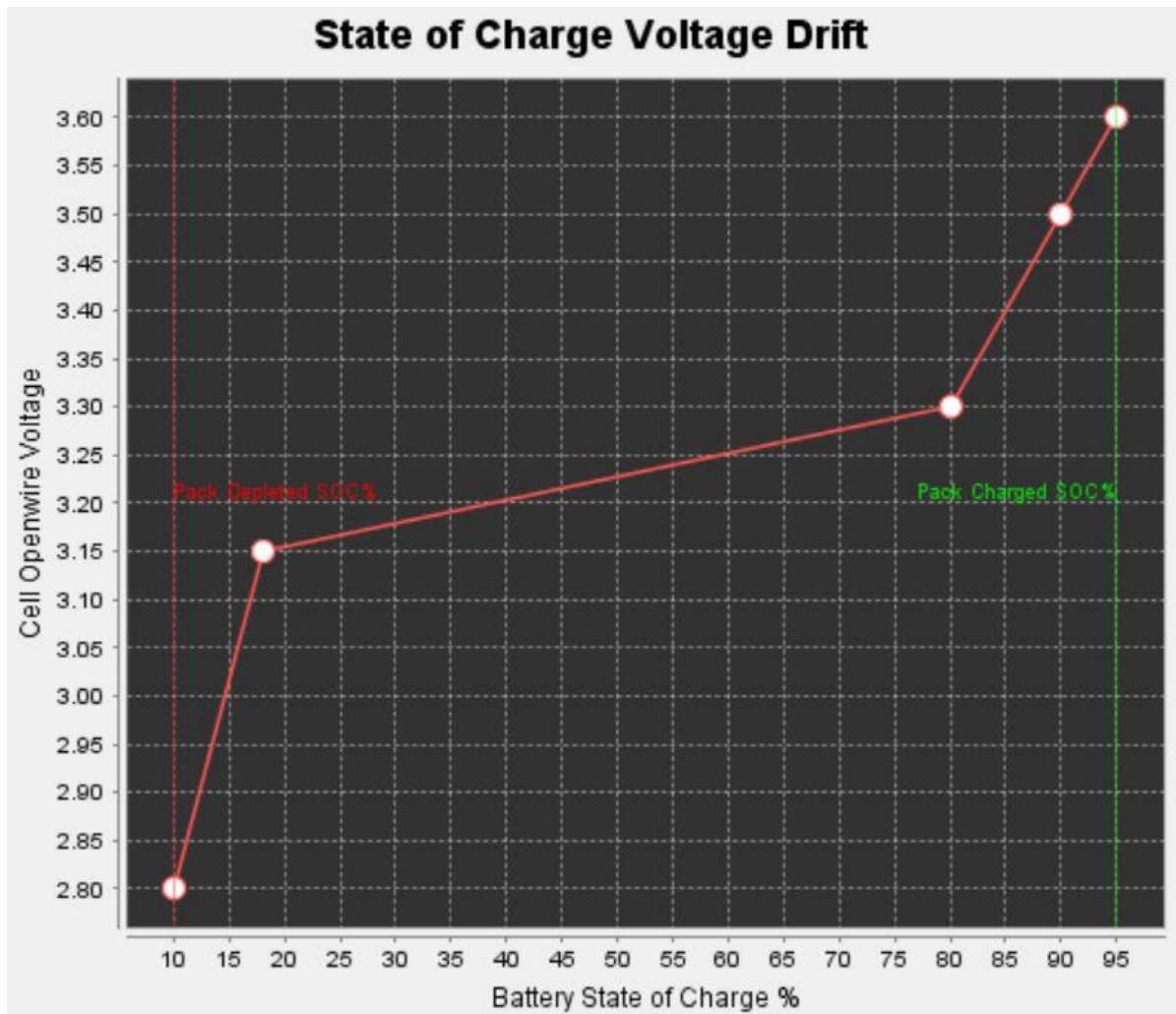


Figure 25 Voltage Profile used to estimate State of Charge.

This method of SOC estimation gives an approximate picture to the user and BMS of the charge levels in the cells. However, this method is inherently limited, as in reality the exact voltage profile on each cell differs based on a variety of factors; and with the age of cells in HiCEV, it is plausible that some cells have degraded more than others. This profile also fails to account for multiple variables which can have a noticeable impact on cell voltages; namely, temperatures, cell currents, and the hysteresis effect of charging and discharging on the voltage profile. Despite this, as an approximation, it is able to reliably estimate when charge and discharge currents should be reduced and when to shut-off the battery pack to prevent excessive discharge.

The SOC profile is used conjointly with a charge current limit profile, which is used to determine safe charge and discharge currents, based on the SOC and temperature. This charge current profile enables currents of up to 100 A until a SoC of 80%, designed to limit the regenerative braking during operation at high SOC. For this reason, the primary limiting factor on the charge current, is the power output of the charger, which is a maximum of 3 kW for the current ways charger used in HiCEV. For HiCEV the desired bus voltage is approximately 360 V, based on reaching a 95% state of charge, the charger operates with a current range of 8.6 - 8.0 A when keeping the cells within 20 – 95% SOC. Towards the end of the charge cycle, this constant current is tapered by the BMS via CAN commands, however, this only occurs at SOC of greater than 90%. Figure 26 below, shows the charge current profile in the BMS and how this affects charging operation.

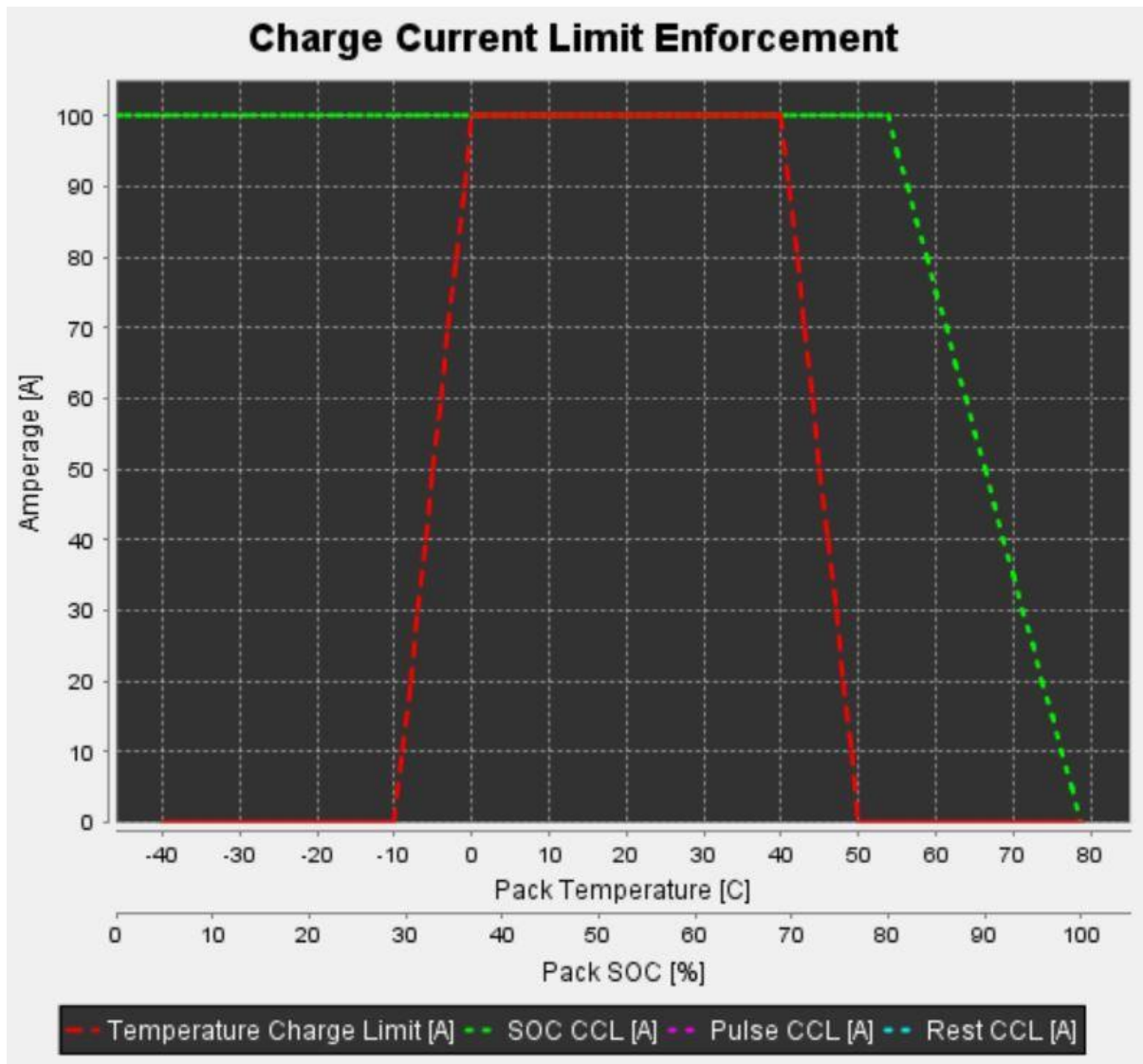


Figure 26 BMS CCL Enforcement Profile.

As the charger is relatively low-power, it remains operating at near full capacity for the entire charge cycle. Therefore, HiCEV is almost entirely charged using constant current charging; however, due to the low current charging, the de-rating of the charger at very high SOC this poses minimal risk to the lifespan of the cells.

3.5 LV Systems and Ignition

HiCEV continues to make use of the existing wiring loom for all vehicle peripherals, powered by a DC/DC converter, which functionally replaces the alternator. Additionally, HiCEV has new integrations to safely monitor and operate the vehicle peripherals. When the DC bus is disconnected, these peripherals can operate off the original 12 V battery, now used as both a backup, and to power the start-up operations. New peripheral systems included in the vehicle largely include cooling integrations, however, power steering and braking systems which typically integrate with ICE engines seamlessly, had to be reworked into the LV bus also. Previously, these peripherals were electrically isolated from the 12 V bus using independent relays operated by the EVCM, since removing this, these peripherals are now controlled by the ignition, such that they turn on when the inverter begins start-up. A full list of aftermarket 12 V systems, expected current requirements, and fusing, can be seen in Table 4; current ratings have been determined by measured currents in the peripherals.

Table 4 12 V peripherals and corresponding current ratings.

Peripheral Description	Current Rating	Fuse Rating
Inverter Fans	3 A	5 A
Inverter Cooling Pump	1.2 A	2 A
Motor Fans	7.5 A	15 A
Motor Cooling Pump	5 A	15 A
Power Steering Pump	50 A	100 A
Power Steering Enable Switch	100 mA	1 A
Vacuum Brake Assist Pump	10 A	15 A

The objective of the control for these peripherals is that the original vehicle peripherals continue to operate as they did with the ICE motor. For this reason, the aftermarket peripherals are simply driven from an ignition switch-controlled relay, which has the benefit of simplicity, however, comes at the expense of the limited controllability. Figure 27 shows the full schematic of the additional 12V systems.

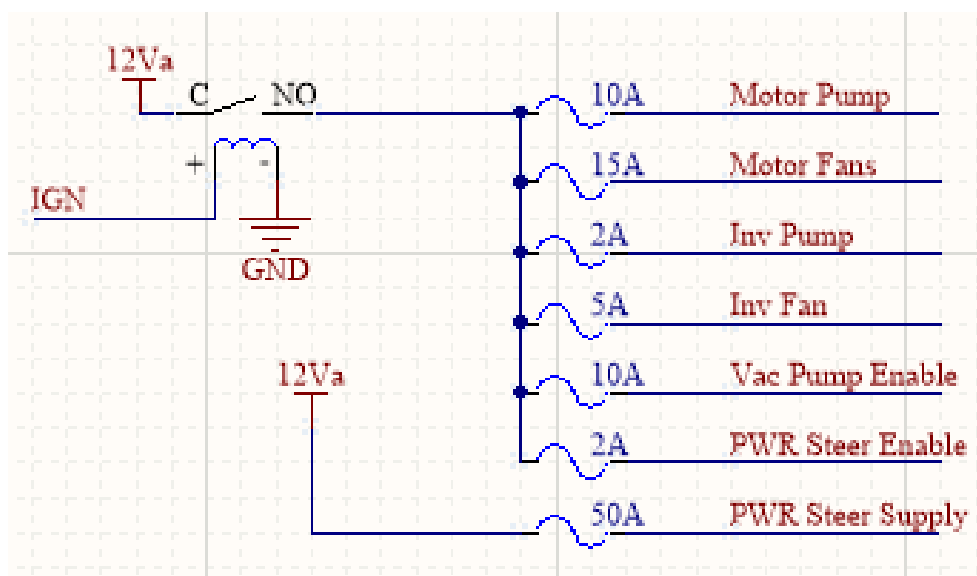


Figure 27 Schematic of aftermarket 12 V components.

The add-on 12 V peripherals each share a single busbar which is switched by the main relay. To avoid wider damage to the bus, each peripheral is independently fused. The power steering pump is an exception to this, as it has significant power draw on the main bus, therefore it connects directly to the 12 V output of the DC/DC converter and is driven via an enable switch. This main busbar, is connected via a designated IP67 rated fuse box, which has been left for expandability should it be required.

The ignition system makes use of the key switch, as seen in most ICE vehicles; this consists of three stages, accessories, ignition, and start. Within the vehicle, HiCEV has easily accessible connection points which are routed through the ignition for the accessories and ignition stages of start-up, which are used to drive relays that in-turn start the vehicle. A full schematic of the ignition systems is shown in Figure 28 below.

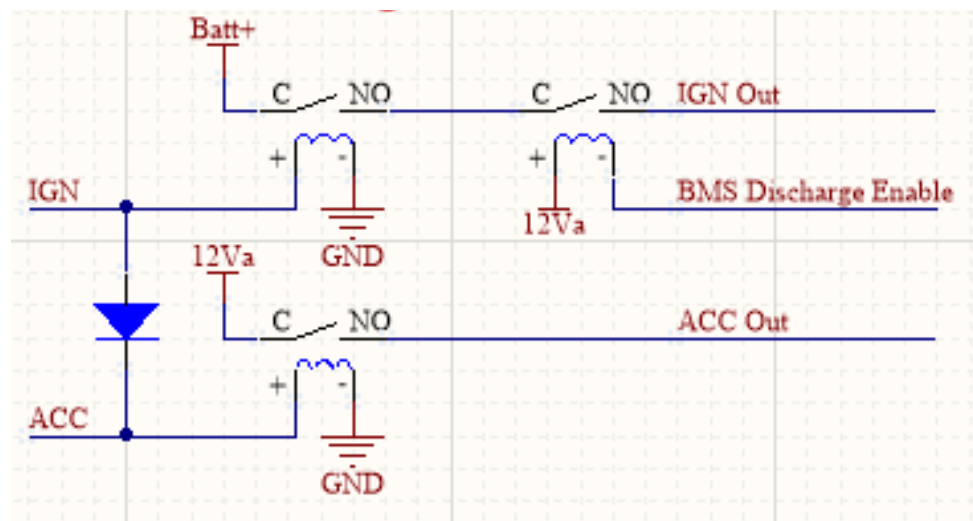


Figure 28 Ignition System Schematic

The BMS and inverter are the primary sub-components which must be switched on during start-up, with it being imperative that the BMS is able to monitor the batteries before high currents are able to be drawn from the bus via the inverter. To account for this, the BMS is used to switch a series connected relay with the ignition. The effect of this is twofold; it both enables the BMS to finish start-up before any loads are applied to the main bus, and it enables the BMS to shut-down the inverter in an emergency. To the driver, this may cause a small delay during start-up, however, provided there are no errors in the battery pack, this delay should be less than 1 second (considerably lower than the original diesel pre-heat function). Due to accessibility issues, the 'start' level of the ignition switch remains unused, however, by turning the key to the 'start' position, it does have the unintended effect of turning off the accessories stage. To account for this, a diode is installed, such that if the user turns the switch too far, the accessories-controlled relay is able to be controlled by the ignition; failing to do this will result in the BMS and therefore the inverter shutting down when the ignition switch is turned to 'start'.

The DC/DC converter in HiCEV is a Sevcon Gen 5 HV DC/DC, capable of outputting up to 1200 W of power to supply the 12 V bus. This was sourced to replace the existing, Meanwell RPB2400-12, for which it was difficult to cool while maintaining the IP67 waterproofing requirement. This converter is rated to output 13.4 V on to the bus which is connected in parallel with the 12 V back-up supply battery. The parallel connection with the cell means that when the vehicle is on, the DC/DC converter is able to charge the 12 V back-up supply, as well as maintain a steady 12 V on the bus while all peripherals are drawing from the bus. As a 1.2 kW converter, the 13.4 supply is able to

support up to 89 A for the peripheral operation, experimental testing has yielded that typically all peripherals operating in idle can draw approximately 40 A; despite this, large loading on the bus from the power steering pump or vacuum pump could threaten the stability of this system. If the current draw on the DC/DC converter exceeds 90 A, the converter is programmed to shut-down, which requires a manual re-start via either the ignition, or the power switch situated on the converter. Though this is not directly reported to the driver, the shut-down of the converter should provide significant noise feedback to the driver as the fan and pump speeds de-rate rapidly.

The DC/DC converter is integrated with the original wiring loom where the alternator was previously used to power the 12 V systems; therefore, the power drawn from the DC/DC converter includes not only additional peripherals but also vehicle systems connected to the original Toyota wiring harness. Using current ratings, it is possible to estimate the peak current loading expected on the 12 V bus and determine the risk of emergency shutdowns for the DC/DC converter. The rated current for the aftermarket peripherals stands at 76.8 A, though it is unlikely that all peripherals will be operating at peak currents simultaneously. Being an older ICE vehicle, many of the peripheral lights, stereo equipment and vehicle monitoring peripherals have a lower efficiency than modern LED alternatives. Despite this, the peak power draw from the main bus from vehicle peripherals, based on worst-case scenario tested measurements, stands at approximately 28 A. The power draw from the 12 V bus, during peak loading conditions, is noticeably greater than the power rating of the DC/DC converter. This does pose risk to the stability of the DC/DC converter operating in HiCEV as it could potentially trigger an over-current shut-down for the converter; however, the parallel connected battery is able to operate as a power source as the bus voltage drops. This enables the system at large to remain stable during high current transients provided the cell remains charged.

The emergency shutdown in HiCEV consists of normally conducting switches which, when triggered isolate the power supply to both the inverter and the BMS. Isolation switches consist of a pressure switch, designed to isolate the 12 V supply during a crash, and a physical isolation switch, within reach of the driver in the cockpit. When the shutdown is pressed, the 12 V supply is immediately cut from both the inverter and the BMS, which causes them to disable output relay drivers disengaging HV connections to the vehicle. Due to the limitation of the existing pressure switch, it is currently configured to isolate the BMS power supply, and does not directly cut power to the inverter. Despite this, due to the ignition circuit, when the BMS is powered off, the Inverter will lose power due to the 'discharge enable' pin being disengaged. In practice, this may contribute to a delayed shutdown during a crash, however, the discharge enable pin being disengaged should isolate the HV rapidly.

3.6 HV Box

The HV box facilitates all HV line connections on the main bus of HiCEV, which consists of the majority of the main components; the inverter, DC/DC converter and the Charger. The HV box primarily operates as a fused switching-junction for the main power connections along the bus, contained in an IP67 rated container to prevent damage to the vehicle. An electrical schematic for the HV box can be seen in Figure 29 below.

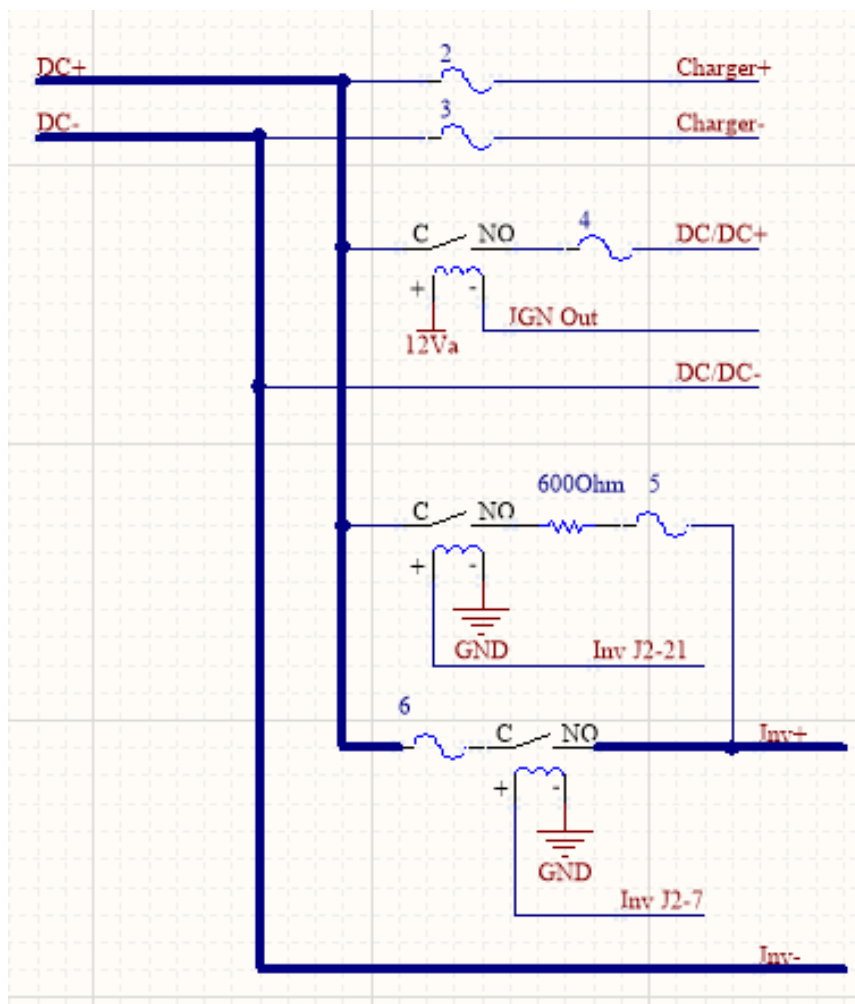


Figure 29 HV Box Schematic.

Electrically, the HV box facilitates the switching of the main power connections to the inverter and DC/DC converter, which are controlled via the BMS using the discharge enable function. This layer of control enables the BMS to ensure that no power is drawn from the main batteries until it is safe to do so.

The HV box has exposed busbar connections with the main high and low connections to the batteries remaining exposed and multiple physical connection points facilitating all HV connections within the box. With this system, the primary insulator between HV connections is the air-gap in the HV box. The breakdown strength of air is very high, at 3.3 kV/mm, which makes it an ideal insulator for the HV bus in HiCEV. At its narrowest points, the HV bus connections are insulated by an air gap of approximately 2 cm, which in theory, should be suitable to insulate up to 66 kV. Because of this, the primary risk to short circuits in the HV box stem from physical movements within the box, which is unlikely due to the physical mounting of the hardware.

Wiring has been intentionally routed in the HV box such that most of the cabling is under a mounted acrylic screen and comes through, primarily to make connections with the main busbar. This was intended to provide the least movement in the cables while driving as HiCEV is exposed to vibrations and mechanical movements. Despite this, due to the mounting of the relays some lengths of cable remain which extend noticeably above the bottom of the box, this was an unintended by-product of providing a layout which enabled the user to access all components easily if required. The physical layout for the HV box is included in Figure 30, notably, all fuses and relays are accessible when the lid is removed.

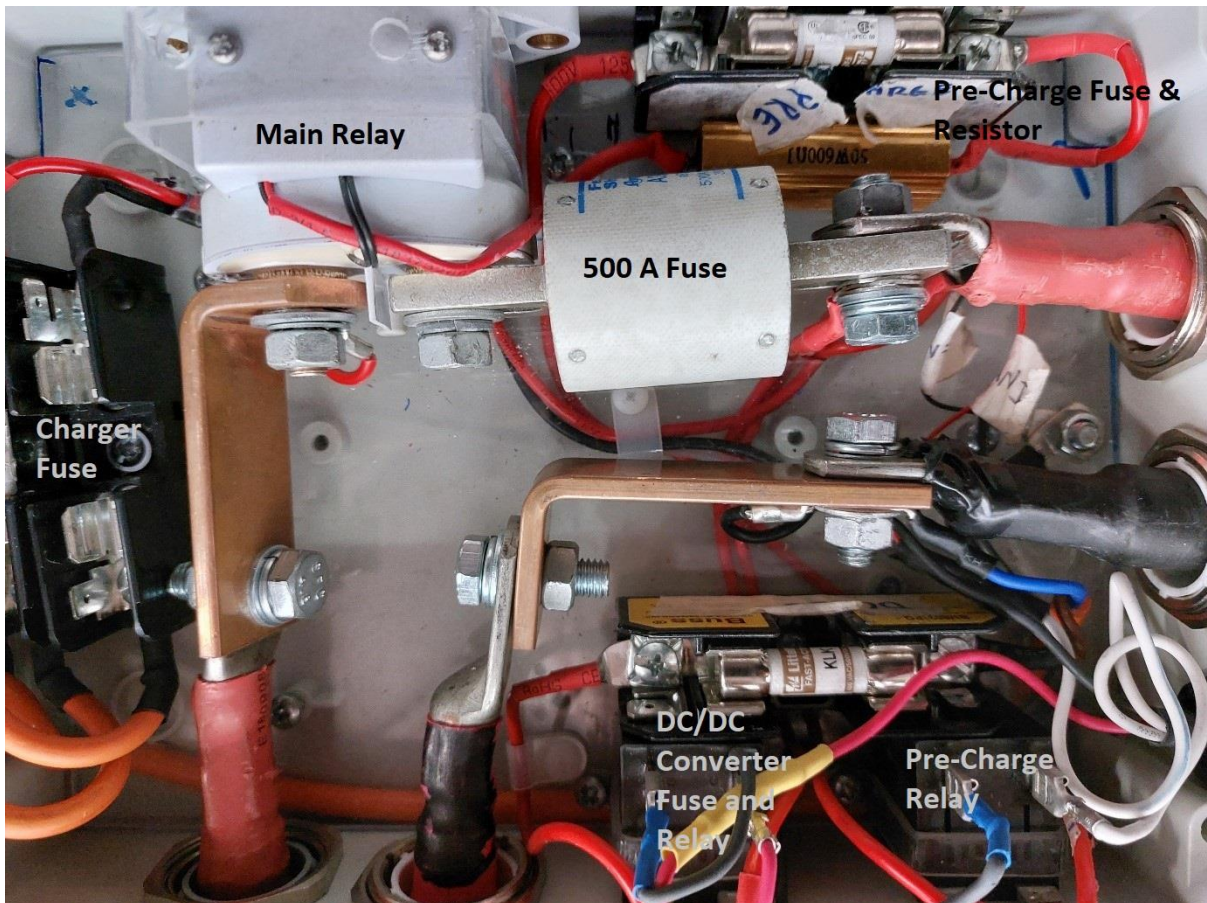


Figure 30 HV box Physical Layout.

3.7 Power Distribution Box

Like the HV box, the power distribution box provides a mechanical IP67 rated structure to facilitate necessary connections for the operation for HiCEV. The power distribution box is used to route the AC connections in HiCEV for integration with the charger. This also poses a secondary function, of providing an alternative 12 V connection for the powering of charger peripherals and the BMS. A full schematic for the power distribution box can be seen in Figure 31 below.

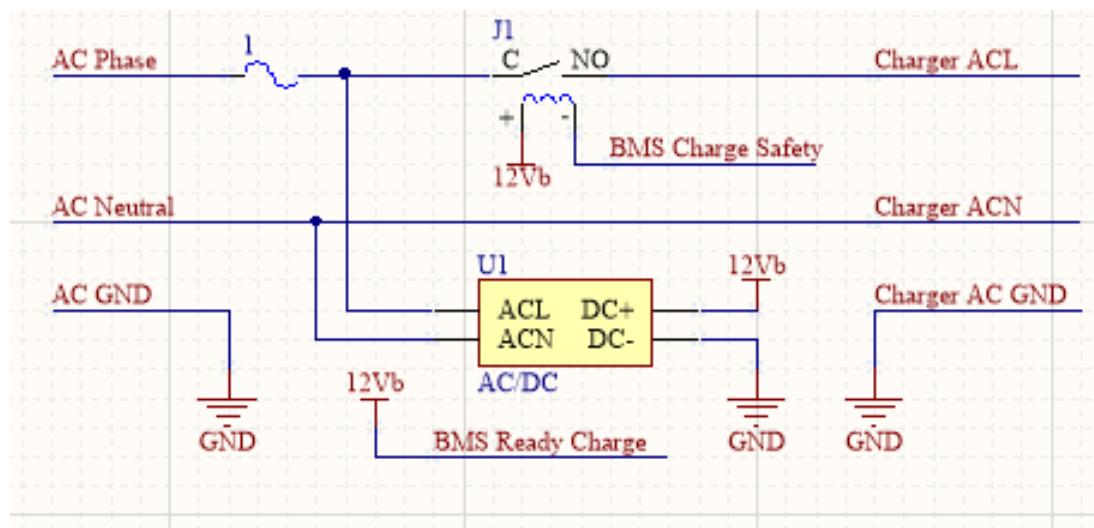


Figure 31 Power Distribution Box Schematic

The charger is BMS controlled via both the charger safety connections and the CAN bus. HiCEV uses a relay on the AC connection to the charger to disengage it when the charge process is complete providing electrical isolation. As the BMS functionally controls the charger 12 V supply from the power distribution box is an essential component of the vehicle. Because of the charger safety relay, the BMS must be active before the charger is powered on. Despite this, the 12 V supply for the BMS and cooling peripherals does remain operable, enabling the user to monitor cells, or for the BMS to balance cells after charging without manually disengaging the charger.

3.8 Braking System

Modern ICE vehicles come with braking assist features which many drivers have been accustomed to. These systems make driving safer, by making braking physically easier to perform for the driver. The main braking system in HiCEV, despite the newly installed regenerative braking, the vehicle still relies on the original drum braking system. In ICE vehicles, a negative pressure gradient is applied to the brake pedal using the vacuum created in the vehicle's intake manifold. However, with an EV conversion, the brake vacuum is generated by a designated vacuum pump, also known as a brake booster.

The brake booster is used with the original assembly of the vehicles braking systems, enabling seamless mechanical integration. However, properties of the pump require that electrically, controlling the pumps operability requires many considerations. Concerns for the braking system include thermal, power and noise pollution issues which potentially arise from operating the pump with 100% duty. However, most notably, the manufacturer ratings for the pump require it to operate below a pressure of -650 mmHg [63]. To maintain a set level of vacuum, the pump has a pressure switch installed in the hose which measures the pressure to maintain between -350 mmHg and -550 mmHg. This pressure switch triggers at a set pressure within the operation range, outputting a 12 V signal when the pressure drops below the set point. The concern with using this pressure switch directly for control is that the vacuum pump would operate in short bursts immediately switching off when the pressure increases above the set-point.

The braking system in HiCEV utilises an asynchronous 555 timer to output an on signal for a set time delay, to cause the pump to create a vacuum for 15 seconds after the vacuum is depleted past the set point. A schematic for this system can be seen in Figure 32 below.

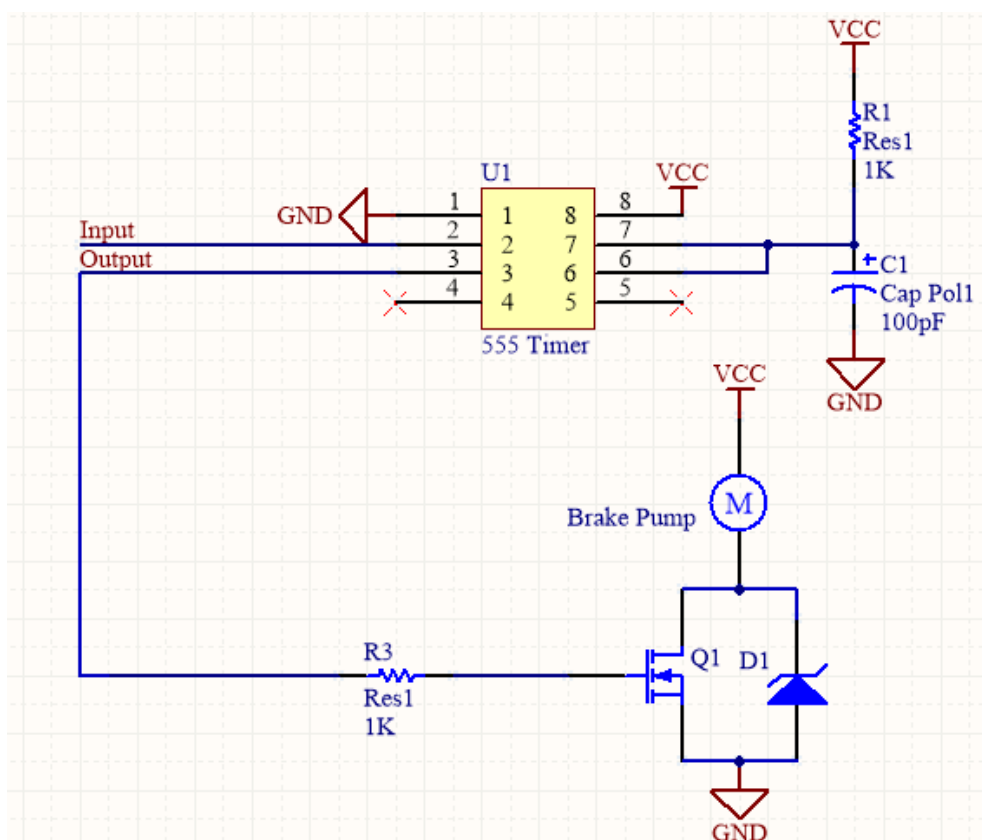


Figure 32 Brake Pump Controller Schematic.

The brake booster requires relatively high currents to operate continuously which mean the output driver for the system is required to have low conduction losses. The system uses an NMOS transistor series connected with the pump to provide this functionality as the conduction losses are limited by the small $R_{DS(ON)}$ of 7 m Ω . The 555 timer is configured to work with a timing resistor and capacitor, with an RC time constant of 15 s. As the capacitor discharges the output for the 555 timer switches off when the voltage at the capacitor drops below the internally referenced comparator voltage of $1/3 V_{DD}$, which occurs after approximately a single time constant, the output changes state, thus turning off the pump.

The brake pump circuit is implemented on a PCB which shares its functionality with the control brake switch used with the inverter. When grounded, the brake switch in the inverter activates regenerative braking; however, the brake switch installed in the vehicle energises to 12 V. This is because the original brake switch is series-connected with the brake lights energising the brake lights when pressed. The board has a NMOS inverter to ground the brake switch input to the inverter when pressed, fulfilling this functionality requirement.

3.9 Cooling Systems

HiCEV operates with typical drivetrain peak powers of approximately 130 kW, which, means that even at high efficiency, thermal losses can be considerable. These concerns primarily affect the DC/DC converter, charger, inverter and motor each of which are cooled through fluid transfer systems. While operating, the charger and inverter are each cooled using standard automotive water-based coolant fluid which cycles through a radiator. In-contrast the motor uses a non-conductive, transmission-oil based cooling loop. The power losses from these components can be estimated based on the estimated usage while driving HiCEV; it is noteworthy, that in practice the motor will likely be operating well below its peak power ratings for most of the drive time. Table 5 below shows the expected power losses for the main components in HiCEV based on both peak and realistic average operating powers, which can be used to estimate the required cooling for HiCEV.

Table 5 Expected Thermal losses in Electrical Components.

Component	η (%)	P_{Peak} (kW)	$P_{Operating}$ (kW)	$P_{Peak Loss}$ (kW)	$P_{Op Loss}$ (kW)
DC/DC	91	1.2	0.6	0.108	0.054
Charger	92	3	3	0.24	0.24
Inverter	97	130	40	3.9	1.2
Motor	95	130	40	6.5	2

It is worth noting that efficiency estimates differ based on the operating power for many of these components, thus power loss estimates are approximate values. Each component also has a different operating temperature threshold which enables the vehicle to remain operational with declining power output as temperatures increase.

Estimating the capacity of vehicle cooling systems remains an inexact science. This is due to the wide range of unknown variables which can contribute to the systems cooling performance. Contributing factors to the cooling performance of a typical radiator system include the thermal mass of the fluid within the system, the radiator surface area, flow rates, and thermal conductivity of thermal contacts. Despite the wide range of unknowns in the system, the cooling capacity for a system can be estimated based on plausible operating characteristic guesses.

Mechanically, a liquid cooling system can be modelled as a series of heat transfers which occurs in stages throughout the cooling loop. The liquid within the loop operates as a thermal mass which transfers heat from electrical losses into the environment via radiators within the loop. A simplified schematic for a water-cooling loop can be seen in Figure 33 below [64].

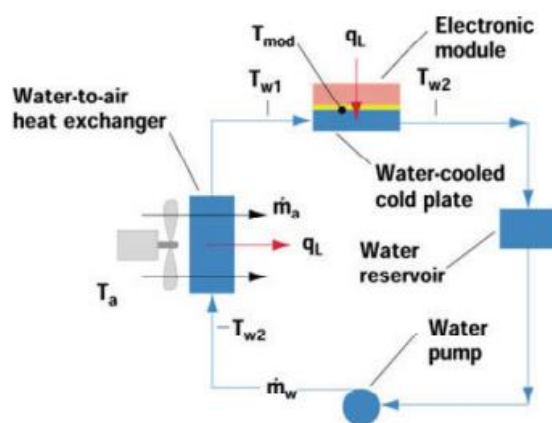


Figure 33 Schematic of heat transfer in a liquid cooling loop [64].

Thermal transfers occur between the power losses from electronic systems and coolant via a thermal contacting plate, typically ridged to maximise thermal exposure to coolant in the system. Within HiCEV components, the surface area exposed to the coolant within the systems remain to be unknown variables which contribute to the high levels of uncertainty in cooling performance within the vehicle. Additionally, with the inverter and motor cooling systems, power consumption in the system is variable contributing to variable performance in the cooling systems based on temperature gradients throughout the cooling loop. HiCEV uses components for which the exact thermal properties are unknown, however, mathematical models can be applied to demonstrate the operation for the cooling system and predict the effective thermal resistance for the systems.

The primary thermal exchanges occur at the points of contact between the electric module and the water, via a conductive plate; and the water and the ambient air via a radiator system. The exact temperature for an electronic module in a water cooling system can be predicted based on the thermal resistance between the module and the water cooling system, and the temperature of the coolant within the system, such that the following equation holds true.

$$T_{mod} = q_L R_{cp} + T_l \quad (12)$$

Throughout operation, the temperature of the cooling liquid will rise due to power dissipation, which is offset by the radiators. The average temperature of liquid in the loop can be predicted based on the energy entering the system from the components, the energy leaving the system through the radiator and the thermal mass of the liquid flowing through the cooling loop. Thermal mass is a product of a liquids specific heat, the amount of energy required to heat the liquid, and the volume of liquid in the system. Reservoirs are often included in cooling systems to increase the volume of liquid in the system, thus taking longer to heat up. The amount of energy dissipated by the radiator at steady state is equivalent to the energy entering the system, such that the following holds true.

$$q_L = \varepsilon C_l (T_l - T_a) \quad (13)$$

Where ε is the effectiveness of the radiator, such that the energy dissipated is proportional to the temperature difference between the ambient air and the liquid within the system and the specific heat of the liquid within the system. The concern with this model is however, that the effectiveness of the heat exchanger is dependent on a variety of factors, notably, flow rate of air, air pressure, flow rate of liquid, and exposed thermal contact. Despite this, using known factors, the overall efficiency for a cooling system can be predicted based on the steady state temperature of the liquid within the water-cooling loop. Within the context of HiCEV, the ability of a cooling system to maintain below maximum full-power operating temperatures can be used to determine the viability of an installed system.

3.10 General Reliability

Reliability of HiCEV is contingent on many factors, inclusive of failsafe protections, adequately meeting specifications, and vehicle monitoring. Without the EVCM these concerns can be exacerbated as monitoring operating temperatures, currents and voltage, becomes difficult for the driver, relying entirely on internal monitoring provided by the hardware. Despite these concerns, development to specification and testing consider both driver safety and longevity for the vehicle.

HiCEV has been designed to operate with failsafe protections for driver safety and general reliability. Fundamentally, this stems from the fusing and emergency shut-down within the vehicle, preventing over-current, over-heating and damage to expensive modules of HiCEV. Within this structure, each module of HiCEV is also able to monitor its own temperature and control outputs based on thermal or over-current de-rating within the vehicle. Peripheral controlled relays are also used to limit the currents within HiCEV, as each peripheral can use relay signals to electrically isolate connections within the vehicle, provided a fault is triggered, or the vehicle stops operating within safety limits. Fusing is used widely within HiCEV as a redundancy measure, design of protection box layouts has operated around accessibility of fusing for easy replacement should it be required.

As part of HiCEV functional requirements, the vehicle must be operable in a farming capacity. To meet this specification, the vehicle requires both a wide range of thermal operability and weather-proofing which was factored in through the design of HiCEV modifications. All electric components within HiCEV are constructed or mounted within IP67 enclosures which are rated for minor submersion in water. To prevent mechanical damage, the wiring has also been routed through dual-lining heat shrink and conduit, which serve the purpose of physically shielding the wiring, whilst also providing water-proofing to prevent water entering any enclosures through wire mounting.

LVVTA recommendations have also dictated many of the wiring enhancements made in HiCEV. Considerable adjustments were made to mounting of cables within the chassis as per recommended 350 mm mounting distance recommended by the LVVTA. LVVTA guidelines were also used to dictate the wiring and cable used within the vehicle, based on current, insulation, and thermal guidelines. Signal and LV relay wiring uses a standard 1 mm diameter threaded cable, current rated for 5 A considerably greater than maximum current ratings for most relays used in HiCEV at 0.125 A. Higher power components on the 12 V bus use high current rated wiring, independently routed to prevent thermal losses from compounding within the wiring loom.

Vehicle system monitoring occurs while operating through the inverter, motor and BMS. The BMS indirectly controls the inverter, by communicating current charge and discharge limits during operation based on cell temperature, voltage and resistance settings. Notably, the inverter can also directly monitor the temperature sensing performed by the motor, and its own temperature, to de-rate current provided over temperature events occur. While driving, the vehicle operator may be unaware of potential issues, however, the Inverter, motor and BMS are able to communicate fault and historical fault codes which enable fast debugging for future use.

Chapter 4: Experimental Results

4.1 Testing Overview

HiCEV operation is reliant on the functionality of a variety of sub-systems within the vehicle, such that reliability is dependent on the operation of each module and the linking interfaces. Each of the modules and integrations within HiCEV can be tested independently to ensure the vehicle is reliably functioning for typical operating conditions. The primary modules within HiCEV consist of the BMS, Inverter, Motor, DC/DC converter and the 12 V sub-systems. In addition to this, integrations, notably, CAN bus, Ignition systems, and driver UI, are tested to ensure that the vehicle remains responsive and safe for operation.

The project objective is to produce a reliable vehicle that is capable of operating in a high-country environment. Testing aims to ascertain whether this is achievable for HiCEV, whilst also establishing electrical performance characteristics for the vehicle and reliability indicators. Electrical performance can be established from data reporting within the Inverter and BMS, as well as external measurements; whilst reliability can be estimated based on the results of testing, as well as testing of various vehicle features which extend reliability. Notably, temperature, shut-down circuits, and vehicle monitoring systems are used while driving to maintain safe conditions with the intent of extending reliability. For general operation, it is important to establish motor, inverter and battery characteristics to ensure that the vehicle is able to operate as intended. Importantly, an objective of HiCEV was for it to operate similarly to the ICE performance, performance can be characterised through testing of the motor, to establish operating torque and speed for the vehicle. The operating characteristics will also have a considerably effect on the driving experience based on acceleration, gear changes and control.

HiCEV design requirements, for reliability and practicality, establish the framework for which HiCEV is tested against. For each component, physical parameters, such as cooling, operating current, efficiency, and functionality, can be monitored to provide experimental evidence that long-term reliability is achievable for HiCEV. Though many of HiCEV features will inherently operate differently to the mechanical expectation, given the distinctions between electric and ICE motor performance; HiCEV should still exhibit predictable performance based largely on the software and hardware metrics. Expected operation can be derived from programmed and hardware parameters which dictate the operability for the vehicle.

Table 6 shows a testing overview for the car, based on the requirements and desired testing outcomes, specific testing procedures have been added to demonstrate how testing will proceed for HiCEV.

Table 6 Testing Overview

Module:	Requirements:	Specific Testing Procedures:
BMS and Battery Pack	<ul style="list-style-type: none"> - Communicate Reliably with Inverter for control. - Monitor cell conditions. - Operate relays to prevent damage to the vehicle. 	<ul style="list-style-type: none"> - Thermal Testing. - Current Measurements - Voltage Profile Measurements - Ensure shut-down operational.
Inverter and Motor	<ul style="list-style-type: none"> - Drive Motor. - Maintain safe temperatures. - Remain within current limits for battery pack. - Integrate with peripherals for reliable vehicle control. 	<ul style="list-style-type: none"> - Test various operating conditions, loading and speed. - Thermal Testing. - Ensure integration with other modules is reliable and stable. - Ensure Safety features are operational.
12 V Bus and peripherals	<ul style="list-style-type: none"> - Ensure DC/DC Converter remains stable under load. - Test braking system for reliability. 	<ul style="list-style-type: none"> - Measure DC current and voltage in various operational conditions. - Ensure Shut-down switch is operational. - Test Thermals of DC/DC converter in typical operating environments.
Battery Charger	<ul style="list-style-type: none"> - Maintain safe operating temperatures. - Integrate with BMS to determine safe operating conditions. 	<ul style="list-style-type: none"> - Test thermal characteristics. - Ensure charge interlock is operational. - Test CAN communications with BMS to ensure current and voltage outputs operate as intended.

4.2 Batteries

The battery management system monitors and tracks battery characteristics throughout general operation. This monitoring bases estimations for battery parameters on programmed characteristics, adjustable via BMS software. The batteries in HiCEV are approximately 10 years old, which contributes to potential degradation and imbalance within cells present in the pack. These issues should be exposed through the voltage and resistance characteristics of the cells as monitored through multiple charge cycles.

Battery testing information stems from the live cell data logging performed by the BMS based on data retrieved from cell taps, the current sensor and temperature sensing. Battery characteristics make it difficult to reliably estimate many key characteristics, such as state of charge and cell resistance, due to the requirement for additional information to accurately estimate these characteristics.

4.2.1 Charge Test

Charge tests were performed by simply discharging cells within HiCEV to a low state of charge, 20%, and proceeding to test both charge time, cell and pack characteristic throughout the charge cycle. Initial testing was performed with a pack current of 6 A, limited by the BMS, due to thermal considerations with the wiring connecting the wall plug to the vehicle. Though possible to operate at 8 A, the AC wiring external to the vehicle was prone to thermal or overcurrent protections. At 6 A, the current in the AC input stage for the charger can be maintained below 10 A, an important threshold for maintaining safe operation in all NZ household plugs.

Charge times can be estimated based on the reported state of charge and the known capacity for the cells. Typical operation for HiCEV would be to begin charging at a depth of discharge of 80%, equating to an 80 Ahr charge requirement. Given the 6 A charge current limitation, the expected charge time can be assumed to be approximately 13.3 hours; though quite substantial, this remains to be viable for overnight charging. At peak power, the charger would be able to facilitate 8 A charge current within HiCEV, however, due to AC line ratings within households, it is safest to constrain this to 6 A. Testing using the 6 A charging current was performed over the course of multiple days and required approximately 10 hours to charge from 20% to 95% based on BMS state of charge estimations.

The state of charge and voltage curves highlight an interesting correlation based on BMS reported data on state of charge. The state of charge in HiCEV typically remains stable at approximately 80% throughout the charge cycle, this correlation is likely caused by the charge current increasing the cell voltage, which is then being compared to the voltage profile within the BMS to report that the state of charge is approximately 80%. When cell voltages increase above the 80% threshold the pack state of charge seemingly rapidly increase towards 95% at the end of the charge cycle, as seen in Figure 34.

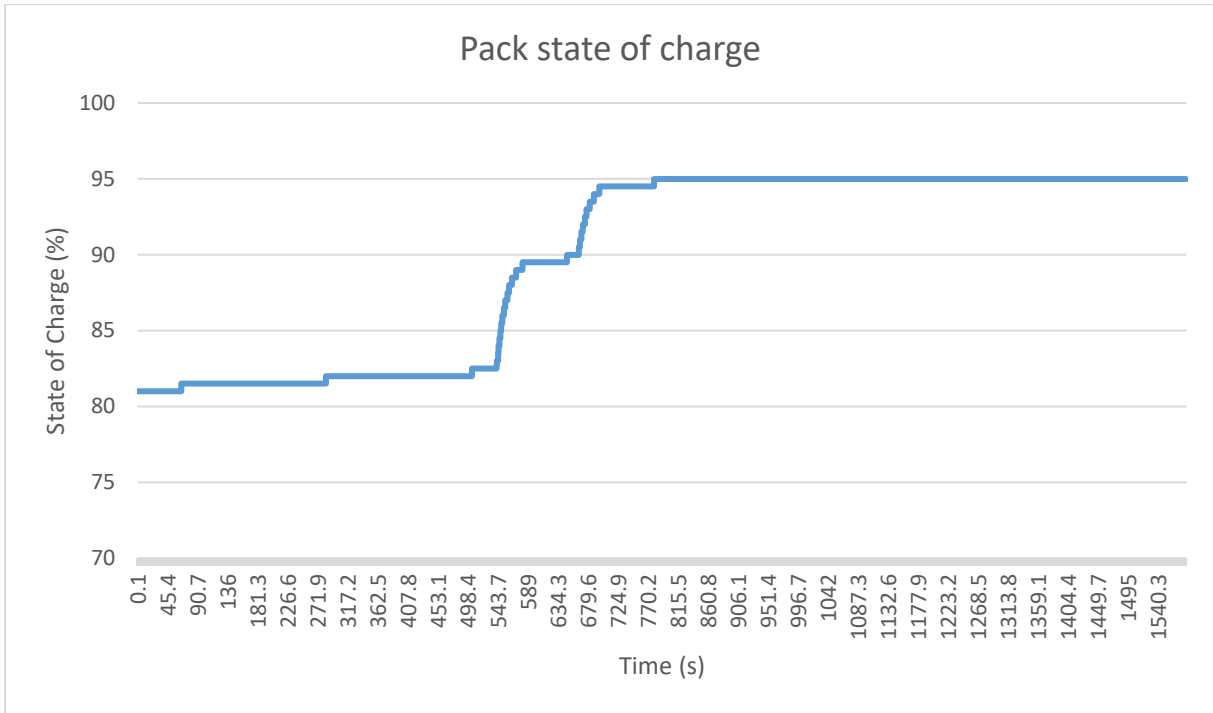


Figure 34 Pack state of charge estimation during charge.

The pack voltage is seen to increase in a relatively linear trend towards the end of the charge cycle; a trend which is mismatched with the state of charge estimations. Despite this, the pack voltage increases at an expected rate based on the charge parameters for the cells. Figure 35 below shows the pack voltage at the end of a charge cycle, and what happens to the pack voltage when the charger is removed. Notably, removing the charge current from the cells results in an immediate drop in cell voltage, followed by a steeper pack voltage drop. These two stages can be explained by the BMS cell balancing, where the first stage after charging is simply the charge current being removed from the cells, and the second stage being current dissipated by passive balancing through the Orion BMS.

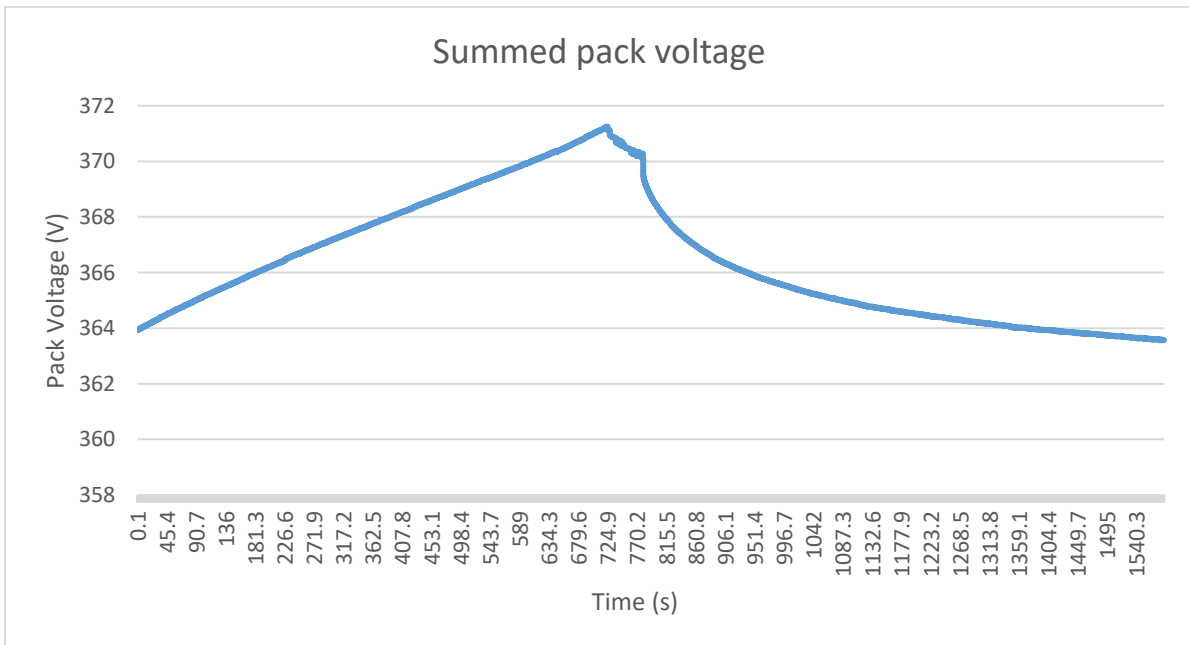


Figure 35 Pack Voltage at end of charge cycle.

Within the lab, the charge current limit was disabled to test the battery charger under load at 3 kW. With this charge method, the current is limited by the peak power output of the charger, which remains constant at 3 kW, and the cell voltage, which increases with state of charge. The charge current throughout the charge cycle resembles the expected trend. The charge current for most of the charge cycle is proportional to the pack voltage, as expected, given the charger is operating at a constant power. This is observed as a decreasing charge current as the bus voltage increases, which based on the 3 kW limit, operates around 8 A at 360 V as expected. It is also worth noting, that the charger self-imposes operating power output limits due to thermal degradation, which has not been observed during testing, indicating that the cooling system is operating as intended. Towards higher state of charge, the charge current declines significantly faster, this is due to the BMS communicating charge current limits based on state of charge, this only occurs towards the end of the charge cycle at state of charge of greater than 90%. Figure 36 below shows the charge current throughout the charge cycle; where pack current gradually decreases until the end of the charge cycle where SOC limits the charge current.

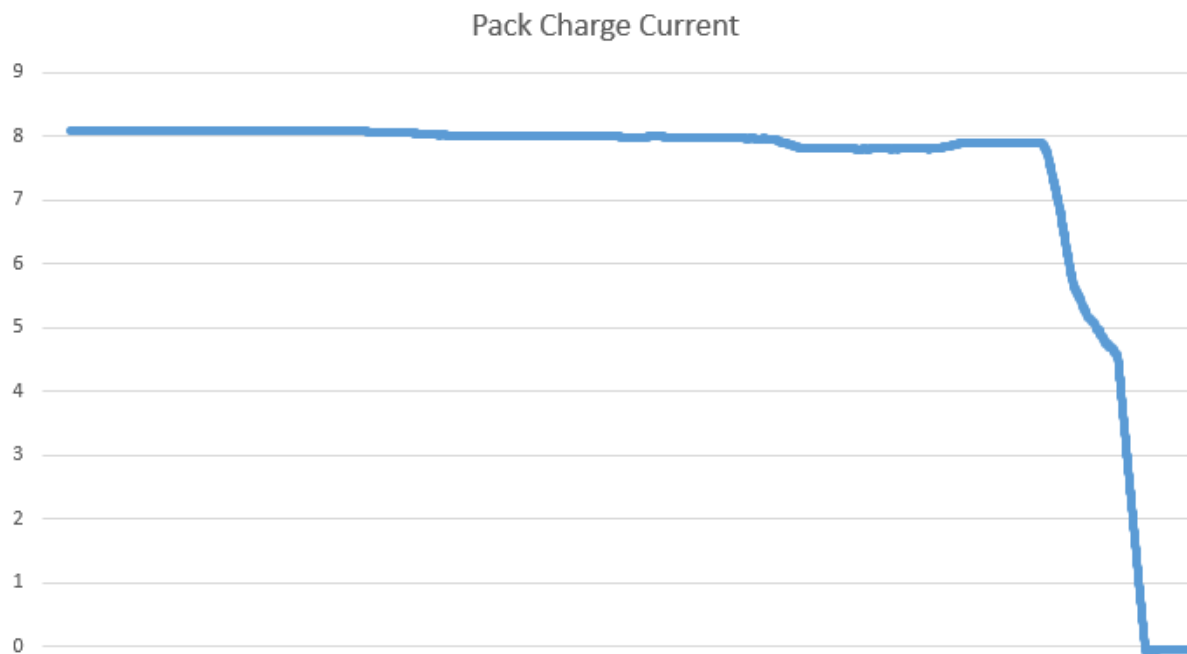


Figure 36 Charge Currents through a full charge cycle.

It is worth noting that this current reduces over the course of minutes, given that the charge cycle can take many hours to complete. This is an expected trend, as the charger operates considerably below the rated charge current of 100 A for the cells.

4.2.2 Cell Balancing Test

The Orion BMS has a built-in cell balancing algorithm that operates via the cell taps to passively discharge cells via a shunt resistor. The cell taps can independently monitor cell voltages to calculate the exact state of charge per-cell, as well as estimate the pack state of charge. The cells with a greater state of charge can be independently discharged through parallel connected shunt resistors. During cell balancing, it can be observed that cells with the greatest voltage are discharged, whilst cells with lower voltage remain stable. Figure 37 shows cell voltages for a variety of cells during the cell balancing procedure; it is worth noting, that the highest charged cells discharge until they are within 0.1 V of the lowest charged cell.

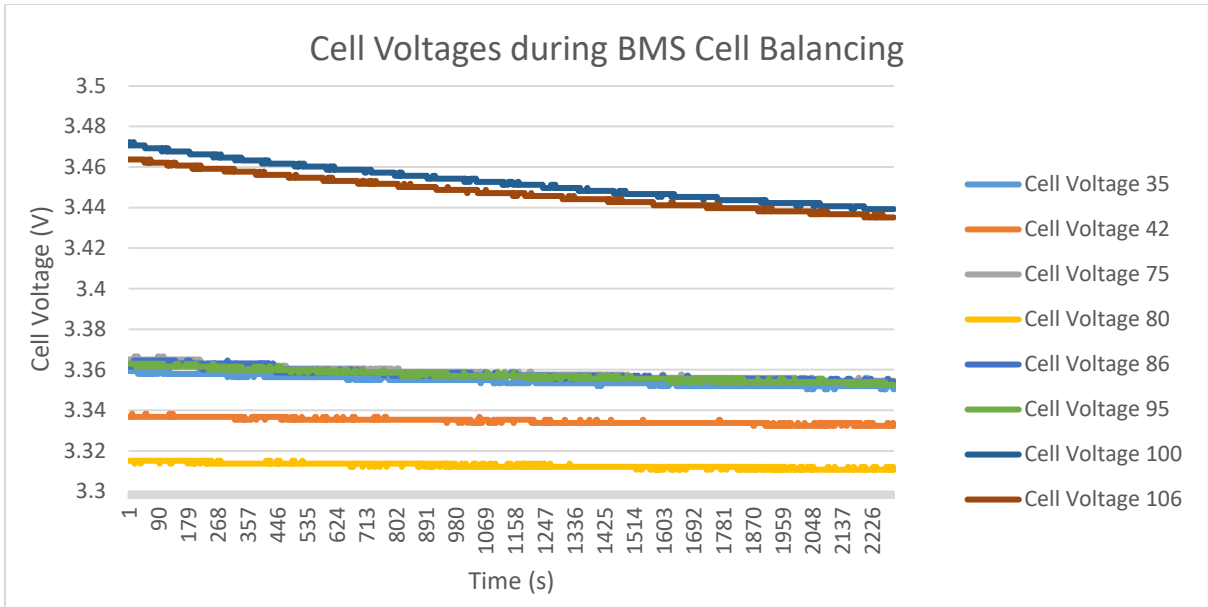


Figure 37 Various cell voltages during BMS passive cell balancing.

4.2.3 Discharge Test

Typical operation for an electric vehicle is that the pack current will differ considerably during general operation, exacerbated by the presence of regenerative braking which facilitates bi-directional current flow, during typical discharge testing. The effect of this is that the pack voltage under variable load, is prone to voltage drifts, also referred to as voltage hysteresis. Voltage hysteresis can be observed in its most basic form as a mismatch between the charge and discharge voltage profile for estimating cell state of charge; compounding this, there is also major distinction based on the magnitude of charge and discharge currents. When testing cells in normal EV driving conditions, the pack current is variable which results in a considerable voltage drift on the pack output. Figure 38 shows the pack voltage across a long-term discharge, notably, despite the variance in the bus voltage due to discharge currents, observably the voltage trends downwards as expected from the cells during discharge.

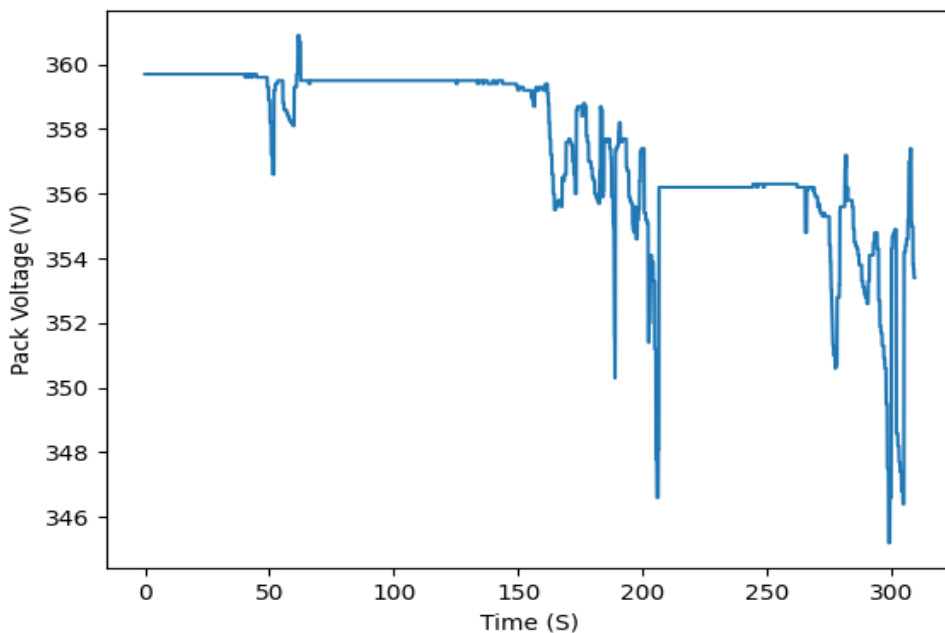


Figure 38 Pack Voltage during drive testing.

Comparing pack current and voltage highlights the effect discharge currents have on the pack voltage. This hysteresis is within expected levels as the per-cell voltage drop expected at 200 A operating current is 0.3 V, this amounts to approximately 30 V with 108 series connected cells. Given that the peak current which the motor can draw under load is 410 A, the expected voltage hysteresis is considerable. Figure 39 shows the pack current over the same discharge period to show the relationship between pack current and pack voltage.

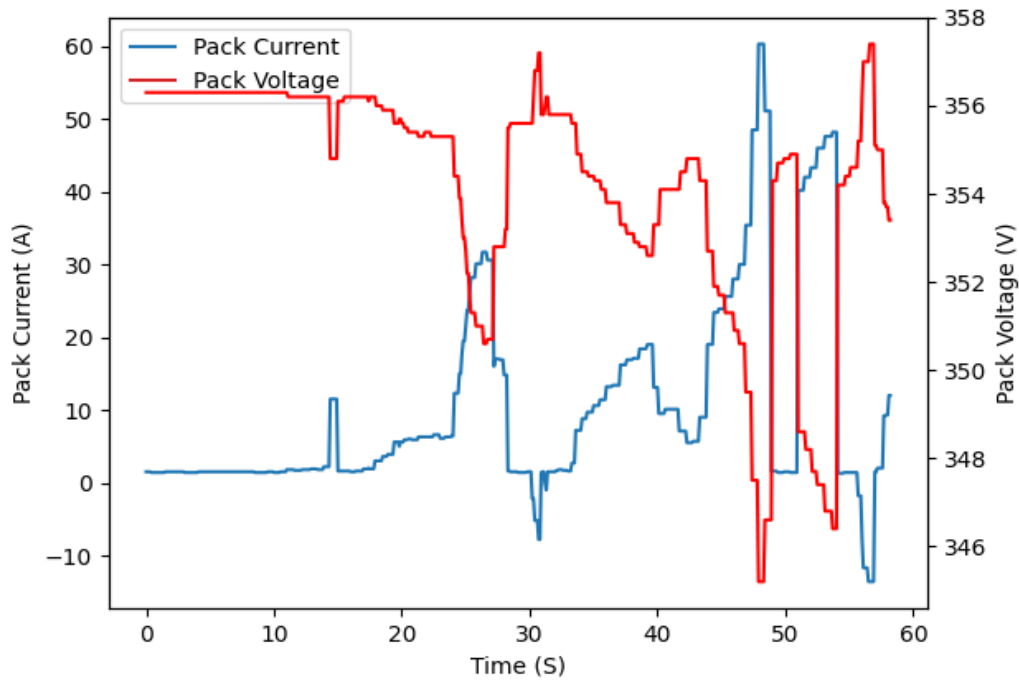


Figure 39 Pack Current during drive testing.

The pack state of charge resembles the trend observed with the charge characteristics whereby, the state of charge holds at 95% and rapidly drops around an inflection point of 360 V. From this, it is easy to conclude that the voltage profile programmed in the BMS to estimate state of charge is misconfigured. The state of charge during discharge can be seen in Figure 40; it is worth noting that this discharge for this occurs non-continuously under normal vehicle operation.

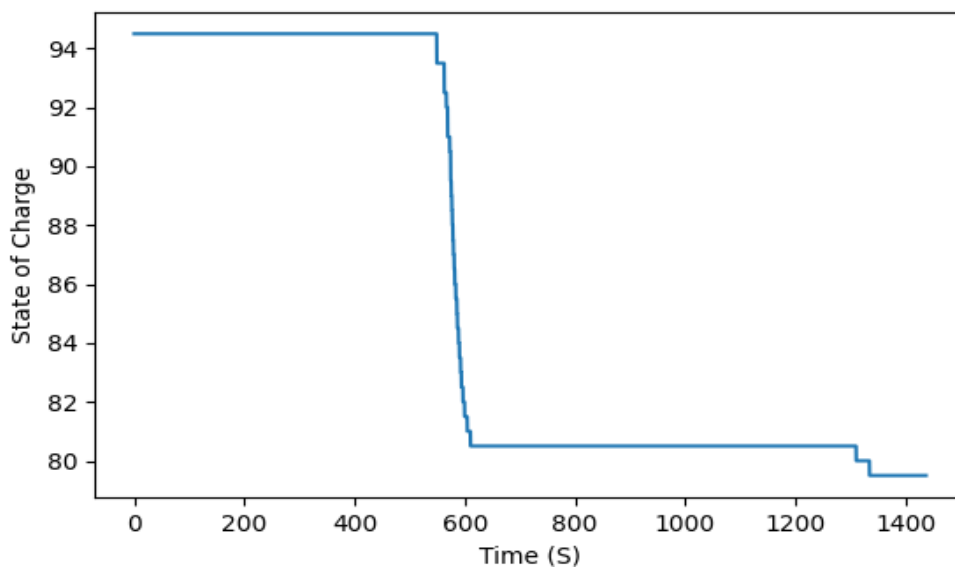


Figure 40 Pack state of Charge during discharge

4.2.4 Voltage Profile Test

The original voltage profile has limitations due to the actual operating characteristics for the cells in HiCEV. Though this does not impact performance in a considerable way, the voltage profile is used to determine current limits and can be used to determine cell state of health. Figure 41 below shows the updated voltage profile for HiCEV's battery cells. The profile has been updated based on the expected behaviour for the Winston LiFePO₄ chemistry, using the Orion BMS pre-programmed profile for use with Winston 100 Ah cells.

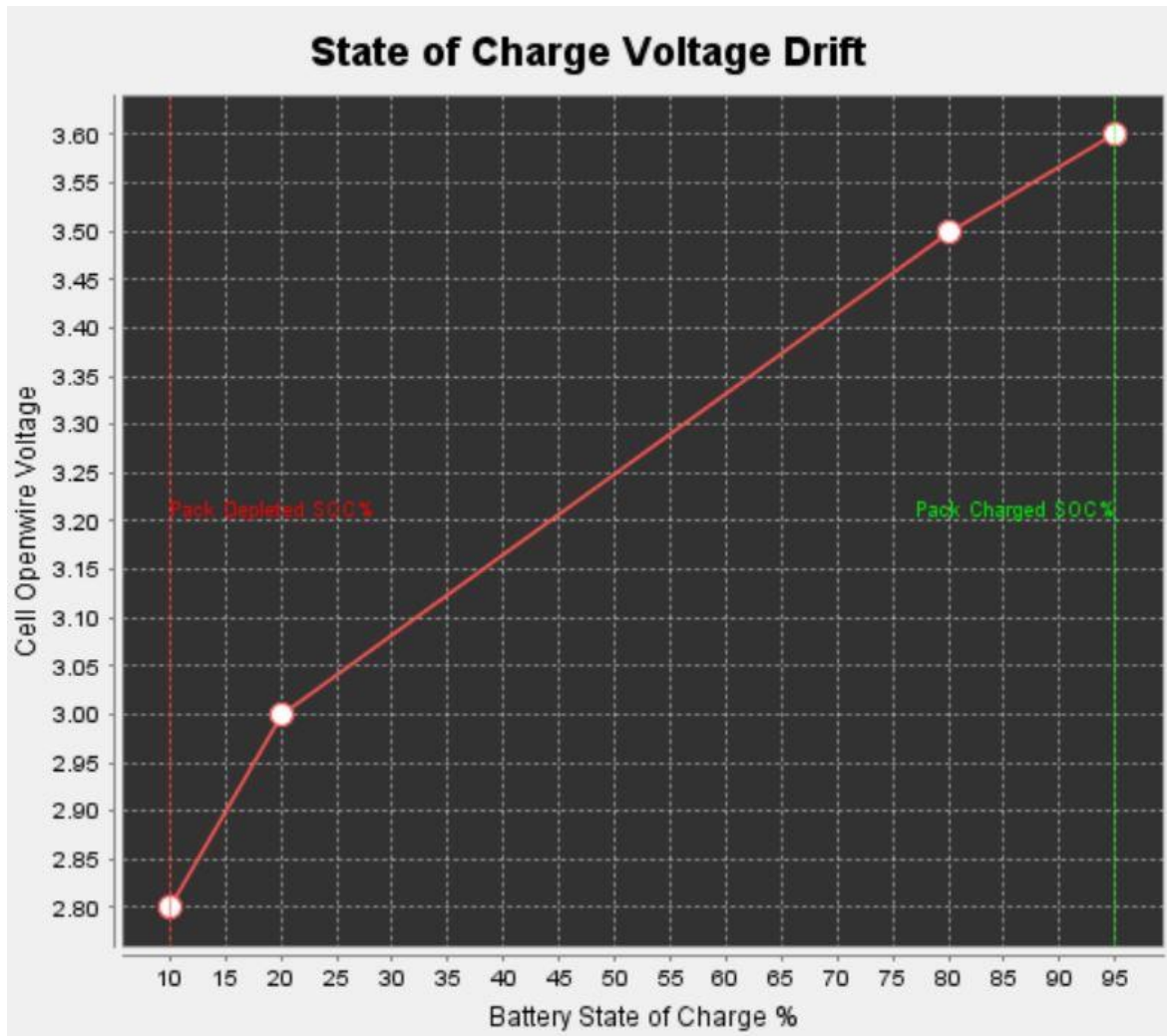


Figure 41 Voltage Profile updated for Winston 100Ah Cells

The updated battery voltage profile provides a significantly more accurate representation of the open cell voltages for the chemistry used in HiCEV. Figure 42 shows the state of charge compared to time when charging at 6 A continuously for several hours.

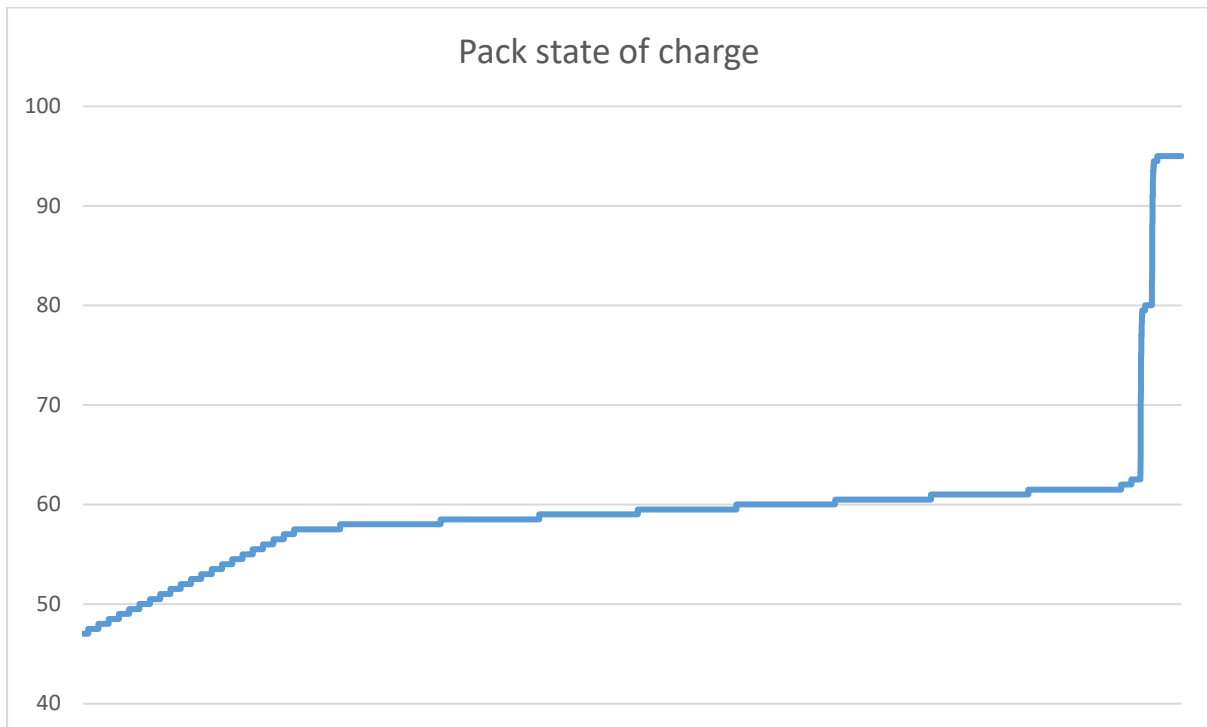


Figure 42 Pack estimated State of Charge using Orion factory calibrated Winston 100 Ah cell profile settings under 6 A continuous current charging.

The updated voltage profile had a noticeable improvement on the cells estimated state of charge at lower charge levels. Despite this, there was a clear jump from approximately 62.5% to 95% state of charge towards the end of the charge cycle, which remains unexplained. Data from cell voltages indicate that around this period, the pack voltage exhibited a similar profile. Figure 43 shows the pack voltage throughout the same charging period seen above.

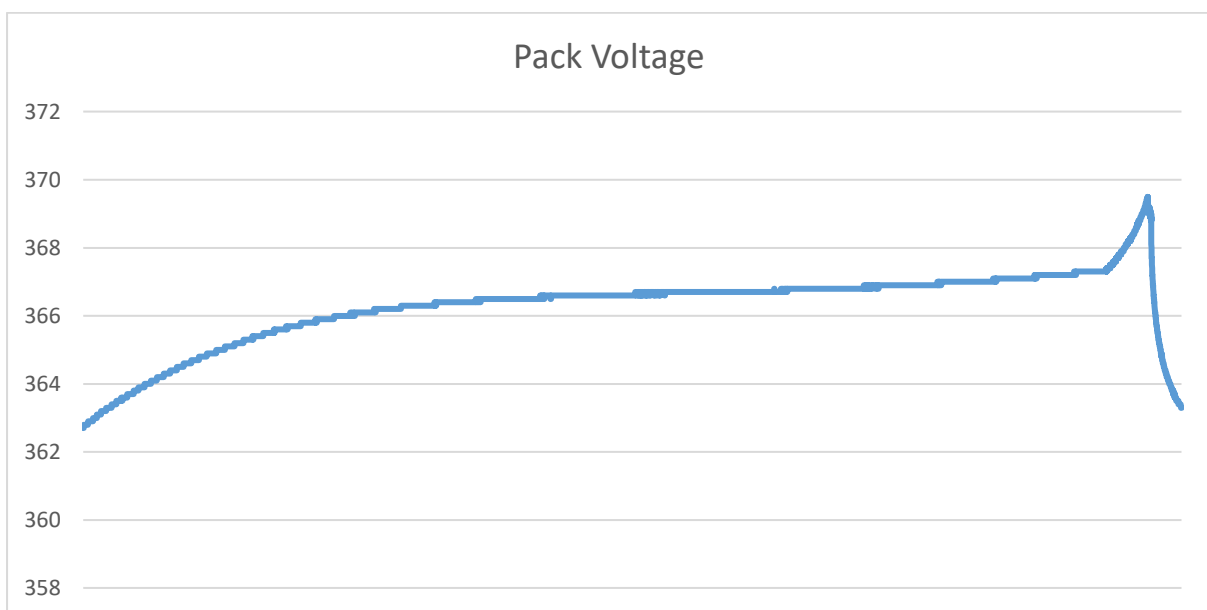


Figure 43 Pack voltage during charge with updated cell profile.

The pack voltage profile throughout this charging period indicate that there may be issues with the BMS or batteries which are causing this behaviour. Noticeably, the state of charge is measuring 95% at a pack voltage of approximately 370 V, which would indicate an average cell voltage of 3.45 V. Using the programmed voltage profile, it is easy to determine that the pack state of charge at this voltage should be closer to 75%. Likely, this anomaly is due to battery health issues, BMS voltage measurements, or poor cell balancing. Given that cell balancing is re-performed with each charge, there is a likelihood that cell balancing issues and state of charge issues stem from individual state of health fluctuations between cells in the pack, or BMS voltage measurements. Given the age of the vehicle, it is conceivable that battery degradation is affecting the operation on the BMS.

Battery degradation manifests itself with multiple symptoms, one of which is reduced charge capacity, which results in faster charges and discharges for individual cells which are further degraded than others [65]. In a large battery pack, like HiCEV's, individual cells with reduced charging capacity can develop imbalances with other cells, which considerably for HiCEV, means cell SOC imbalances. These cell imbalances are important to note, because in HiCEV, the BMS calculates SOC based on the individual cell voltages, as opposed to using the pack voltage. Figure 44 shows an extreme case of cell imbalances while charging, where the cell with the highest voltage in the pack is almost fully charged, and the lowest voltage cell, along with several other cells are still mid-charge. This imbalance could also be the by-product of several years of non-use of HiCEV's cells; however, given these cells have been previously fully charged and balanced prior to performing this test, it is an unlikely explanation.

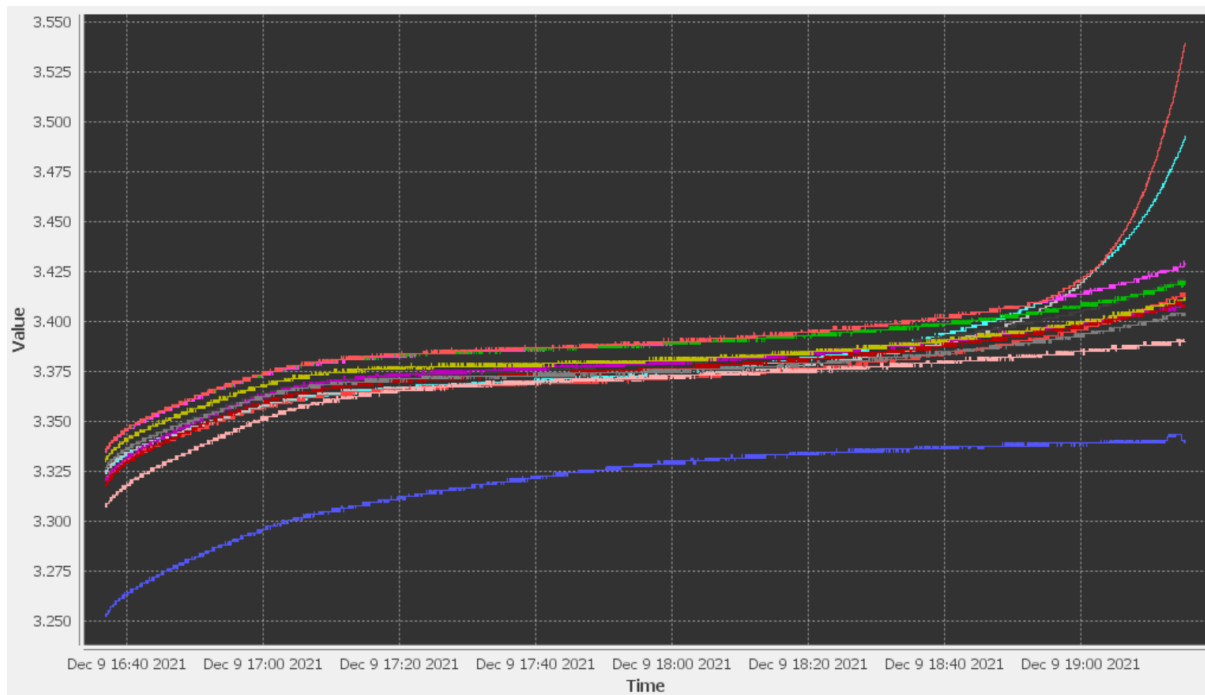


Figure 44 Individual cell voltages throughout charge period.

The effect that the highest charge cells have on the pack estimated state of charge is also very noticeable, as the state of charge estimation increases substantially as the high SOC cells are saturated. The state of charge throughout the same time scale resembles the trend observed in Figure 42. Notably, the state of charge follows the voltage trend of the highest cells in the pack, as opposed to the average cell voltages which are still within the linear region of the voltage profile.

4.2.5 Battery and BMS Reliability

It is well established that life cycle for lithium-ion cells varies based on a variety of environmental and physical design factors. As HiCEV's battery pack has aged, performance and capacity of the cells within the pack has likely degraded due to the effects of long-term storage and a number of charge cycles. Throughout battery testing, several cells exhibited signs of degradation through both voltage and cell resistance measurements reported by the BMS. During drive testing, this became apparent when the BMS reported several "weak cell fault" events, which were triggered by measured cell resistance exceeding 450% of the nominal value. Though the cell faults have no bearing on typical operation, the cell resistance is used by the BMS to estimate safe operating current for the pack; with excessive resistances limiting pack peak discharge currents to as low as 38 A, which is substantially lower than typical current while accelerating. The effect of this, was that the inverter drawing moderate amounts of current during acceleration would result in the BMS discharge enable shutting down the inverter and DC-DC converter while driving. The details of one such "weak cell fault" can be seen in Appendix 4, while an example of BMS calculated cell resistances can be seen in Figure 45.

Live Cell Data									
Highest Resistance:	7.11	[001]	Highest Cell Volt:	3.314	[108]	Pack SOC:	78.0%	<input checked="" type="radio"/> Internal Resistances	
Lowest Resistance:	0.13	[069]	Lowest Cell Volt:	3.270	[080]	Pack Current:	-0.4A	<input type="radio"/> Live Cell Voltages	
Avg Cell Resistance:	1.55		Avg Cell Voltage:	3.307		Pack Voltage:	357.1V	<input type="radio"/> Open Cell Voltage	
Delta Cell Resistance:	6.98		Delta Cell Voltage:	0.044		Current Limits:	+47A / -32A		
							Relay Status:	Discharge:OFF, Charge:OFF, Safety:OFF	
Cell 1	Cell 2	Cell 3	Cell 4	Cell 5	Cell 6	Cell 7	Cell 8	Cell 9	Cell 10
7.110	1.130	3.890	0.980	1.030	1.050	1.080	1.490	1.210	1.090
7.010	1.350	3.090	1.150	1.020	1.030	1.080	0.230	1.100	1.070
1.030	1.090	4.940	1.350	1.190	2.580	2.100	1.130	0.900	1.710
3.530	1.140	1.040	1.140	0.440	0.990	1.070	1.630	2.660	1.150
1.230	1.010	1.240	1.060	1.080	2.700	1.150	1.070	2.530	1.030
0.990	0.420	1.310	1.090	1.040	7.080	1.010	1.060	1.100	1.200
0.950	1.040	1.270	1.090	0.850	1.770	0.960	0.970	0.130	0.990
5.040	1.050	0.920	1.630	1.070	1.010	1.060	1.040	0.990	4.580
0.960	1.060	0.920	1.000	0.980	0.240	1.020	0.960	3.140	1.000
1.080	1.000	1.050	3.210	1.760	1.840	1.000	0.960	1.180	1.010
1.010	1.000	2.390	1.110	1.160	0.900	0.940	3.180	0	0

Figure 45 Cell Resistances calculated by Orion BMS during discharge test.

Cell resistance is calculated by measuring the voltage drop across a cell under load, due to the magnitude of resistance present within a typical cell, the BMS requires relatively high current to calculate cell resistance to an acceptable degree of error. HiCEV also has some interesting features which may also affect this calculation as the calculation relies on zero resistive loss between cells. In practice, the cells are linked by copper bus-bars which have a small associated resistance, as well as the connections the batteries via screw terminals, which accounts for some variability among cells calculated resistance; the magnitude of which, should be negligible, provided they are installed correctly. In addition to this, the BMS cell taps also account for some volatility in the cell resistance measurement. Like the terminal connections, cell taps are crimped and connected via the screw terminal which can account for variable resistive losses contributing to anomalies when recording cell voltages. The physical wiring for the cell taps may also be prone to $\frac{di}{dt}$ noise on varying cell voltages, as well as parasitic capacitive and inductive coupling with nearby HV high-current cabling. Despite this, the majority of cells within the pack reported to be within the expected threshold for cell resistances, which implies the internal resistance issue remains likely to be a wiring, cell or BMS input concern.

Throughout testing, the BMS was configured to disengage the discharge enable pin if the current limits on the batteries exceeded the pack discharge current limit. Testing the BMS under-load resulted in the inverter and motor cutting out, due to the discharge enable pin disengaging the 12 V supply to the inverter. The cause of this was the current limit calculation, which among other variables, uses cell resistance to determine safe discharge current limits. Because of how cell resistance requires flowing current to calculate, the inverter would often operate until a high enough current for the BMS to calculate internal resistance; at which point, the discharge current may be exceeding the new calculated allowable current limits, causing the BMS to shut off connected peripherals.

HiCEV previously operated under EVCM control which makes it difficult to conclude when the discharge current limit enforcement first became an issue. The reason for this, is that using EVCM for control and start-up, resulted in bypassing the BMS discharge enable, and thus, the current limit enforcement. Though it is possible to continue using the pack with discharge current limit enforcement disabled through Orion BMS software, establishing the health of the cells in question remains highly important, as cell longevity has considerable bearing on the long term reliability of HiCEV. BMS calculations can be verified by performing a discharge test and using cell voltage drops to determine the internal resistance of the cells.

The test set-up consisted of a large 4.6 Ω load which was connected across the battery pack, which was used to discharge the cells at approximately 80 A. This known current enabled the BMS to calculate the internal resistance of cells in the pack, by measuring the voltage drop across the cell throughout discharge; similarly, the testing used multimeters, to measure the specific cell voltages before and after the load was applied. The measurements were used with ohm’s law, such that the voltage drop across the cell, with a known loading current could be applied to calculate the exact internal resistance levels using the equation below.

$$R_i = \frac{V_{oc} - V_{cc}}{I} \quad (14)$$

Several cells within the pack were flagged as ‘high-risk’ for testing purposes, due to BMS measurements, or physical visible damage to the cells. Initial testing used multimeters which are accurate to 3 sig. fig., used to verify the test set-up, and calculate approximate internal resistances for the given cells. The results of this test can be seen in Table 7.

Table 7 Battery Cell Calculated Internal Resistances compared to Orion measurements.

Cell Number	Open Circuit Voltage (V)	Closed Circuit Voltage (V)	Measured Resistance (mΩ)	BMS Reported Resistance (mΩ)
23	3.35	3.23	1.54	7.07
54	3.34	3.21	1.67	1.09
56	3.34	3.19	1.92	7.04
69	3.32	3.17	1.92	1.80
71	3.39	3.18	2.69	6.35
80	3.31	3.07	3.08	5.82
98	3.35	3.20	1.92	0.96

The readings from this test were substantially different from the measurements as calculated by the BMS. Despite this, the testing method was limited in that the precision of the multimeters used was low, and the discharge current was decreasing throughout the test period from 80 A to 77 A, influencing measured results. For this reason, the test was repeated with higher precision Fluke 8845A multimeters, which operated to 5 sig. fig., whilst live data was recorded by the BMS such that the voltage drops observed on the cell taps could be directly compared to voltage drops on the multimeters. The results of this test can be seen in Table 8, where cells 23, 71 and 80 were selected due to their reported cell resistances and their accessibility within the pack for measurements.

Table 8 Battery Internal Resistances, and Discharge Voltages, compared with Orion measurements.

Cell Number	Open Circuit Voltage (V)	Closed Circuit Voltage (V)	BMS Open Circuit Voltage (V)	BMS Closed Circuit Voltage (V)	Measured Resistance (mΩ)	BMS Reported Resistance (mΩ)
23	3.27350	3.18016	3.3256	2.8250	1.19667	7.44
71	3.26951	3.17502	3.2080	2.8460	1.21141	6.06
80	3.28901	3.10823	3.2823	2.7864	2.31769	5.79

It is clear from this, that the cell voltages are not dropping as substantially as the BMS reads under-load, and that the open-circuit voltages are slightly mismatched to the BMS readings from the cell taps. The likely cause of this drift is due to faulty cell tap wiring, or an internal BMS measurement issue. For this reason, the BMS cell taps were removed and probed with a multimeter to determine the resistance between the cell terminals, and the connection to the BMS. What was found, having measured all cells from 70 to 90, was that there were no anomalies with the resistances from the cell to the BMS, with all measurements being within the range of 0.017 mΩ and 0.019 mΩ. From this finding, it was determined that the likely source of the battery issues stemmed from a measurement issue within the BMS; to verify this, a back-up Orion BMS 2 was connected to HiCEV to compare results. Table 9 shows the calculated internal resistances for various cells in the tests using the Orion BMS 2.

Table 9 Internal Resistances from Discharge Test using Orion BMS 2.

Cell Number	Measured Resistance (mΩ)	BMS 2 Reported Resistance (mΩ)
23	1.54	3.08
54	1.67	1.20
56	1.92	2.18
69	1.92	1.13
71	2.69	1.76
80	3.08	1.77
98	1.92	1.14

The resistances from this test more closely resembled the calculated resistances from discharge testing. Despite this, cell 23 remained to show a significantly greater internal resistance than measured, likely highlights a loose cell tap, or damage within the cell. As cell 23 is located beneath the cab of HiCEV, it is difficult to ascertain this, the cell tap has been tightened, though the crimp cannot be easily modified due to its positioning under the vehicle. Given the results of this test, some internal resistances do indicate a declining state of health within the pack. Prior to returning

the vehicle to the sponsor, it is also advisable that the BMS is replaced with the BMS 2, however, due to the extent of rewiring involved this is impractical for short term testing. To continue testing, the BMS software has been modified to disable the discharge current limit enforcement, such that the BMS can continue to be used.

It is also plausible that the cell resistances change over the period of continuous discharge, contributing to the high variance in cell resistances as calculated by the BMS 1, BMS 2 and external voltage probes. To properly ascertain the performance of cells, replacing affected cells is the most viable method to determine whether BMS concerns are due to cell state of health, or BMS hardware faults. Notably, BMS 2 tests were measured over a shorter discharge period, as the objective of the BMS 2 tests were to see the calculated internal resistances on the BMS 2, as opposed to record data manually, which was extending the period of the testing. In a similar vein, the data manually recorded throughout testing is somewhat compromised due to the period of discharge affecting exact voltage measurement.

To verify the findings, the battery voltages were monitored using the BMS 2 and an oscilloscope for the duration of 20 seconds with a known discharge current of 80 A. Using the oscilloscope data was logged, such that the measured voltage throughout the test can be directly compared to the voltages measured by the battery management system. The results of this test, measuring cell 71, can be seen in Figure 46.

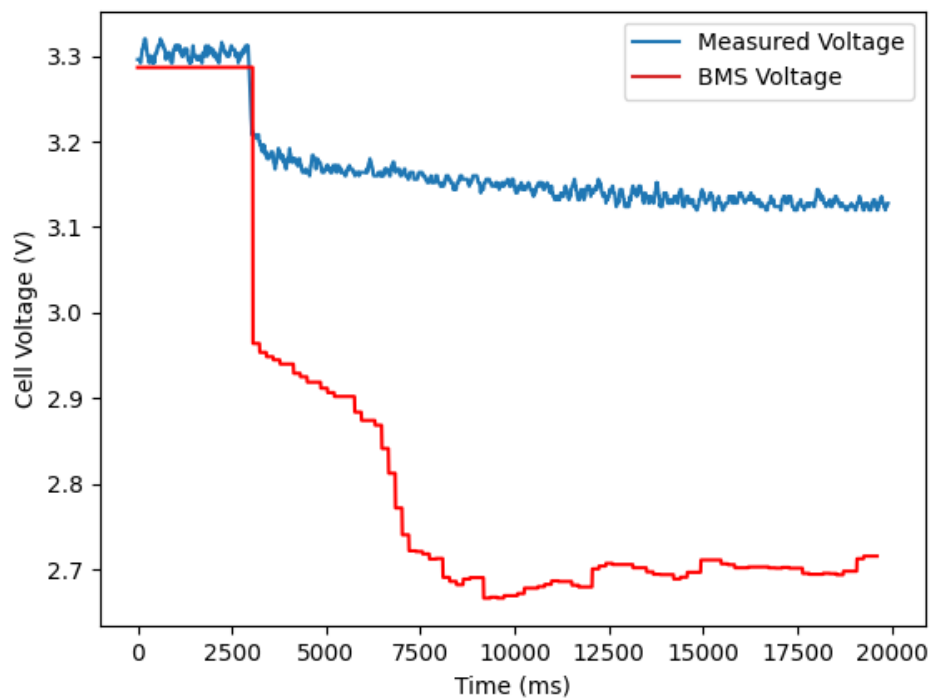


Figure 46 Cell 71 Voltage Measurements over 20 s measurement period.

The results in Figure 46 show the battery voltages as measured by both the BMS and an oscilloscope on the same time scale. Notably, this shows a large disparity between the BMS monitoring and the physical battery voltage, indicating either cell tap wiring or a BMS voltage measurement issue as a probable cause for the fault.

To verify if the issue was due to wiring, cell 71 and 69 were swapped in the battery pack and the Orion BMS 2 was wired into the system fully, with the expected result being the faulty cell would move in the pack, thus moving the fault as measured by the BMS. The full internal resistance calculations from this test can be seen in Appendix 5 where cell 71 and 69 have been marked. Given the results of this test, that the fault persisted with the BMS 2 installed, and the fault did not move with the battery cells, it is most likely that the fault is a wiring issue which remained constant between all tests. Due to time constraints, fully rewiring the cell taps unfeasible, however, the findings are positive as it indicates that cells within the pack are physically still safe to use.

As the batteries were removed from the vehicle to perform the above tests, benchtop discharge testing was also carried out to further verify the results of the above tests. The cells which were tested were 69, 70, 71, and 80. Cells 69 -71 were tested to get a benchtop comparison of cell internal resistances and voltage drop when discharging the cells independently of the pack, cell 80 was also removed from the vehicle as when measured, the cell voltage was considerably below the average voltage of the surrounding cells. The cells were each discharged at 50 A, for a period of 5 minutes, over which the voltage drop was measured. Table 10 below shows the results from this test.

Table 10 Benchtop Cell discharge test

Cell:	Start Voltage Open Circuit (V)	Start Voltage Closed Circuit (V)	Estimated Cell Resistance (mΩ)	End Voltage Closed Circuit (V)
69	3.32	3.25	1.4	3.17
70	3.31	3.22	1.8	3.15
71	3.32	3.24	1.6	3.16
80	3.23	3.12	2.2	3.04

The results of this test verify in a more controlled environment that the internal resistance for several cells in the pack is within normal ranges. Despite this, when recharging cells back to the initial 3.32 V starting point to rebalance cells with the pack, cell 80 had a rapid voltage drop back to 3.26 V, indicating possible cell damage which is worth further investigation.

4.2.6 Charger Thermal Testing

The CurentWays charger in HiCEV is rated to operate up to 3 kW, making use of a water-cooling system consisting of a radiator, and a pump controlled by the charger itself. Notably, due to the relatively low power output of the charger, a fan is absent from the cooling system, limiting the radiators effectiveness. The charger itself, drives a cooling relay based on internal charger temperature measurements, where at 40 °C the charger enables the cooling system, switching on the pump. The charger power output is also temperature dependant, as the operating power begins to decline from 55 °C and reduces power output to 0 at a temperature of 75 °C. Table 11 shows temperatures taken from a 6 A (approx. 2200 W) charge over the course of 3 hours to determine the operation temperature under typical charging conditions. The results were measured using a thermocouple to determine both the ambient, and approximate charger temperature through surface temperature measurements near known hot points on the charger.

Table 11 Charger Thermal Test Results.

Time (minutes)	Charger Temperature (°C)	Ambient Temperature (°C)
0	28.0	24
5	32.3	24
10	37.1	24
15	43.1	24
20	43.3	24
25	41.5	24
30	42.7	24
60	50.5	25
90	54.7	25
120	45.6	26
180	45.4	25

This initial test also verified the functionality of the charger I/O pins which were being applied for peripheral control. This can be seen in the data from 20 to 25 minutes, where the measured temperature begins to decline because the water pump turns on at 40 °C. From this test, it also became clear that at the 90-minute mark, the pump alone would not suffice as a long-term cooling solution for the charger; for this reason, a small AC fan was set up to produce some airflow over the radiator, which rapidly reduced the temperature of the system (detailed below). It is reasonable to conclude from this, that the coolant flowing in the system was sufficiently operating to cool the charger, however, without the radiator airflow, the coolant itself was heating up reducing the performance of the cooling system. To rectify this, a fan should be installed in HiCEV to sufficiently cool the charger.

Follow up testing was performed with an AC fan temporarily stationed to maintain low airflow through the radiator to verify this finding. The results of this test can be seen in Table 12.

Table 12 Charger Thermal Test with Airflow Applied.

Time (minutes)	Charger Temperature (°C)	Ambient Temperature (°C)
0	22.3	23
5	31.2	23
10	35.6	23
15	36.2	23
20	37.2	23
30	39.3	22
60	41.4	22
90	41.9	20
120	42.6	20
180	42.8	20

Throughout the charge period of 3 hours, the temperatures of the charger did not exceed 43 °C which is substantially within the ideal operating limit of below 55 °C. However, the measurements taken by the external thermocouple do not precisely represent the internal temperatures for the charger, this was apparent when the pump switched on at 34.4 °C, 7 minutes into testing, where it is set to turn on at 40 °C. Despite this, the trend observed shows that the charger temperature increases slowly later into the test, which implies that the cooling system is approaching an equilibrium wherein energy expelled by the charger is similar in magnitude to the energy being expelled by the cooling system, and the thermal fluid in the cooling loop is a relatively stable temperature.

4.3 Inverter

The inverter manages most of the control within the vehicle as well as monitoring of motor characteristics during operation which are reported to the end user for debugging information. Throughout testing, the software was modified in the inverter to achieve a more reliable end result, based on the vehicle performance, and issues as they arose. For the most part, perceived reliability issues with the inverter were resolved by diagnosing issues with the battery management, however, optimisations were made to facilitate reliable and safe operation for the end user. The inverter testing can be partitioned into functional, ensuring systems work as intended, and operation testing, where the vehicle performance can be scrutinised more closely via data reported through the RS232 ports.

4.3.1 Inverter Functional Testing

The inverter software operates under a state machine which integrates with various peripherals within the vehicle. The state machine operates as a checklist which the vehicle performs on start-up, wherein, each state moves forward to the next state based on the conditions met through integrations with peripherals. The most important components of this are the integrations made with the ignition, pre-charge, BMS, and core control inputs. Inverter software enables monitoring of these systems during general operation, to see how the vehicle responds given various control inputs.

The inverter is set-up such that the pre-charge occurs when 12 V is first applied to the control stage, which occurs when the BMS is powered on and enabling discharge, and the ignition switch has been activated. Pre-charge testing, through powering on the inverter, has shown that the feature is operating as intended. For safety purposes, when pre-charge fails, usually because the isolation switch is open, the inverter registers a DC bus under-voltage fault, that requires the inverter to be power cycled. In practice, this is unlikely to cause any major damage, however, this is important to note as the pre-charge system also controls the main bus relay, which when closed directly connects the vehicle batteries to the inverter bus capacitance, which could enable high transient currents that could be damaging to the vehicle. When the pre-charge is successful, the main relay is closed and the inverter moves on to checking for peripheral inputs.

The peripheral inputs, namely, the accelerator potentiometer, the forward enable switch and brake switch are essential for the inverter to move into a drivable state. The state machine checks whether the vehicle accelerator potentiometer is within the allowable range for start-up, which is between the minimum programmed voltage for the potentiometer, and the minimum accelerator input, where torque begins to be applied. If this condition is met, when the brake and forward enable switches are grounded, the vehicle moves into a driving state. Given HiCEV's manual transmission, the forward enable is grounded as the gearbox can be used to drive the vehicle in reverse; thus, by pressing the brake pedal, the vehicle moves into a drivable state. From extensive testing, start-up issues typically arose from the BMS (discussed in section 4.2.5), as opposed to the Inverter; given that the inverter power is reliant on the discharge enable functionality.

The inverter functionality during operation then becomes contingent on the peripheral reporting as well as its integration with the BMS to ensure it does not exceed current limits. It is worth noting that the BMS reports maximum discharge and charge current limits to the inverter in real-time, however, these variables differ from the discharge current limits calculated by the BMS. The maximum limit, is a calculated current limit based on the battery chemistry and state of charge; whilst the instantaneous current limits are calculated by the BMS based on real-time monitoring of cell temperatures, resistances and the pack estimated state-of-health. This difference is important to

consider, as during testing, it was assumed shut-downs were the result of inverter software concerns, as opposed to the BMS. This was assumed because the inverter software reportedly updates control in real time to the limits reported by the BMS, which under normal circumstances would not allow current limits to be exceeded. Because of this, the inverter control software was modified to better reflect the operation of the inverter under its own control, as opposed to the EVCM control, as concerns were raised to whether inverter software was causing unwanted behaviour.

4.3.2 Inverter Software Modifications

Reliability during initial testing phases was sub-par, with the motor cutting out during driving on various occasions at low-speed. Initial debugging, suggested that this was likely due to parameter values set within the inverter software, as the BMS had not logged any faults. Additional modifications were also made to inverter software to acclimate the control to the driving conditions within HiCEV, where control parameters, like torque limits, had a substantial bearing on driving experience.

In the initial testing phases, one of the most noticeable trends was in the DC bus voltage that was substantially lowering under high-loading currents. This typically coincided with vehicle shut-down events, which put attention on the inverter's allowable DC bus voltages. The inverter has a range of allowable bus voltages, which spanned from 220 V to 400 V, based on the inverter's minimum rating, and the maximum probable battery pack voltage. However, it also had an allowable hysteresis voltage, which was rated at only 30 V, such that when the voltage of the DC bus drops by 30 V during discharge, it would reduce torque commands. From the recorded data, it could be seen that shut-down events while driving typically coincided with exceeding this 30 V hysteresis range; to compensate, the vehicle allowable DC bus hysteresis was updated to allow the bus voltage to sag by as much as 80 V under load, which is consistent with the expected bus voltage under high-current discharge. However, modifying this made the vehicle more unreliable, with shut-downs common while accelerating at low-speeds. Vehicle shut-down events are highlighted in Figure 47, showing the DC current drop to 0 instantaneously, on a voltage drop of 30 V.

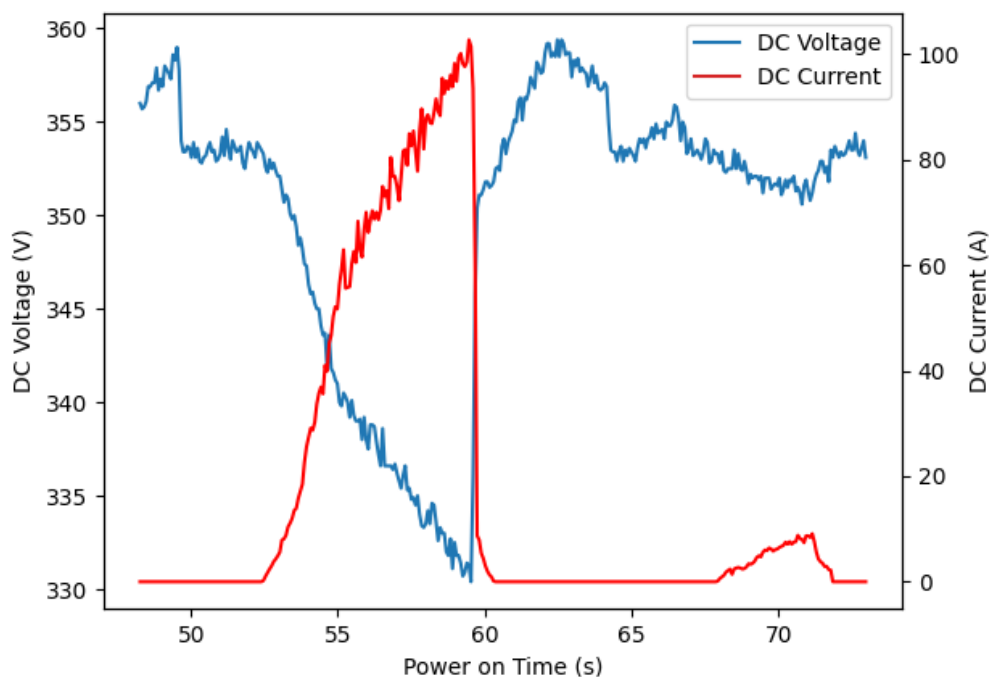


Figure 47 Inverter Current dropping to 0 on shutdown, compared to voltage hysteresis.

Further testing yielded that the BMS was the cause of these faults (as discussed previously), shutting down the vehicle, by disabling the discharge enable pin, thus immediately powering off the control stage for the inverter. The likely cause for the BMS shutting down the inverter, is that at high currents the BMS recalculates the internal resistances for the cells in the pack, it is potentially coincidental that this occurred at voltage drops resembling the hysteresis parameter in the inverter software. The DC voltage hysteresis may have been contributing to increased reliability when testing at low speeds, as the torque commands were scaling to prevent high-current discharges which were triggering the BMS to shut-down the vehicle. Despite this, due to realistic operating conditions, established in Peirce Hennessy's work, the variable has been left to allow a voltage drop of 80 V before scaling torque commands [14].

Motor and vehicle operating parameters were also closely scrutinised as a result of the vehicle shut-downs and debugging. It became apparent from this that many of the motor parameters in the inverter software left a buffer region to prevent the inverter software from reducing commands given by the previously installed EVCN via CAN. When the inverter was switched over to control the vehicle, these parameters were involved with controlling torque and current for the motor, which were above the motor ratings. This was modified to prevent any issues that may arise from applying overly heavy current commands to the motor when under load. Inverter parameters that were modified can be seen in Table 13. Modifications were made based on the allowable parameters specified by the inverter manufacturer [21].

Table 13 Motor parameters updated in inverter software.

Parameter	Former Value	Updated Value
IQ Limit, ID Limit	495 A	425 A
Motor Over-Speed	12000 RPM	10000 RPM
Break Speed	3600 RPM	1700 RPM
Torque Limit	410 Nm	320 Nm

The manufacturer specifies parameters based on the inverter, bus voltage and motor, which have been updated to represent the set-up in HiCEV. Notably, these parameters assume a bus voltage applied of 320 V, which due to operating conditions, is unlikely to occur in practice. Under load, the DC bus voltage is likely to drop by as much as 80 V due to the internal resistance of the pack at high operating currents, this will likely affect the realistic torque and currents that are applied to the motor. Due to ongoing testing on the batteries, the break speed was reduced from 3600 rpm to 1700 rpm. The break speed is the threshold at which the inverter current commands begin to reduce to accommodate the motor at constant power operating speeds. Reducing the break speed parameter to 1700 rpm is to produce the desired effect of reducing the peak DC current loading on the batteries during testing. It is also worth noting based on previous testing performed by UC students a DC voltage to drop to as low as 290 V when accelerating is to be expected; the parameters above assume 320 V, notably, when break speed is returned to 3600 rpm the performance may be hindered by the bus voltage [14].

Drivability is also a major consideration when programming inverter parameters as many hardware limited parameters are impractical for real-world conditions. For HiCEV, regenerative braking and coasting torque are such examples of parameters for which pushing the theoretical maximum is impractical for usability. Several test drives were used to update these parameters for practical operation. Due to the hardware set-up, HiCEV has two modes of regenerative braking, through coasting, from the driver lifting their foot of the accelerator, or active braking, from triggering the

brake switch. Coasting occurs frequently when driving, and from testing has been set to regenerate at a braking torque of 40 Nm, whilst braking causes regeneration to ramp braking torque up to 120 Nm. These parameters were determined as the result of a limitation of HiCEV's hardware, being that it uses a braking switch as opposed to a braking potentiometer. Consequently, pressing the brake results in ramping up to maximum braking torque, as opposed to controlling braking torque based on how depressed the pedal is. This will affect the overall efficiency as when braking heavily, the regenerative braking will be limited to the peak regen torque of 120 Nm.

4.3.3 Inverter Thermal Testing

Throughout operation, the inverter self-reports the internal operating temperatures through the RS232 interface. With this, the temperatures can be monitored and compared under various testing conditions. The primary source of heat in the inverter stems from conduction and switching losses within the power switching devices (IGBTs). Under high current, these losses are increased, contributing to an increased expected thermal loss on the system. This trend can be observed in Figure 48, when comparing the DC current with the operating temperature for the inverter throughout recorded testing periods.

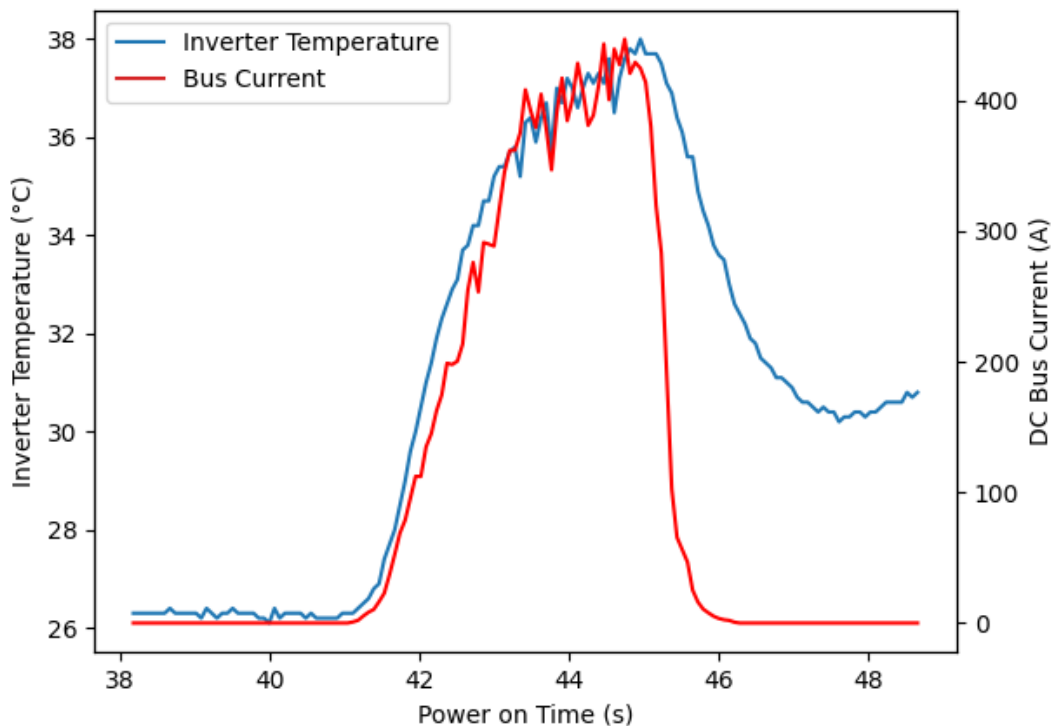


Figure 48 Inverter Temperature and Current Profile

Inverter programming limits the DC current to approximately 175 A during typical operating conditions, however, a simple discharge test does not illustrate the expected thermal efficiency of the cooling system under sustained discharge. Under long-term operating conditions, the coolant within the system is likely to heat up contributing to decreased thermal efficiency, however, conversely, the vehicle is unlikely to maintain high current discharge throughout the period of operation. To gauge the cooling performance of the inverter cooling loop, HiCEV was driven for approximately half an hour in various gears, performing stop-start and acceleration tests. Though this is not a perfect representation of the realistic operating conditions for the vehicle, acceleration requires substantial power and current contributing to abnormally high-power usage at low speeds. The results of this test can be seen in Figure 49.

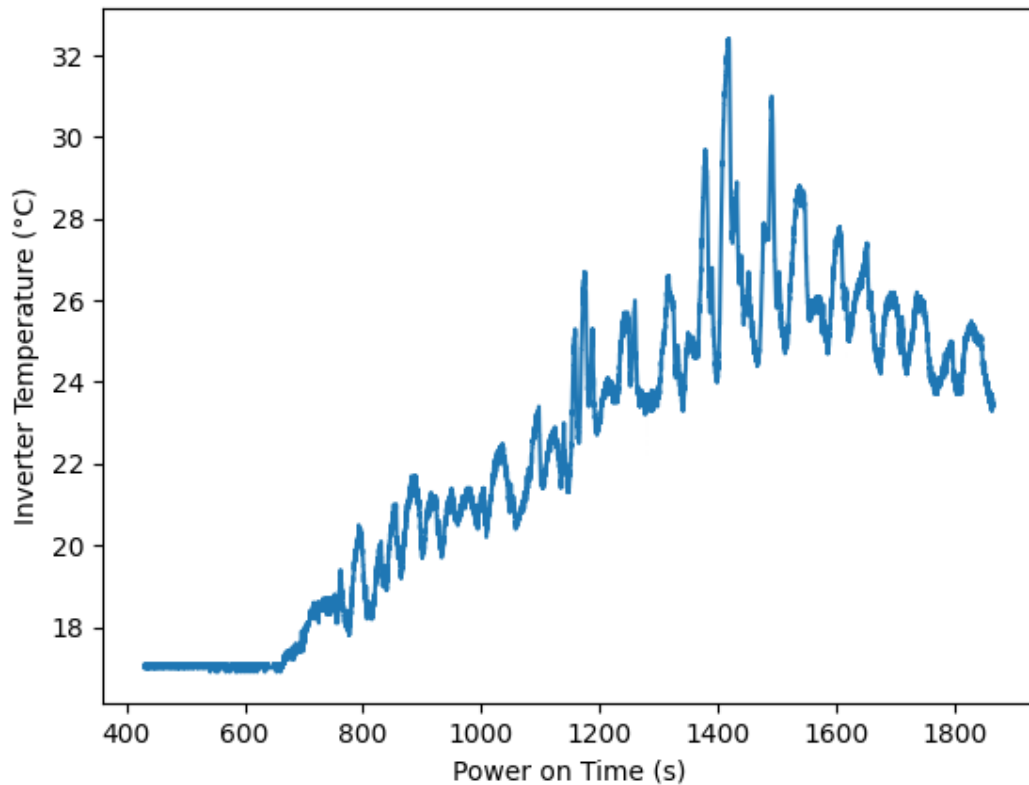


Figure 49 Long-Term operation Inverter temperature profile.

The average temperature of the inverter notably increased progressively throughout this test, this is likely due to the thermal fluid within the cooling loop increasing in temperature as well. Despite this, for the duration of this test, the temperature was maintained below 32 °C, partly this was due to the low ambient temperature of 17 °C at the time of testing; however, this remains substantially below the 60 °C thermal performance de-rating for the inverter.

4.3.4 Operational Testing

The built-in motor control for the inverter converts a simple potentiometer input into a torque command to be applied to the motor based on a variety of software parameters. This torque is modulated using quadrature and direct components of current which are applied to the stator windings. When operating, the magnitude of the currents, notably the quadrature current, should reflect the torque command, as the two properties are proportional. Overlaying the two parameters, as seen in Figure 50 below, shows that the accelerator input closely resembles the current applied to the motor. In EV's this is an important parameter to maintain as torque control resembles the ICE vehicle throttle control many drivers are accustomed to, as opposed to speed control. In practice, this results in a greater acceleration when the pedal is depressed as desired.

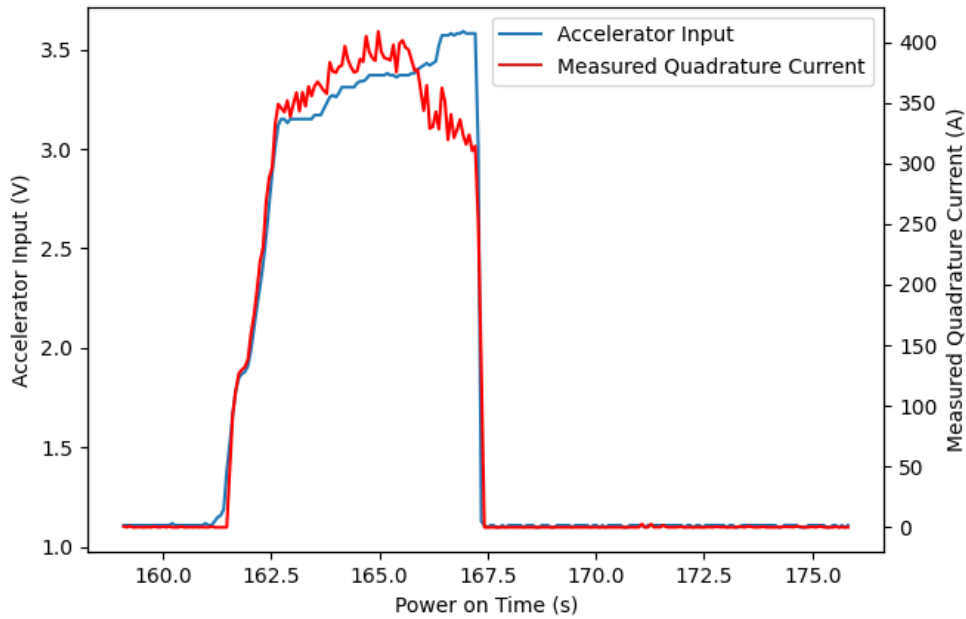


Figure 50 Quadrature Current vs Accelerator Input

Inverter software, as well as motor hardware characteristics have imposed limitations on the magnitude of current available at high operating rpm due to the break speed for the motor. Additionally, the full operating range for the acceleration input is clamped due to the ‘coasting’ ability built-in to the inverter, which applies regenerative braking to the motor at low input voltages.

Comparisons can be made between the requested and measured values for the applied quadrature currents to determine the source of current limitations within the vehicle. Figure 51 shows this relationship, where it is apparent that the software is reducing the quadrature current commands due to the motor reaching the programmed break speed, as opposed to the motor back-EMF limiting the motor current. This is an expected result as the inverter parameters assume a DC bus voltage of 320 V, when HiCEV operates with a 360 V bus voltage.

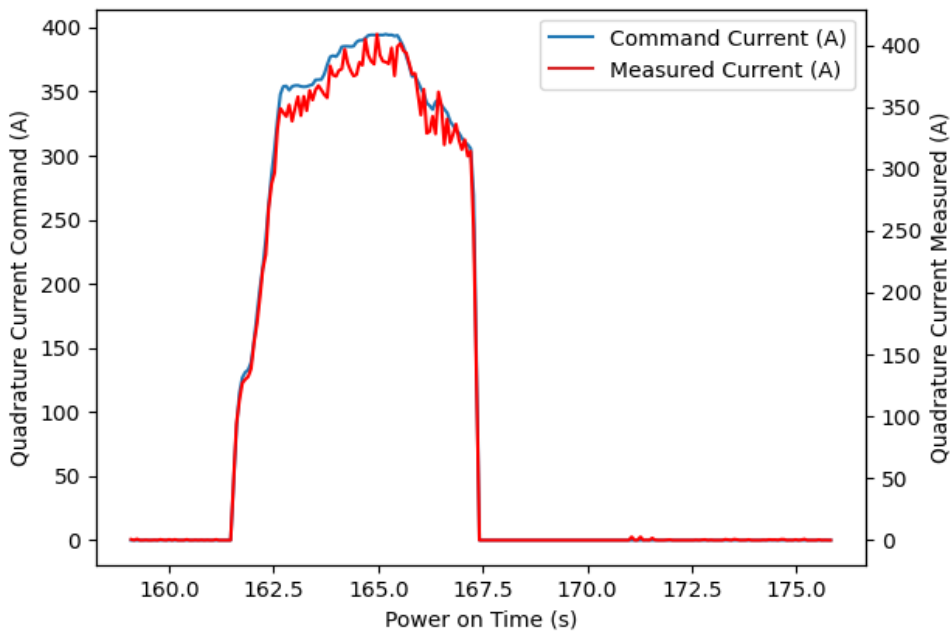


Figure 51 Requested Quadrature Current vs Measured Quadrature Current

Based on the results of battery testing, as well as the known bus voltage sag to occur within HiCEV, it is desirable to continue operating with the current limits as seen in the tests performed above. This does clamp the peak power output for the vehicle, however, low-speed torque availability is still present, which is useful when operating the vehicle in farm environments. The power availability for the vehicle can be increased by increasing the 'break speed' variable to be appropriate to the bus voltage. It is also worth noting that at low state of charge, the bus voltage in HiCEV will be below the 360 V nominal, and during normal operating conditions, the bus voltage is likely to drop considerably.

4.3.5 Vehicle Efficiency

The inverter self-reports information that can be used to estimate the vehicle's efficiency at various stages of acceleration. Notably, using the voltage and current measurements, the input power can be established by simply finding the product of the DC bus voltage and the DC current. Similarly, the motor power, or output power from the DC/DC converter, can be estimated by using mechanical parameters of torque and motor speed. Efficiency estimates can be made by dividing the output power by the input power. Figure 52 shows the electrical efficiency as reported by the inverter throughout an acceleration test, where the motor speed is provided for reference.

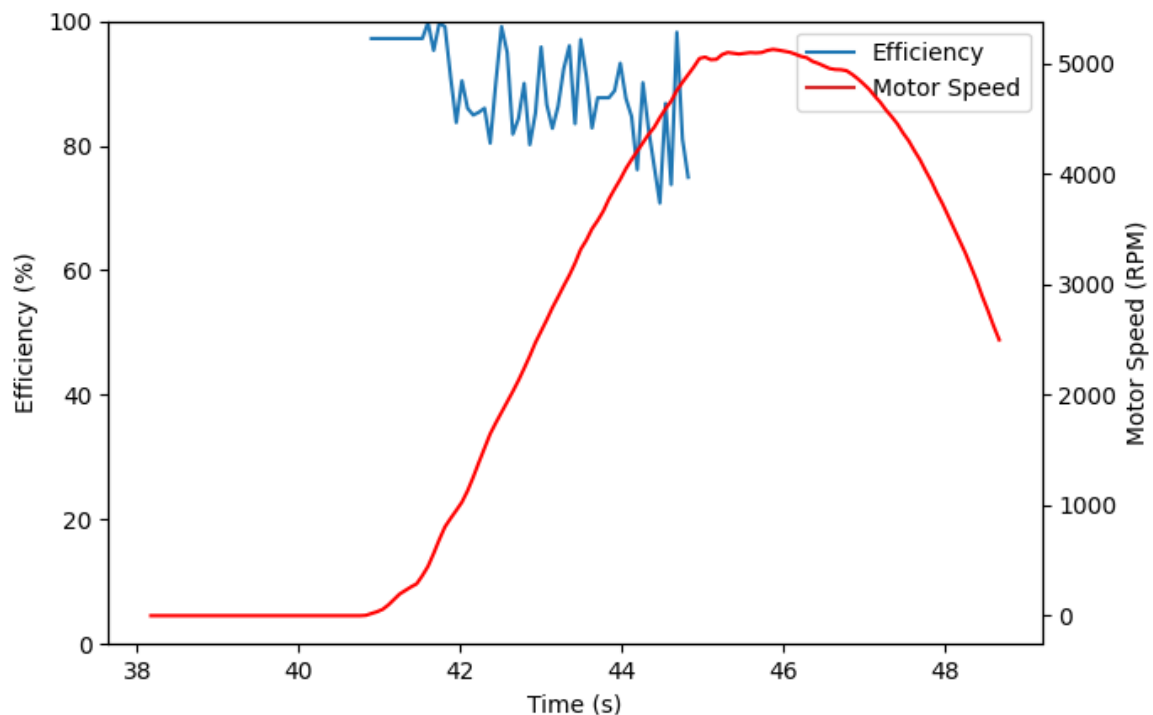


Figure 52 Efficiency vs Motor Speed

For the majority of the operating range, particularly at lower speeds, the efficiency is within reported ranges for the inverter and motor combination, with the Inverter rated for 96%, and the motor rated for 85 – 95% varying with exact operating characteristics. It is worth noting that from this test the efficiency estimates have been established from reported data from the inverter, with measurement inaccuracies associated with the operating environment. A full graph of the calculated input (electrical) and output (mechanical) power, can be seen in Appendix 6.

4.4 Motor Characteristics

The variable frequency drive controller in the inverter enables the motor to be controlled via torque commands, which can be used to characterise the torque-speed parameters for the motor.

Following the results of battery testing, the motor testing was performed with the maximum recommended 'break speed' of 3600 rpm, enabling motor testing to be performed at the full power the inverter is rated for. The inclusion of the gear box and differential in the powertrain for HiCEV also facilitates low speed testing of vehicle characteristics using low gearing options to achieve high motor speeds at low vehicle speed. The results of one such test, in 1st gear can be seen in Figure 53 below, where the vehicle was accelerated with maximum torque commands until the vehicle speed reached 40 km/h.

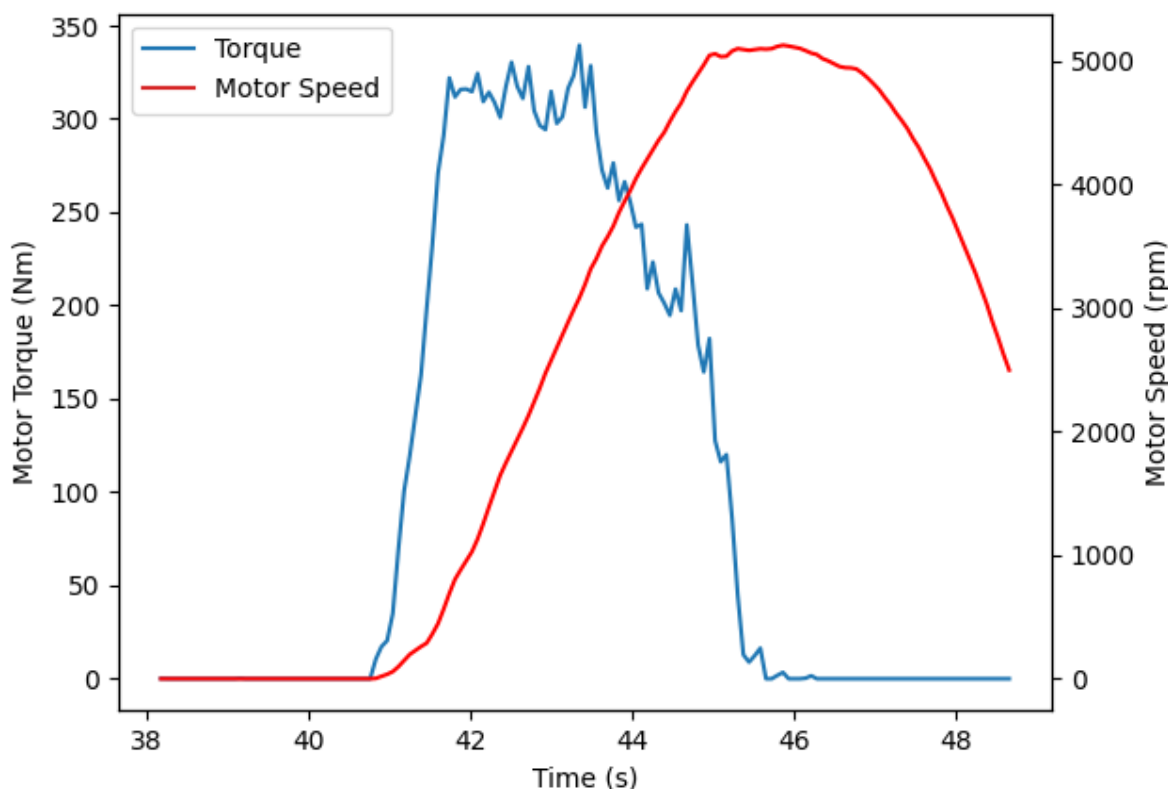


Figure 53 Torque and Speed Characteristics 1st Gear Acceleration.

It becomes apparent that at higher motor speeds, the torque output for the motor begins to decline. In these tests, the break point for the motor was at 3600 RPM, and the maximum motor speed was 5000 RPM, both of which were enforced by the motor controller in the inverter. Under this break speed, the practical operating speed for the motor in various gears can be estimated based on the motor speed requirements and the gear ratio for the original Land Cruiser. Table 14 below shows the vehicle speed at which the motor will reach the break and maximum speed in each gear.

Table 14 Motor Break Speed per Gear

Gear	Break Speed (km/h)	Max Speed (km/h)
1	28.2	39.1
2	52.3	72.6
3	84.9	117.9
4	122.0	169.4
5	145.5	202.1

As expected, the test showed a noticeable break speed which occurred at approximately 3600 rpm. In higher gears, the motor torque remained constant at 320 Nm for the duration of the acceleration test, and did not reach the break speed. The peak power output for this was approximately 130 kW, a considerable improvement on the original ICE powertrains 95 kW output. Additionally, due to electric motor torque speed characteristics, the acceleration at low speed is noticeably greater than ICE counterpart vehicles, due largely to the torque-speed characteristic exhibited by the system.

The results for the power-speed characteristics similarly exhibited the expected trend when performing low speed testing. In lower gears, it was possible to observe the vehicle ramp up in power output linearly proportionally to the rotor speed under a constant torque until the break speed, where the power output stabilised in the constant power region of operation. Like the previous results, the motor characteristics are largely dictated by inverter software controls limited in part by the bus voltage, rather than hardware limitations in the motor. Figure 54 best demonstrates the constant torque region for the motor, with the motor speed being significantly correlated to the motor power when accelerating in 3rd gear.

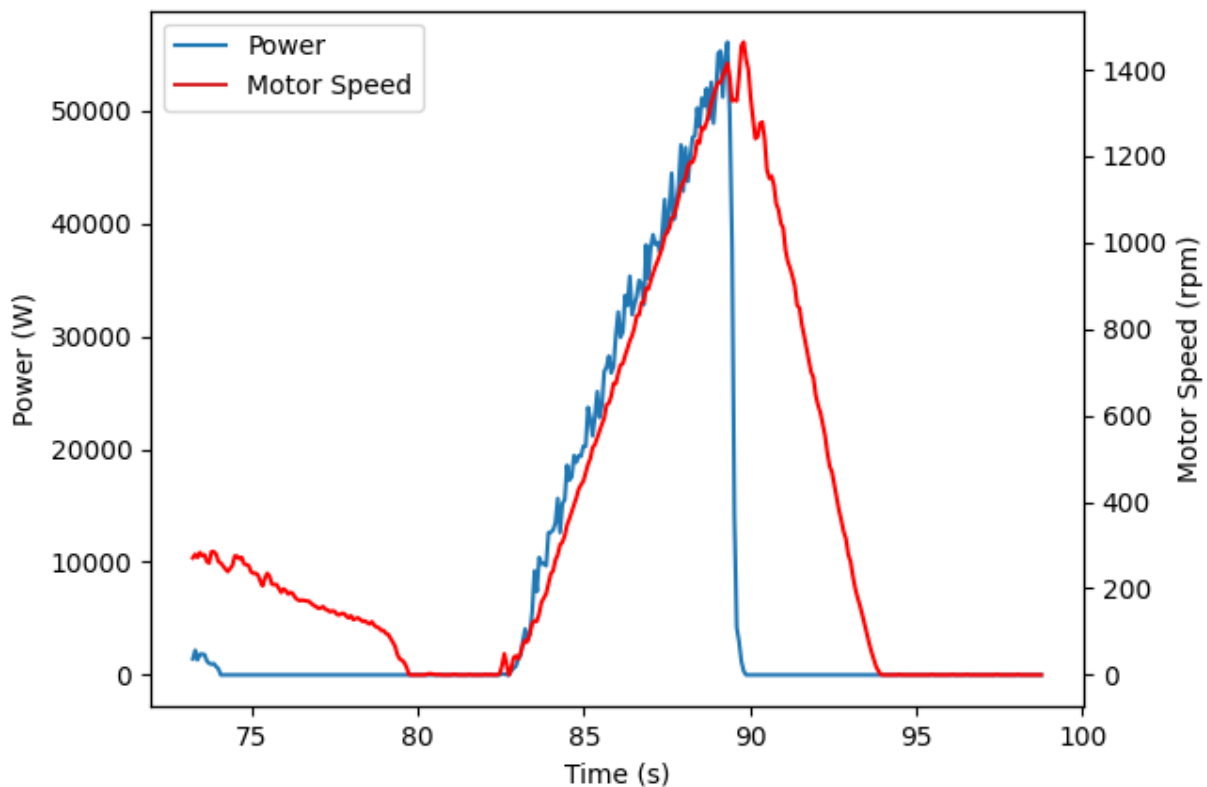


Figure 54 Power and Speed Characteristics in 3rd Gear Acceleration Test

In 1st gear, accelerating exhibits a similar trend with an increasing power at lower motor speeds, transitioning into constant continuous power at higher motor speeds. Given the motor characteristics, this is shown to exhibit the expected trend; it is however worth noting that in the constant power operating region the torque experiences a significant drop off that in practice, results in slowed acceleration, despite operating at a high continuous power. HiCEV gears enable the driver to work around this by changing gear to remain in high torque operation once these motor speeds have been reached. Figure 55 below shows the vehicle power in relation to vehicle speed when performing an acceleration test in gear 1, whilst similarly Figure 56, shows the motor torque for comparison throughout the same test period.

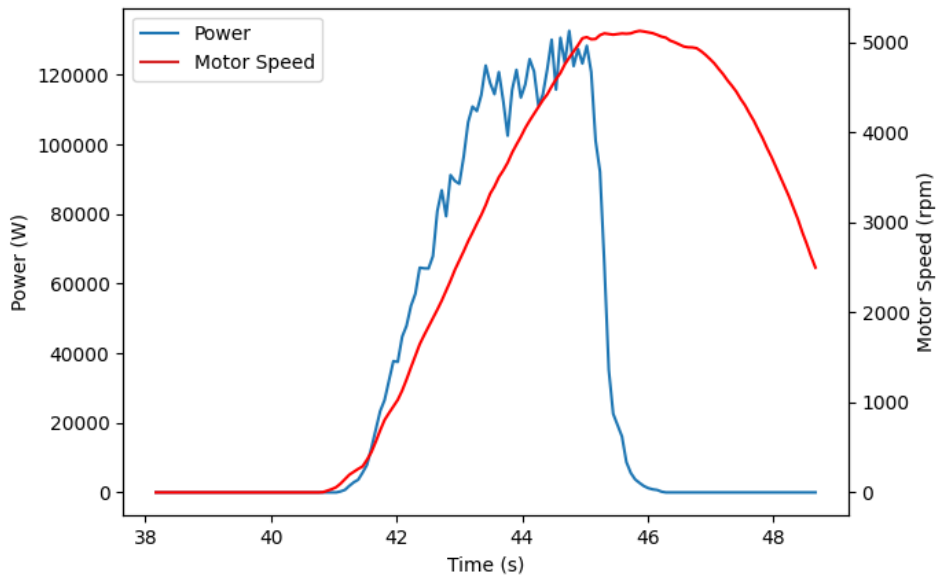


Figure 55 Power and Speed Characteristics during 1st Gear Acceleration test

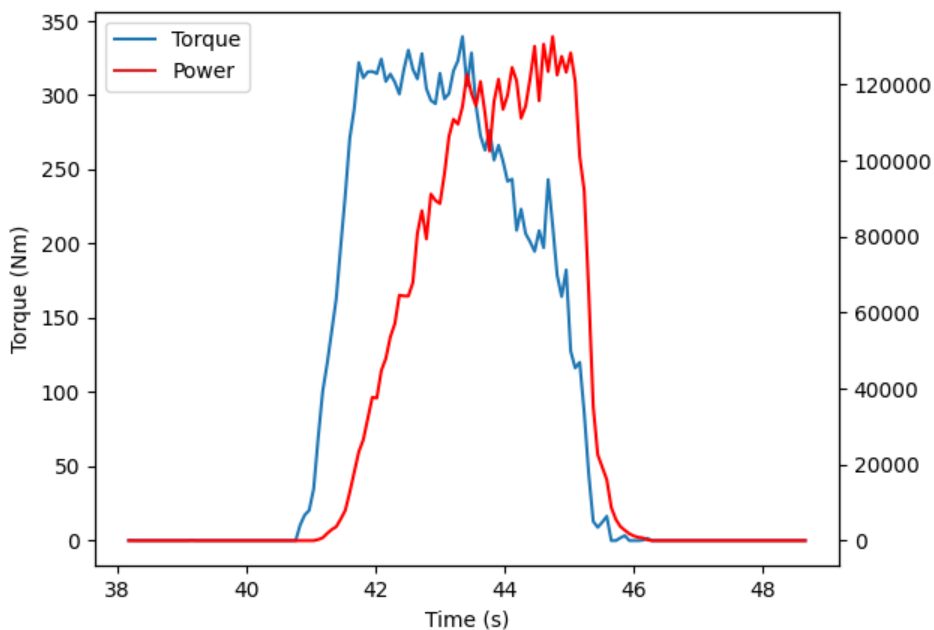


Figure 56 Power and Torque Characteristics during 1st Gear Acceleration test

4.5 DC/DC Converter

Throughout testing the installed DC/DC converter in the vehicle had to be changed due to faulty hardware in the Sevcon Gen 5. The cause for the fault in the DC/DC converter is unknown, however, the Meanwell DC/DC converter previously installed in the vehicle was readily available to continue testing. The Meanwell converter is an RPB-1600, rated for up to 100 A of continuous current, marginally more powerful than the Sevcon solution. Unfortunately, due to the nature of the Meanwell converter requiring open air cooling, it is unable to be pursued as a long-term solution for HiCEV and an alternative DC/DC converter will need to be sourced.

Testing performed on the 12 V systems showed that typical 'idle' currents required by the DC/DC converter are approximately 30 A, with peaks of over 100 A occurring during operation. In large part, these peaks are caused by the use of the power steering pump which can pull up to 60 A under load. To stabilise the system, the DC/DC converter is connected in parallel with the back-up battery to prevent over-loading from the systems causing significant undervoltage on the 12 V bus. When the Sevcon DC/DC converter failed, the most notable symptom was that the vehicle shut-down when loaded up by the power steering pump, this was due to under voltage on the 12 V bus causing HiCEV's peripherals, notably, the inverter, to shut down.

4.6 LV Systems

Low voltage systems in HiCEV consist of all vehicle peripherals, which are driven by the back-up battery and the DC/DC converter. This primarily consists of cooling peripherals for the vehicle, however, included on the bus is the original Land Cruiser wiring loom, designed to operate from the alternator originally installed in the vehicle. The majority of retro-fitted systems were operable

4.6.1. Brake Pump Circuit

The brake pump circuit receives feedback from a vacuum switch mounted in the brake booster vacuum hose, which when grounded, will drive the output on for a set period of 15 s. An issue encountered with this set-up is that the vacuum switch, when vacuum is weak, is susceptible to latch in a grounding position, which causes the circuit to malfunction. This typically occurs when the vehicle has been sitting around for several days without use, or the brake pedal has been pressed while the pump is not powered on. To solve this, temporarily, a switch has been added to the vacuum pump that can be used to manually drive the pump for several seconds to fix the latching condition. Provided the vehicle is used frequently, this is unlikely to provide issues in the future; however, with infrequent usage the pump is susceptible to latching up.

If this becomes problematic in the future, vacuum switches with built in trigger operating regions are available and can be retro-fitted to the brake booster pump. This can be used to directly drive a relay series connected with the pump supply voltage. Alternatively, the trigger circuit could be modified to simply drive the pump at intervals regardless of the vacuum levels in the booster. This is non-ideal as a solution however, as it would mean driving the pump while there is already a vacuum present when the vehicle was sitting 'idle', whilst also potentially providing too little vacuum to drive the brakes for down-hill driving.

4.6.2 CAN Communication

CAN communication is used to integrate the primary peripherals of HiCEV, namely the Inverter, Charger and BMS to each other and PC software. The charging and discharging processes are both controlled by the BMS, as such, the inverter and charger are never powered on simultaneously. CAN bus monitoring occurs within the BMS and Inverter and can be used to report back to the user. To verify the CANbus was operational as expected, it was tested using an oscilloscope, which yielded that the CAN high signal was switching between 0 and 5 V, whilst the CAN L signal remained grounded, which can be seen in Figure 57.

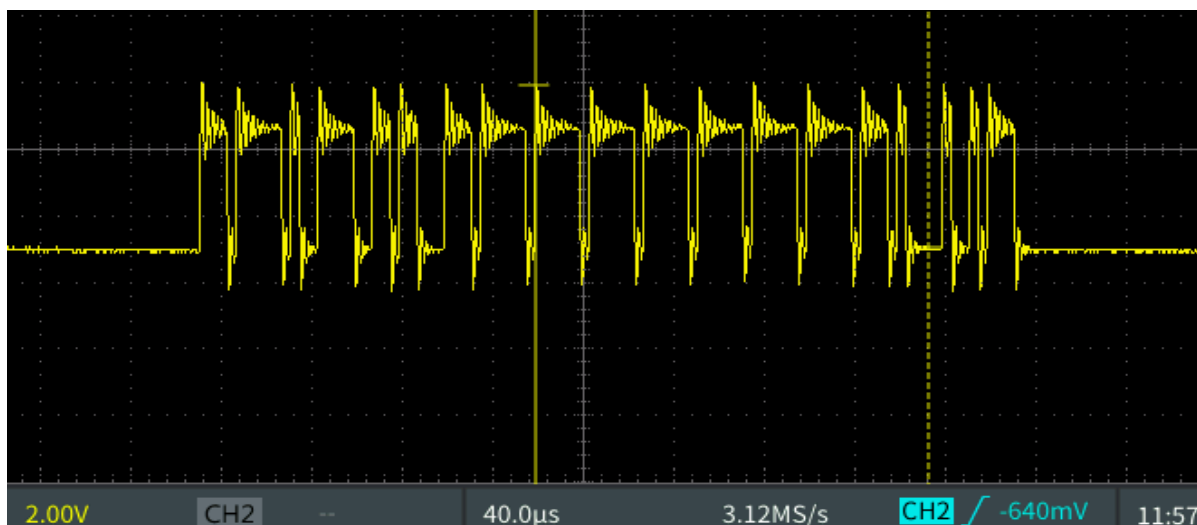


Figure 57 CAN High Signal.

CAN bus operation allows for the bus to continue working while one of the cables is grounded, which meant that this issue likely went undiagnosed for some time. Notable, despite the oscilloscope readings showing this fault, the vehicles CAN communication continued to operate reliably as expected. The message captured in Figure 57 is the BMS reporting maximum CCL and DCL to the inverter, with a message length of 4 bytes, of which, only 2 are used for reporting current limits. This is particularly noticeable, as it illustrates the 'bit stuffing', wherein, the bytes consisting of 0x00 messages have '1' bits in every 5 bits sent, to indicate to the receiving node that a fault has not occurred.

To debug this CAN bus fault, a multimeter was used to test for any short circuit connections within the bus. It immediately became clear that the fault was within the CAN low signal which was being grounded somewhere in the CAN bus. To establish where it was, nodes were disconnected, starting with the BMS, to test for conduction between the CAN shield and the CAN Low signal. Initial testing showed that removing the BMS from the CAN bus resolved the short connection issues, and that on further inspection, the short circuit was internal to the BMS, as determined by the removal of the main I/O header from the BMS resolving the short circuit. Fortunately, this error has an easy work around using the Orion BMS, as the BMS has 2 independent CAN buses, wherein the second CAN bus requires an external termination resistor. Alternatively, given issues previously experienced with the BMS, it is also viable to replace the BMS with the BMS 2 model, which should have working CAN bus connections. The initial response was to use the second CAN bus in the BMS 1, which required external termination, the results of which can be seen in Figure 58.

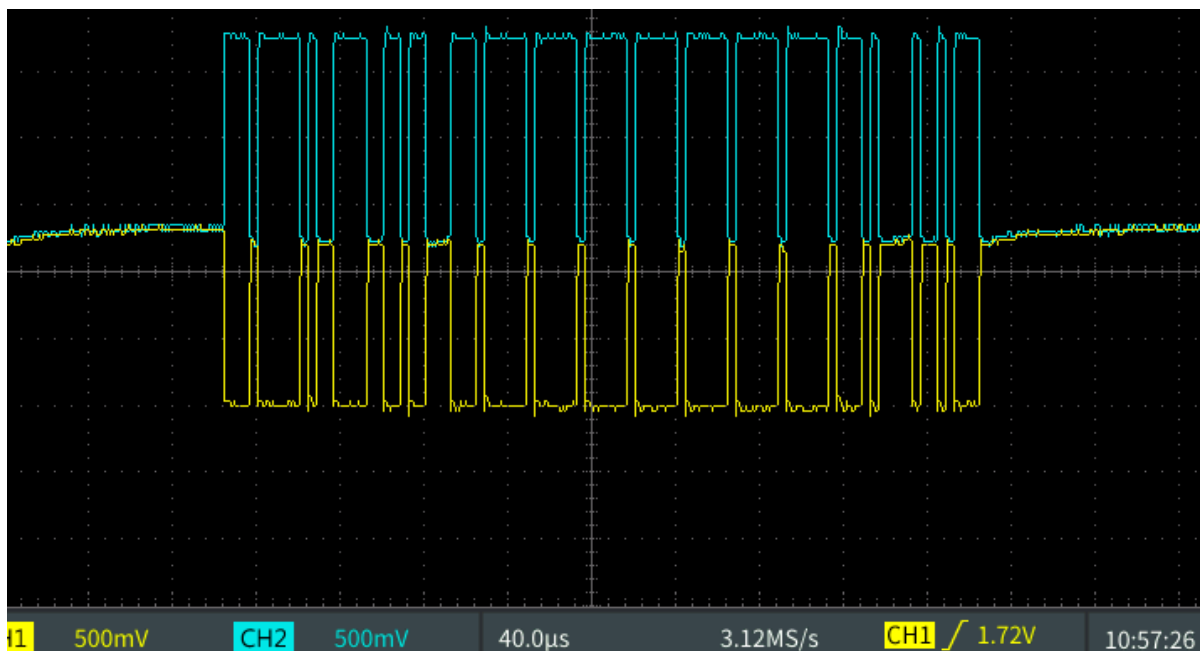


Figure 58 CAN bus using external termination resistor on BMS.

It is evident from the above that switching to the second CAN network for the BMS remedies the situation, as we now see a set of differential signals transmitting the same message as in Figure 57. This should contribute to enhanced reliability in signal integrity when transmitting data to the inverter and BMS, and reduce the frequency of communication faults with external monitoring devices used in testing.

4.6.3 Ignition Systems

Testing the vehicle required minor modifications to be made to the 'ignition' system for the vehicle. Notably, as the BMS induced reliability concerns, it was bypassed when turning on power to the inverter and DC/DC converter. To bypass the BMS, a switch was wired in series with the discharge enable wiring near the BMS, which when closed shorted directly to the chassis of the vehicle. In practice, what this meant, was that the BMS discharge enable check was bypassed, thus having the two relays it connects to, one supplying the inverter, the other the DC/DC converter, always conducting. This essentially means the ignition system consists of the key switch, turning on the BMS during the first stage, and the inverter at the second stage with no intermediate safety checks or delay involved. Though this presented no faults in and of itself, it was purely used as a temporary bypass for the purposes of testing, and it is recommended that the switch is removed prior to returning the vehicle to the sponsor. A schematic for the vehicle ignition during testing can be seen in Figure 59.

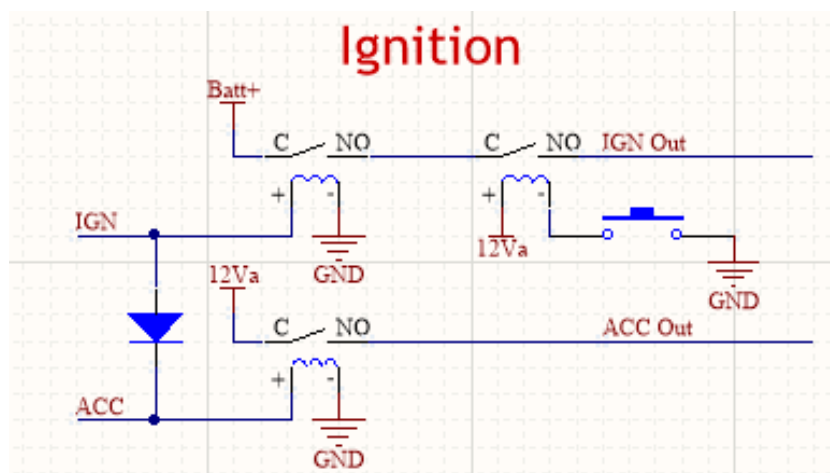


Figure 59 Modified Ignition System Schematic

4.7 Drive Testing

HiCEV aims to integrate the electrical systems with the existing vehicle drivetrain to maintain a similar drivability to the original ICE systems. However, electrical motor characteristics differ substantially from ICE counterparts, which contributes to major noticeable differences when driving with the modifications, despite the integrations which have been made to the existing powertrain to maintain a similar experience. In large part, the variability comes from the fundamental operating characteristics of the motor. In ICE motors, peak torque outputs can vary substantially with motor speed, which is why gearboxes are implemented into ICE vehicle systems. The gearbox in an ICE system enables the motor to continue operating within a higher torque operating range at a variety of vehicle speeds. With the electric motor, the vehicle can remain within its high torque range for a wider range of vehicle speeds which is why many EVs are designed around a single or very few gears. In practice, the most noticeable difference that stems from this is in the acceleration in lower gears, as the electric motor is capable of producing high torque at lower speeds. Another significant change from the ICE vehicle drivability is in the gear changes and starting. In ICE vehicles, due to risk of motor stalling when loaded at low motor speeds, the clutch is slowly applied as the throttle is feathered to increase the motor speed. Unlike ICE vehicles, EVs have no risk of stalling from this, and in HiCEV it has been noted that the most effective way to change gear is to quickly engage the clutch with no throttle, as the throttle typically accelerates the motor rapidly, heating up the clutch. Conversely, when slowing down, the motor will perform regenerative braking which when the clutch is removed from the motor, will cause the motor to instantly slow down with no load applied, when the clutch is then reapplied, the motor will rapidly speed up based on the vehicle speed and the gearing being applied to the motor. Ultimately, this means that downshifting the vehicle, especially into lower gears, when slowing for a corner will result in a shaky response from the vehicle. This concern can be somewhat mitigated in HiCEV by using the vehicle with a higher gear ratio for the majority of road driving. A fortunate side effect of the electric drivetrain, is that it can be used like this, in gear 3, vehicle acceleration is respectable, with HiCEV able to reach speeds of 30 km/h in approximately 5 s, and peak continuous operating torque maintained until a 'break' speed of 85 km/h, which is ideal for open road driving conditions.

Chapter 5: Discussion and Conclusions

5.1 Project Objectives

5.1.1 Functional Requirements

With the exception of reliability issues, largely due to existing wiring faults in the BMS cell taps, the functional requirements for HiCEV have been met to varying levels of success. In the introduction to the project, there were three main functional objectives for HiCEV, inclusive of the ability to drive round safely and stably with the modifications, the ability to perform regenerative braking and the ability for the vehicle to charge from any domestic AC outlet in NZ. Features of the vehicle, inclusive of the modifications to control and the vehicle mechanical components, contribute to the variance in the level of success for meeting these operating requirements.

With the BMS bypass enabled, HiCEV has largely maintained reliable drivability throughout many tests with the current set up. The primary concerning factor which inhibits the vehicle from meeting all functional requirements stem largely from the gear changes, which with the electric powertrain, and without the presence of a brake potentiometer, can be very jittery as the motor speed changes rapidly to match the operating speed of the gearbox. In part, this stems from another functional requirement, being the ability for the vehicle to use regenerative braking to improve the range of the batteries. Unfortunately, as the control is not configured for a manual gear box, the control assumes that under a 0 acceleration input, the vehicle should apply a small regenerative braking torque, that when the clutch is lifted will slow the motor to 0 rpm in a short space of time, accounting for the jumpy gear changes. With this exception, the integration of the motor into the existing gear system has been largely successful, the gearbox is usable to enable the driver to adjust the vehicle torque as required, and in higher gears, the effect of motor acceleration in gear changes is minimal. Though not fully representative of the original driving experience, HiCEV has been able to replicate a manual vehicle with an electric drive train, though realistically, only 2-3 gears are likely to be used by the operator through normal driving conditions.

Another significant functional requirement for HiCEV is the ability for it to charge from any standard AC power outlet. In HiCEV, this meant integrating an existing charger with the vehicle which is controlled via the BMS. Functionally, this was operating as intended, however, current limits on the BMS were set to 6 A to prevent the vehicle charging from triggering any breakers in NZ households. This means that while functionally, the vehicle is capable of charging virtually anywhere, meeting the functional requirement, charge times may exceed 12 hours, rendering the vehicle unusable for extended operation.

5.1.2 Mechanical Requirements

The LVVTA standards authority dictated many of the mechanical requirements for the vehicle at the start of the project scope. Since then, significant improvements have been made to essentially all electrical systems, through the mounting and tidying of wiring in the vehicle. This has the effect of not only making the vehicle safer to use, but also making the vehicle tidier and easier to repair. As part of the project, a significant portion of the existing wiring loom was removed from the vehicle and replaced with new wiring which met LVVTA requirements, through wire ratings, colour coding and mechanical mounting. Despite this, there are a few LVVTA requirements that are more difficult to reliably prove due to its existing implementation in the vehicle, and the cost associated with testing. The most substantial of these stems from the battery requirements, with the battery boxes needing to be able to withstand 30 times their weight in impact force; due to cost, and time requirements the existing battery boxes and battery set up was left as originally implemented.

5.2 Future Work

5.2.1 Brake Pump

The brake pump circuit relies on a pre-installed sensor which is designed to operate with ICE vehicles. In ICE vehicles, vacuum pressure is maintained using the intake manifold on the engine, the switch enables a light on the dashboard indicating a fault in the braking system. In HiCEV, this same switch is used with the brake pump circuit to trigger the operation of the pump. In practise, when the vacuum level is severely dissipated, or left on low vacuum for extended periods of time, the vacuum switch latches in position, this has the effect of stopping the trigger that enables the pump. The system can be improved by using an off-the-shelf vacuum sensor, which is sold by the pump manufacturer, with an operating trigger region automating the operation of the pump. It is recommended for future reliability, HiCEV should be retro-fit with a switch similar to this to enable the vehicle to reduce inconvenience to the vehicle operator.

5.2.2 Batteries and BMS

The results of the extensive battery testing pointed to a fault in the wiring set up for the cell taps in HiCEV. Given that there are existing replacement taps, which are compatible with the BMS 2, it is advisable that the cell taps are rewired, and tested with the BMS to enable the vehicle to operate reliably with the BMS in place. To properly continue battery testing, it is also advisable that all batteries are balanced, to ensure that the BMS state of charge estimations can operate with a higher degree of reliability.

5.2.3 DC/DC Converter

The current DC/DC converter installed in HiCEV is intended as a short-term solution to enable continued operation testing of the vehicle until a replacement is found. The primary drawback of the existing solution is that it fails to meet waterproofing requirement which is necessary for all components in the vehicle. To improve reliability, it may be advisable to replace the DC/DC converter with a modular, parallel connected system, as smaller DC/DC converters are easier to cool, and in the event of a failure, would not prevent the vehicle from continuing to operate.

5.2.4 Testing and Further Integrations

HiCEV is an unregistered vehicle, which has inhibited testing as it is unable to be legally tested on NZ roads. This has limited much of HiCEVs testing to lower speed, though due to motor characteristics and presence of gearing much of the electrical and mechanical data for characterising performance was still achievable at these lower speeds. Despite this, the vehicle is intended as a farm vehicle with occasional on road use, which will require substantial further testing on long term, higher speed operation.

The inverter could also use further integrations with the remainder of the vehicle to operate more efficiently. A notable feature which is missing in HiCEV is the presence of a brake potentiometer as opposed to simply using the existing brake switch, due to this, regenerative braking is scaled based on the time the switch is pressed as opposed to scaling to the potentiometer voltage input, which can lead to unnatural braking at times, as well as a lower overall regenerative braking torque when braking hard from a higher speed. Additional integrations which the inverter is capable of operating with include the ability to use the full 3-stage ignition, control error signal LEDs and control its own cooling systems.

5.3 Conclusions

HiCEV sought out to produce a prototype vehicle to test the viability of using EV conversions for farm vehicle operation. The primary objectives for the prototype is to accomplish normal vehicle operation in the required off-road and on-road conditions required by farm vehicles. To meet these objectives, several criteria were set, regarding vehicle operation, water-proofing, and LVVTA standards, which would enable the vehicle to be registerable for use on NZ roads. Work on HiCEV had been performed with the intent on meeting these objectives, whilst also proving desired electrical operation in many of the existing and modified systems.

In its current state, HiCEV has met its primary electrical operating requirements. The vehicle is now able to operate under the control of the inverter to perform all functional objectives, though due to BMS wiring, reliability has been hindered. The work performed has facilitated water-proofing through the use of more off-the-shelf IP67 rated components, rewiring, and sealing of cable glands throughout the vehicle. Similarly, all modifications made to the vehicle have followed LVVTA guidelines, though several components, namely existing HV wiring and BMS wiring, require further mounting to the chassis to fully meet specifications.

Modifications were primarily focussed on restoring the functionality of HiCEV, given the EVCM faults that prevented operation since previous student work. In doing so, the majority of the vehicle was rewired to bypass all EVCM functionality, which reduced the overall complexity of the system, but introduced concerns regarding the monitoring of each sub-system. For this reason, testing emphasised the performance of many of the existing vehicle systems, inclusive of the cooling, BMS, inverter and motor systems.

Results from tests show that the majority of vehicle systems work as intended; with the exception being the battery and BMS systems which have caused many shut-downs due to measurement errors. BMS measurement faults were causing the vehicle to shut-down due to mismeasurement of battery internal resistance, the internal resistances measured through external means yielded that the cell internal resistances were as low as 1.12 m Ω where the BMS was reporting internal resistances of up to 7.44 m Ω . Testing on the inverter and motor yielded expected results, with a constant continuous torque of 320 Nm sustained by the motor until a 'break' speed of 3600 rpm. This performance was as expected based on the motor characteristics, enabling the inverter to reach near its peak continuous power rating of 130 kW. One concern with the set up for the motor is the torque drops off rapidly at higher motor speeds, contributing to a strange driver experience, however, this concern can be addressed using the existing manual gearbox installed in the vehicle. Overall, the objective of maintaining similar performance to the original vehicle was largely maintained, though the distinctions between electrical and mechanical drive systems, led to significant unavoidable changes in the vehicle drivability.

References

- [1] European Commission, "Causes of Climate Change," [Online]. Available: https://ec.europa.eu/clima/change/causes_en. [Accessed 07 28 2021].
- [2] A. Sendy, "The cost of charging a Tesla-and how it compares to gas vehicles," Solar Reviews, 9 July 2021. [Online]. Available: <https://www.solarreviews.com/blog/how-much-does-it-cost-to-charge-a-tesla-is-it-the-same-as-the-cost-to-charge-other-electric-vehicles>. [Accessed 28 July 2021].
- [3] New Zealand Transport Authority, "Clean Car Programme overview," NZTA, 2021. [Online]. Available: <https://www.nzta.govt.nz/vehicles/clean-car-programme/overview/>. [Accessed 28 July 2021].
- [4] Environmental Protection Agency, "Sources of Greenhouse Gas Emissions," [Online]. Available: <https://www.epa.gov/ghgemissions/sources-greenhouse-gas-emissions>. [Accessed 29 July 2021].
- [5] Meridian Energy, "The top six advantages of driving an EV," [Online]. Available: <https://www.meridianenergy.co.nz/ev/advantages>. [Accessed 29 July 2021].
- [6] EV Specifications, "2011 Nissan Leaf SL - Specifications," 2021. [Online]. Available: <https://www.evspecifications.com/en/model/b1e92>. [Accessed 28 July 2021].
- [7] Enelx, "EV Charging," 11 November 2019. [Online]. Available: <https://evcharging.enelx.com/resources/blog/577-how-long-does-it-take-to-charge-a-tesla>. [Accessed 29 July 2021].
- [8] ChargeNet, "ChargeNet Map," 2021. [Online]. Available: <https://charge.net.nz/map/>. [Accessed 29 July 2021].
- [9] P. Chhabra and K. Rudesuela, "Electric Vehicle Safety: Concerns and Considerations," Nickel Institute, 5 March 2021. [Online]. Available: <https://nickelinstitute.org/blog/2021/march/electric-vehicle-safety-concerns-and-considerations/>. [Accessed 29 July 2021].
- [10] A. Maclean, "How safe are electric cars?," Driving Insights, [Online]. Available: <https://drivinginsights.co.nz/driver/how-safe-are-electric-cars/>. [Accessed 29 July 2021].
- [11] Ministry of Business, Innovation and Employment, "Electricity Statistics," 2021. [Online]. Available: <https://www.mbie.govt.nz/building-and-energy/energy-and-natural-resources/energy-statistics-and-modelling/energy-statistics/electricity-statistics/>. [Accessed 2 August 2021].
- [12] Ministry of Business, Innovation and Employment, "New Zealand Energy Strategy 2011 - 2021," 2011. [Online]. Available: <https://www.mbie.govt.nz/dmsdocument/142-nz-energy-strategy-lr-pdf>. [Accessed 2 August 2021].

- [13] International Energy Agency, "Electricity," 2021. [Online]. Available: <https://www.iea.org/fuels-and-technologies/electricity>. [Accessed 2 August 2021].
- [14] P. Hennessy, "Designing and Prototyping of a High Country Electric Vehicle," University of Canterbury, Christchurch, 2016.
- [15] Low Volume Vehicle Technical Association, "Electric and Hybrid Vehicles," 2002. [Online]. Available: https://www.lvvta.org.nz/documents/standards/LVVTA_STD_Electric_and_Hybrid_Vehicles.pdf. [Accessed 26 July 2021].
- [16] Glenthorne Station, "Location and Map," 2021. [Online]. Available: <https://www.glenthorne.co.nz/location-map>. [Accessed 26 July 2021].
- [17] IEC, "IP Ratings," IEC, 2021. [Online]. Available: <https://www.iec.ch/ip-ratings>. [Accessed 26 July 2021].
- [18] A. Abdalrahman, "Digital control techniques for grid-connected inverters," 2013. [Online]. Available: https://www.researchgate.net/publication/259563184_Master_of_Science_dissertation_Digital_control_techniques_for_grid-connected_inverters_Ain_Shams_University_2013_By_Ahmed_Abdalrahman_Ahmed. [Accessed 5 August 2021].
- [19] C. Buttay, Artist, *Principle of the delta Pulse Width Modulation (PWM)*. [Art]. 2006.
- [20] Roboteq, "How Resolvers work," [Online]. Available: <https://www.roboteq.com/applications/all-blogs/14-how-resolvers-work>. [Accessed 5 August 2021].
- [21] Cascadia Motion Systems, "HVH 250 Series Motors - HVH Motor Application Manual," 2021. [Online]. Available: <https://www.cascadiamotion.com/productlist/11-motors/bw-motors/12-hvh250>. [Accessed 2 August 2021].
- [22] Portescap, "How to Optimize Performance and Minimize Size in High Speed Applications," 2012. [Online]. Available: <https://www.portescap.com/en/resources/motor-specifications-and-literature/white-papers/optimizing-blcdc-motors-for-high-speed-applications>. [Accessed 9 August 2021].
- [23] Vector Magnets, "Permanent Magnet Synchronous Motor," 2021. [Online]. Available: <http://m.vectormagnets.com/n1854547/Permanent-magnet-synchronous-motor.htm>. [Accessed 4 August 2021].
- [24] J. Murphy, "Machine Design - What's the Difference Between AC Induction, Permanent Magnet, and Servomotor Technologies?," 2012. [Online]. Available: <https://www.machinedesign.com/motors-drives/article/21831709/whats-the-difference-between-ac-induction-permanent-magnet-and-servomotor-technologies>. [Accessed 4 August 2021].

- [25] M. Ridwan, M. Nur Yuniarto and Soediyo, "Electrical equivalent circuit based modeling and analysis of brushless direct current (BLDC) motor," IEEE, 2016. [Online]. Available: <https://ieeexplore.ieee.org/document/7828706>. [Accessed 6 August 2021].
- [26] Bright-Hub Engineering, "BLDC Motor Back EMF Explained," 2010. [Online]. Available: <https://www.brighthubengineering.com/machine-design/75825-do-you-know-why-electric-motors-generate-reverse-electromotive-force/>. [Accessed 6 August 2021].
- [27] A. Paliawadana, R. Daskith Akbo and L. S. Wickramaratne, "Design of the Propulsion System for an Electric Formula Car," December 2017. [Online]. Available: https://www.researchgate.net/publication/322116711_Design_of_the_Propulsion_System_For_an_Electric_Formula_Car#pf43. [Accessed 10 August 2021].
- [28] Kilowatt Classroom, "VFD Fundamentals," Kilowatt Classroom, LLC, 2003. [Online]. Available: <https://controltrends.org/wp-content/uploads/2010/10/VFFundamentals.pdf>. [Accessed 14 January 2022].
- [29] Y. Chin, "A permanent magnet synchronous motor for an electric vehicle - design analysis," 2004. [Online]. Available: <https://www.semanticscholar.org/paper/A-permanent-magnet-synchronous-motor-for-an-vehicle-Chin/1f6f6ad98429bff0239e82e7ebcde646147850f1>. [Accessed 11 August 2021].
- [30] Y. Solbakken, "Space Vector PWM Intro," Switchcraft, 1 May 2017. [Online]. Available: <https://www.switchcraft.org/learning/2017/3/15/space-vector-pwm-intro>. [Accessed 5 August 2021].
- [31] W. Salah, D. Ishak and K. Hammadi, "Minimization of torque ripples in BLDC motors due to phase commutation - A review," *Przeglad Elektrotechniczny*, pp. 183-187, January 2011.
- [32] C. Lewin, "Field Oriented Control (FOC) - A Deep Dive," [Online]. Available: <https://www.pmdcorp.com/resources/type/articles/get/field-oriented-control-foc-a-deep-dive-article>. [Accessed 11 August 2021].
- [33] Microsemi, "Park, Inverse Park, Clarke, Inverse Clarke Transformations MSS Software Implimentation," 2013. [Online]. Available: https://www.microsemi.com/document-portal/doc_view/132799-park-inverse-park-and-clarke-inverse-clarke-transformations-mss-software-implementation-user-guide. [Accessed 11 August 2021].
- [34] Mathworks, "Clarke Transform," 2021. [Online]. Available: <https://au.mathworks.com/help/physmod/sps/ref/clarketransform.html>. [Accessed 11 August 2021].
- [35] M. E. Iranian and A. Zabihinejad, "Modeling and Implementation of Generator and Network Simulator for Static Exciters using Matlab and Labview," 2011. [Online]. Available: <https://scialert.net/fulltext/?doi=jas.2011.414.425>. [Accessed 11 August 2021].
- [36] Cummins Engineering, "Spot the Difference: Lithium-Ion versus Lead-Acid Battery Electric Technology," 2019. [Online]. Available: <https://www.cummins.com/news/2019/06/17/spot-difference-lithium-ion-versus-lead-acid-battery-electric-technology>. [Accessed 12 August 2021].

- [37] A. Beck, "Lithium Iron Phosphate vs. Lithium-Ion: Differences and Advantages," 2019. [Online]. Available: <https://blog.epectec.com/lithium-iron-phosphate-vs-lithium-ion-differences-and-advantages>. [Accessed 12 August 2021].
- [38] B. Chapman, "How does a Lithium-Ion battery work?," 23 September 2019. [Online]. Available: <https://letstalkscience.ca/educational-resources/stem-in-context/how-does-a-lithium-ion-battery-work>. [Accessed 16 August 2021].
- [39] BYJU, "Standard Electrode Potential," [Online]. Available: <https://byjus.com/chemistry/standard-electrode-potential/>. [Accessed 16 August 2021].
- [40] COMSOL, "Lithium-Ion Battery Internal Resistance," [Online]. Available: <https://www.comsol.com/model/lithium-ion-battery-internal-resistance-19131>. [Accessed 16 August 2021].
- [41] K. M. Deen, "Why is there a sudden potential drop during discharging in Li-Ion battery," 2019. [Online]. Available: https://www.researchgate.net/post/Why_there_is_sudden_potential_drop_during_discharging_in_Li_ion_battery. [Accessed 16th August 2021].
- [42] A. Urban, D.-H. Seo and G. Ceder, "Computational understanding of Li-ion batteries," *Computational Materials*, vol. 16002, 2016.
- [43] RELiON, "Performance Characteristics," [Online]. Available: <https://reliionbattery.com/products/lithium/rb5>. [Accessed 20 February 2022].
- [44] J. S. Edge, S. O'Kane, R. Prosser, N. Kirkaldy, A. Patel, A. Hales, A. Ghosh, W. Au, J. Chen, S. Li, M.-C. Pang, L. Bravo-Diaz, A. Tomaszewska, M. W. Marzook and K. Radhakrishnan, "Lithium ion battery degradation: what you need to know," 25 January 2021. [Online]. Available: <https://pubs.rsc.org/en/content/articlehtml/2021/cp/d1cp00359c>. [Accessed 19 August 2021].
- [45] E. Osmanbasic, "Battery Management Systems - Part 3: Battery Charging Methods," 22 February 2020. [Online]. Available: <https://www.engineering.com/story/battery-management-systemspart-3-battery-charging-methods>. [Accessed 18 August 2021].
- [46] "Battery Charging Methods and Terminology," Helios Power Solutions, [Online]. Available: <https://www.heliosps.com/knowledgebase/battery-charging-methods-terminology/>. [Accessed 18 August 2021].
- [47] Battery University, "BU-409: Charging Lithium-ion," 2018. [Online]. Available: <https://batteryuniversity.com/article/bu-409-charging-lithium-ion>. [Accessed 18 August 2021].
- [48] Orion BMS, "Troubleshooting, Internal Resistance Values Incorrect," 2019. [Online]. Available: <https://www.orionbms.com/troubleshooting/internal-resistance-values-incorrect-by-significant-amount/>. [Accessed 20 August 2021].
- [49] R. Roderick, "A Look Inside Battery-Management Systems," *Electronic Design*, 27 March 2015. [Online]. Available: <https://www.electronicdesign.com/power->

management/article/21800666/a-look-inside-batterymanagement-systems. [Accessed 23 August 2021].

- [50] Orion BMS, "How Cell Balancing Works," [Online]. Available: https://www.orionbms.com/manuals/utility/param_balancing_description.html. [Accessed 23 August 2021].
- [51] S. N. Kevin Scott, "Active Battery Cell Balancing," Analog Devices, [Online]. Available: <https://www.analog.com/en/technical-articles/active-battery-cell-balancing.html>. [Accessed 24 August 2021].
- [52] S. Hemavathi, "Overview of cell balancing methods for Li-ion Battery technology," 13 August 2020. [Online]. Available: <https://onlinelibrary.wiley.com/doi/10.1002/est2.203>. [Accessed 24 August 2021].
- [53] Orion BMS, "Orion BMS Manuals," [Online]. Available: <http://www.orionbms.com/manuals/pdf/wiring.pdf>. [Accessed 24 August 2021].
- [54] PicoTech, "CAN and CAN FD bus decoding," [Online]. Available: <https://www.picotech.com/library/oscilloscopes/can-bus-serial-protocol-decoding>. [Accessed 25 August 2021].
- [55] Pico Technology, "CAN and CAN FD bus Decoding," [Online]. Available: <https://www.picotech.com/library/oscilloscopes/can-bus-serial-protocol-decoding>. [Accessed 25 August 2021].
- [56] NewBedEV, "Is the CAN bus protocol a master and slave protocol?," [Online]. Available: <https://newbedev.com/is-the-can-bus-protocol-a-master-and-slave-protocol>. [Accessed 25 August 2021].
- [57] W. Voss, "Controller Area Network (CAN Bus) - Bit Timing and Synchronization," CopperHill Technologies, 2018. [Online]. Available: <https://copperhilltech.com/blog/controller-area-network-can-bus-bit-timing-and-synchronization/>. [Accessed 26 August 2021].
- [58] CSS Electronics, "CAN Bus Explained - A Simple Intro (2021)," 2021. [Online]. Available: <https://www.csselectronics.com/pages/can-bus-simple-intro-tutorial>. [Accessed 25 August 2021].
- [59] CAN in Automation, "Cyclic redundancy check (CRC) in CAN frames," [Online]. Available: <https://www.can-cia.org/can-knowledge/can/crc/>. [Accessed 26 August 2021].
- [60] S. Corrigan, "Introduction to the Controller Area Network (CAN)," Texas Instruments, 2002. [Online]. Available: https://www.ti.com/lit/an/sloa101b/sloa101b.pdf?ts=1629943421135&ref_url=https%253A%252F%252Fwww.google.com%252F#:~:text=EOF%E2%80%93This%20end%2Dof%2D,is%20stuffed%20into%20the%20data.. [Accessed 26 August 2021].
- [61] Ewart Energy Systems, "Orion BMS Manuals and Troubleshooting," 2018. [Online]. Available: https://www.orionbms.com/manuals/pdf/troubleshooting_soc_jumps.pdf. [Accessed 15 September 2021].

- [62] Borg Warner, "HVH250-115 Electric Motor," 2016. [Online]. Available: <https://www.cascadiamotion.com/images/catalog/remy-pds---hvh250-115-sheet-euro-pr-3-16.pdf>. [Accessed 20 September 2021].
- [63] YT Tech. Corp, "VBS-EV-12 Brake Pumps," YT Tech. Corp, [Online]. Available: <https://www.yutai.tw/evp.html>. [Accessed 28 September 2021].
- [64] Advanced Thermal Solutions, "Calculating the Loads for a Liquid Cooling System," [Online]. Available: https://www.qats.com/cms/wp-content/uploads/ATS_White_Paper_Calculating-loads-liquid-cooling.pdf. [Accessed 28 October 2021].
- [65] J. Edge, S. O'Kane, R. Prosser, N. Kirkclady, A. Patel, A. Hales, A. Ghosh, W. Ai, J. Chen, J. Yang, S. Li, M. Peng, L. Diaz, A. Tomoszewska, M. Marzook, K. Radhakrishanan, H. Wang, Y. Patel, B. Wu and G. Offer, Royal Society of Chemistry, 21 March 2021 . [Online]. Available: <https://pubs.rsc.org/en/content/articlelanding/2021/cp/d1cp00359c>. [Accessed 20 February 2022].
- [66] Nissan, "Nissan Leaf," 2021. [Online]. Available: <https://www.nissan.co.nz/vehicles/browse-range/leaf.html>. [Accessed 28 July 2021].
- [67] Tesla, "Tesla Model S," 2021. [Online]. Available: https://www.tesla.com/en_nz/models. [Accessed 28 July 2021].
- [68] D. Collins, "What's the difference between BLDC and synchronous AC motors?Motors," 15 December 2015. [Online]. Available: <https://www.motioncontroltips.com/faq-whats-the-difference-between-bldc-and-synchronous-ac-motors/>. [Accessed 3 August 2021].
- [69] Lumen Physics, "Magnetic Fields Produced by Currents: Ampere's Law," [Online]. Available: <https://courses.lumenlearning.com/physics/chapter/22-9-magnetic-fields-produced-by-currents-ampere-law/>. [Accessed 6 August 2021].
- [70] T. Schwanen, "The five major challenges facing electric vehicles," BBC, 19 September 2019. [Online]. Available: <https://www.bbc.com/news/uk-49578790>. [Accessed 25 February 2022].
- [71] H. Tabuchi and B. Plumer, "How Green Are Electric Vehicles?," The New York Times, 2 March 2021. [Online]. Available: <https://www.nytimes.com/2021/03/02/climate/electric-vehicles-environment.html>. [Accessed 25 February 2022].

Appendix

Appendix 1 Graphing Program for SCI Data

```
from numpy.core.fromnumeric import size
from numpy.lib.shape_base import tile
import pandas as pd
import matplotlib.pyplot as plt
pd.set_option('mode.chained_assignment', None)
cols = ['Pwr on Time', 'Accel Input', 'Motor Torque', 'Vehicle Torque', 'DC Voltage', 'DC Current', 'Motor Speed', 'Flux',
'Motor Voltage', 'IQC', 'IQF', 'IDC', 'IDF', 'Modulation', 'Inv Temperature', 'Motor Temperature', 'Fault Low', 'Fault High',
'Shudder', 'Brake Pot']

ten = ['Motor Torque', 'Vehicle Torque', 'DC Voltage', 'DC Current', 'Flux', 'Motor Voltage', 'IQC', 'IQF', 'IDC', 'IDF',
'Inv Temperature', 'Motor Temperature', 'Shudder']
hundred = ['Accel Input', 'Brake Pot']
df = pd.read_csv('Drive Test.csv', dtype=str, usecols=[0,1,2,3,4,5,6,7,8,9,10,11,12,13,14,15,16,17,18,19])

df.columns = cols

for col in cols:
    if col in ten:
        df[col] = df[col].apply(lambda x: int(x, 16))/10
    elif col in hundred:
        df[col] = df[col].apply(lambda x: int(x, 16))/100
    else:
        df[col] = df[col].apply(lambda x: int(x, 16))

for i in df.index:
    if df['Motor Speed'][i] > 60000:
        df['Motor Speed'][i] = 0
    if df['Motor Torque'][i] > 6000:
        df['Motor Torque'][i] = 0
    if df['Vehicle Torque'][i] > 6000:
        df['Vehicle Torque'][i] = 0
    if df['DC Current'][i] > 6000:
        df['DC Current'][i] = 0
    if df['IQC'][i] > 6000:
        df['IQC'][i] = 0
    if df['IDC'][i] > 6000:
        df['IDC'][i] = 6535 - df['IDC'][i]

power = []
for i in df.index:
    power.append((df['DC Voltage'][i]*df['DC Current'][i])/1000)

df.insert(20, "Power", power, True)

n = 0
for i in df.index:
    if i >= 1:
        cmp = df['Pwr on Time'][i-1] % 65535
        if ((df['Pwr on Time'][i] * 2500) < cmp):
            n += 1
        df['Pwr on Time'][i] = (n * 65535 + df['Pwr on Time'][i])/3

plt.figure(1)
plt.subplot(411)
plt.plot(df['Pwr on Time'], df['Motor Speed'], 'g')
plt.ylabel('Motor Speed \n(rpm)', size=12)

plt.subplot(412)
plt.plot(df['Pwr on Time'], df['DC Current'], 'r')
plt.ylabel('DC Current \n(A)', size=12)

plt.subplot(413)
plt.plot(df['Pwr on Time'], df['Motor Voltage'], 'b')
plt.ylabel('Motor Voltage \n(V)', size=12)

plt.subplot(414)
plt.plot(df['Pwr on Time'], df['Inv Temperature'], 'purple')
plt.xlabel('Time (ms)', size=12)
plt.ylabel('Motor Temp \n(C)', size=12)

plt.show()
```

Appendix 2 SCI Data Acquisition Formatting Table

Format	Variable Type	Range	Unit	Multiplier
Temperature	Signed Integer	± 3000.0	°C	10
Low Voltage	Signed Integer	± 300.00	Volts	100
High Voltage	Signed Integer	± 3000.0	Volts	10
Torque	Signed Integer	± 3000.0	N.m.	10
Current	Signed Integer	± 3000.0	Amps	10
Angle	Signed Integer	0 to ±359.9	Degrees	10
Angular Velocity	Signed Integer	± 30000	RPM	N.A.
Boolean	Unsigned Byte	0 OR 1	Binary	N.A.
Frequency	Signed Integer	± 3000.0	Hz	10
Power	Signed Integer	± 3000.0	kW	10
Flux	Signed Integer	0 to 30.000	Webers	1000
Proportional Gain	Unsigned Integer	0 - 655.00 OR 0 - 6.5535	N.A.	100 OR 10000
Integral Gain	Unsigned Integer	0 - 6.5535	N.A.	10000
Derivative Gain	Unsigned Integer	0 - 655.35	N.A.	100
Low-pass Filter Gain	Unsigned Integer	0 - 6.5535	N.A.	10000
Time	Unsigned Long Integer OR Unsigned Integer	See Parameter Description	See Parameter Description	See Parameter Description
Per-unit Value	See Parameter Description	See Parameter Description	See Parameter Description	See Parameter Description

Appendix 3 CurrentWays 3 kW charger operation datasheet

3KW CHARGER FAMILY					
Nominal	Model #	Cooling	Constant Current Below	Constant 3KW Power	
				MIN	MAX
72V	CA11C03	Air	60V (50A)	60V	96V
	CL21C03	Liquid			
96V	CA11E03	Air	75V (40A)	75V	128V
	CL21E03	Liquid			
112-225V	CA11L03	Air	112V (26.8A)	112V	225V
	CL21L03	Liquid			
225-450V	CA11H03	Air	225V (13.3A)	225V	450V
	CL21H03	Liquid			

Appendix 4 Weak Cell fault report

DCL Reduced Due To SOC: 0.0	Lowest cell voltage: 3.236
DCL Reduced Due To Cell Resistance: 1.0	Highest cell voltage: 3.323
DCL Reduced Due To Temperature: 1.0	Highest cell voltage ID: 108.0
DCL Reduced Due To Cell Voltage: 0.0	Lowest cell voltage ID: 80.0
DCL Reduced Due To Pack Voltage: 0.0	Highest opencell ID: 108.0
Reduced Due To Voltage Failsafe: 0.0	Lowest opencell ID: 80.0
Multi-Unit Comm Failsafe: 0.0	Highest resistance ID: 11.0
CCL Reduced Due To SOC: 0.0	Lowest resistance ID: 69.0
CCL Reduced Due To Cell Resistance: 1.0	Average cell voltage: 3.305
CCL Reduced Due To Temperature: 1.0	Lowest open cell voltage: 3.237
CCL Reduced Due To Cell Voltage: 0.0	Highest open cell voltage: 3.325
CCL Reduced Due To Pack Voltage: 0.0	Average open cell voltage: 3.306
CCL Zero Because Charge Complete: 0.0	Lowest cell resistance: 0.96
HEM mode: 17.0	Highest cell resistance: 3.19
Maximum cell number: 108.0	Average cell resistance: 1.57
Pack charge current limit: 75.0	
Pack discharge current limit: 102.0	

Appendix 5 BMS 2 internal resistance measurement with cells 69 and 71 swapped in the pack.

Live Cell Data

Highest Resistance: 3.87 [011]	Highest Cell Volt: 3.317 [100]	Pack SOC: 49.0%	<input checked="" type="radio"/> Internal Resistances
Lowest Resistance: 1.02 [065]	Lowest Cell Volt: 3.231 [080]	Pack Amps: 0.0A	<input type="radio"/> Live Cell Voltages
Avg Cell Resistance: 1.38	Avg Cell Voltage: 3.305	Pack Voltage: 356.9V	<input type="radio"/> Open Cell Voltage
Delta Cell Resistance: 2.85	Delta Cell Voltage: 0.086	Current Limits: +84A / -62A	
	Temperature: 22°C / 22°C	Relay Status: Discharge:OFF, Charge:OFF, Safety:OFF	

Cell 1	Cell 2	Cell 3	Cell 4	Cell 5	Cell 6	Cell 7	Cell 8	Cell 9	Cell 10
1.920	1.240	2.240	1.120	1.150	1.160	1.250	1.540	1.310	1.210
3.870	1.390	1.810	1.240	1.150	1.160	1.200	1.150	1.220	1.190
1.160	1.210	3.340	1.380	1.280	2.000	1.730	1.230	1.060	1.600
1.740	1.230	1.150	1.220	1.160	1.270	1.190	1.570	2.110	1.230
1.280	1.120	1.310	1.170	1.190	1.920	1.230	1.180	2.010	1.160
1.140	1.150	1.350	1.200	1.170	2.960	1.120	1.170	1.210	1.280
1.120	1.170	1.360	1.190	1.020	1.480	1.130	1.130	1.090	1.120
● 2.350	1.160	1.100	1.500	1.270	1.150	1.180	1.160	1.130	1.360
1.100	1.190	1.070	1.140	1.140	1.180	1.160	1.110	1.700	1.120
1.200	1.140	1.180	3.400	1.900	1.670	1.150	1.110	1.270	1.150
1.140	1.130	1.890	1.210	1.250	1.060	1.080	1.250		

Appendix 6 Mechanical and Electrical Power vs Time

